Univerzita Karlova

1. lékařská fakulta

Studijní program: Molekulární a buněčná biologie, genetika a virologie

Studijní obor: Molekulární a buněčná biologie, genetika a virologie

Mgr. Soňa Baranová

Intravitální diagnostika neurodegenerativních onemocnění.

Intravital diagnostics of neurodegenerative diseases

Disertační práce

Vedoucí závěrečné práce: doc. Ing. Karel Holada, Ph.D.

Praha, 2024

Prohlášení:

Prohlašuji, že jsem závěrečnou práci zpracovala samostatně a že jsem řádně uvedla a citovala všechny použité prameny a literaturu. Současně prohlašuji, že práce nebyla využita k získání jiného nebo stejného titulu

Souhlasím s trvalým uložením elektronické verze mé práce v databázi systému meziuniverzitního projektu Theses.cz za účelem soustavné kontroly podobnosti kvalifikačních prací.

V Praze, 4.4.2024

Soňa Baranová

Identifikační záznam:

BARANOVÁ, Soňa. *Intravitální diagnostika neurodegenerativních onemocnění*. [*Intravital diagnostics of neurodegenerative diseases*]. Praha, 2024. Počet stran 100. Disertační práce (Ph.D.). Univerzita Karlova, 1. lékařská fakulta, Ústav imunologie a mikrobiologie. Vedoucí závěrečné práce: Holada, Karel.

Acknowledgment

In the first place, I would like to thank my supervisor doc. Ing. Karel Holada, Ph.D. for his support through the whole Ph.D. study. Without his expertise and professional advice, the completion of presented theses would not be possible.

I would also like to thank our collaborators prof. MUDr. Radoslav Matěj, Ph.D. and Ing. Magdalena Brůžová, Ph.D. from National Reference Laboratory for Prion Diseases, with their help with patient's samples.

My gratitude also goes to RNDr. Tibor Moško, Ph.D. for his help with RT-QuIC experiments and Alena Šteflová Lisáková for exceptional technical support in the laboratory. I would also like to thank to former Ph.D. students in our laboratory, namely Maruška and Jakub for their help since the beginning.

Finally, I thank my husband Peter, for supporting me in every step during the Ph.D. study and for cooking the best food.

Abstract

Prionopathies, also called transmissible spongiform encephalopathies (TSE) and synucleinopathies are neurodegenerative diseases that are associated with the accumulation of misfolded proteins (prion and α-synuclein) mostly in the central nervous system. To this day, early and definite diagnosis remains unavailable during the patient's lifetime, mainly due to the absence of reliable biomarker which makes clinical diagnosis more challenging. Therefore, the gold standard in diagnostics remains direct *post-mortem* evaluation of misfolded proteins within brain tissue by western blot and immunohistochemistry. In the recent years, seeding amplification assays (SAAs) like Real-Time Quacking-Induced Conversion (RT-QuIC) emerged for ultra-sensitive *ante-mortem* diagnosis of neurodegenerative diseases. SAAs exploit ability of pathological misfolded proteins present in patient's samples to change the conformation and initiate aggregation of native recombinant protein substrate by prion-like seeding mechanism.

In the presented dissertation thesis, we exploited second-generation RT-QuIC assay (55°C, 700 rpm, cycles of 1 min double-orbital shaking and 1 min incubation) utilizing recombinant hamster shortened prion protein (rHAPrP90-231) to evaluate prion seeding activity in *post-mortem* TSE (n=38) and non-TSE (n=30) cerebrospinal fluid (CSF) and corresponding skin samples. In CSF, we were able to achieve 100% sensitivity and specificity after dilution of samples to remove the effect of present inhibitors. In the skin samples, the sensitivity and specificity of the assay was 89.5% and 100%, respectively. Interestingly, the analysis showed higher median prion seeding dose in the skin samples than in corresponding CSF. To further explore diagnostic potential of skin, we analyzed skin (head apex and ear lobe) from mice inoculated intracerebrally or subcutaneously with RML prion strain. Subcutaneously infected mice showed positive RT-QuIC results in the skin from the apex and ear lobe 12 days and 40 days before the onset of symptoms, correspondingly. However, intracerebrally infected mice displayed positive prion seeding activity in skin only after the onset of symptoms. Moreover, we examined prion seeding activity in two siblings with a genetic Creutzfeldt-Jakob disease with a novel five octapeptide repeats insertion (5-OPRI, R1-R2-R2-R3-R4-**R2-R2-R3-R3-R4**) in the *PRNP* gene. Duration of the disease was more than 10 years in both patients. In the first case, positive seeding activity was detected in every type of tested sample (frontal lobe, cerebellum, CSF, skin). On the contrary, in the second case, no RT-QuIC positivity was detectable suggesting the possible presence of different prion strain. We successfully adopted a protocol for RT-QuIC analysis of formalin-fixed paraffin-embedded brain tissue of TSE patients and demonstrated its ability to detect prions in cohorts of TSE (n=30) and control non-TSE (n=30) patients.

Furthermore, we established RT-QuIC assay adapted for synucleinopathies (42°C, 400 rpm, cycles of 1 min double-orbital shaking and 1 min incubation). We validated α-syn seeding activity in 15 *post-mortem* brain homogenates and CSF samples with definite Dementia Lewy bodies (DLB, n=6), Alzheimer disease with Amygdala Lewy bodies (AD/ALB, n=3) and Creutzfeldt-Jakob disease with DLB (CJD/DLB) comorbidity (n=6) with 100% and 92.9% sensitivity, respectively. We also reported detection of α-syn higher seeding activity in a few non-TSE control samples. However, in two of them, secondary synucleinopathy was confirmed after the neuropathological reevaluation which was prompted by our RT-QuIC results.

Key words: diagnosis, neurodegenerative diseases, prion, CJD, α-synuclein, synucleinopathy, RT-QuIC

Abstrakt

Prionopatie, taktiež nazývané transmisívne spongiformné encefalopatie (TSE), a synukleínopatie predstavujú skupinu neurodegeneratívnych ochorení, ktoré sú asociované s akumuláciou nesprávne zložených proteínov (prión a α-synukleín) prevažne v centrálnom nervovom systéme. Kvôli absencii spoľahlivého biomarkera je včasná a definitívna diagnostika počas života pacienta nedostupná. Zlatým štandardom preto zostáva priama *post-mortem* detekcia patologicky zložených proteínov v mozgovom tkanive pomocou western blotu a imunohistochémie. Avšak v posledných rokoch sa pre ultra-senzitívnu *ante-mortem* diagnostiku zaviedli metódy so spoločným názvom ”seeding amplification assays (SSAs)” akou je aj Real-Time Quacking-Induced Conversion (RT-QuIC). SAAs využívajú schopnosť patologicky zložených proteínov, ktoré sú prítomné v pacientskej vzorke, zmeniť konformáciu a iniciovať agregáciu monomérneho rekombinantného proteínu v substráte vďaka ”prion-like” mechanizmu.

V prezentovanej dizertačnej práci sme analyzovali prión konvertujúcu aktivitu v *post-mortem* TSE (n=38) a non-TSE (n=30) vzorkách cerebrospinálneho moku (CSF) a korešpondujúcich vzoriek koží pomocou druhej generácie RT-QuIC metódy (55°C, 700 rpm, cykly 1 min dvoj orbitálneho trepania a 1 min inkubácia) s využitím rekombinantného skráteného priónového proteínu škrečka zlatého (rHAPrP90-231) ako substrátu. Vo vzorkách CSF, sme boli schopní dosiahnuť 100 % senzitivitu a špecificitu až po nariedení vzoriek, ktoré odstráni efekt inhibítorov prítomných vo vzorke. Vo vzorkách kože sme dosiahli 89,5 % senzitivitu a 100% špecificitu. Prekvapivo, analýza vzoriek ukázala vyššiu priemernú prión konvertujúcu aktivitu vo vzorkách koží než v CSF. Na bližšie preskúmanie diagnostického potenciálu kože, sme analyzovali vzorky kože (z apexu hlavy a ušného laloku) z myší, ktoré boli intracerebrálne alebo subkutánne inokulované priónovým kmeňom RML. Subkutánne inokulované myši vykazovali RT-QuIC pozitívny signál v koži z apexu a ušného laloku 12 a 40 dní pred nástupom klinických príznakov. Avšak myši, ktoré boli inokulované intracerebrálne vykazovali pozitívnu prión konvertujúcu aktivitu v koži až po nástupe symptómov. Navyše sme otestovali prión konvertujúcu aktivitu u dvoch súrodencov s genetickou Creutzfeldt-Jakobovou chorobou (CJD) s novou mutáciou piatich oktapeptidových repetitívnych inzercií (5-OPRI, R1-R2-R2-R3-R4-**R2-R2-R3-R3-R4**) v *PRNP* géne. U obidvoch pacientov bola doba ochorenia dlhšia ako 10 rokov. V prvom prípade sme detegovali prión konvertujúcu aktivitu v každej testovanej vzorke (frontálny lalok, mozoček, CSF a koža). Naopak, v druhom prípade sme nedetegovali žiadnu RT-QuIC pozitivitu čo naznačuje možnú prítomnosť iného priónového kmeňa. Úspešne sme zaviedli protokol na RT-QuIC analýzu parafínových vzoriek mozgu fixovaných vo formalíne od pacientov s TSE a demonštrovali schopnosť metódy detegovať prióny v kohorte pacientov s TSE (n=30) a kontrolných non-TSE (n=30) pacientov.

Okrem toho sme zaviedli RT-QuIC metódu adaptovanú na synukleínopatie (42°C, 400 rpm, cykly 1 min dvoj orbitálneho trepania a 1 min inkubácie). Validovali sme α-syn konvertujúcu aktivitu u 15 *post-mortem* vzoriek mozgových homogenátov a CSF s definitívnou diagnózou Demencie s Lewyho telieskami (DLB, n=6), Alzheimerovej choroby s amygdala Lewyho telieskami (ALB, n=3) a Creutzfeldt-Jakobovej choroby s DLB (CJD/DLB, n=6) komorbiditou so 100 % senzitivitou a 92,9 % špecificitou. Taktiež sme reportovali detekciu vyššej α-syn konvertujúcej aktivity u pár non-TSE kontrolných vzoriek. Avšak pri dvoch vzorkách bola potvrdená sekundárna synukleínopatia po neuropatologickej reanalýze na podnet našich RT-QuIC výsledkov.

Kľúčové slová: diagnostika, neurodegeneratívne ochorenia, prión, CJCH, α-synukleín, synukleínopatia, RT-QuIC

Content

List of Abbreviations

AD	Alzheimer disease
ALB	Amygdala Lewy bodies
AU	Arbitrary units
AUC	Area under the curve
α-syn	Alpha-synuclein
$\alpha\text{-syn}^{D}$	Pathological alpha-synuclein
BBMM	BugBuster master mix
BH	Brain homogenate
BCA	Bicinchoninic acid
BSE	Bovine spongiform encephalopathy
CBD	Corticobasal degeneration
CD	Corneal donor
CJD	Creutzfeldt-Jakob disease
Cryo-EM	Cryogenic electron microscopy
CSF	Cerebrospinal fluid
DLB	Dementia with Lewy bodies
DLBCL	Diffuse large B-cell lymphoma
dpi	Days post inoculation
EDTA	Ethylenediaminetetraacetic acid
EEG	Electroencephalogram
FFI	Fatal Familial Insomnia
FFPE	Formalin-fixed paraffin-embedded
FTLD	Frontotemporal lobar dementia
gCJD	Genetic Creutzfeldt-Jakob disease
GndHCl	Guanidine hydrochloride
GPI	Glycosylphosphatidylinositol
GSS	Gerstmann-Sträussler-Scheinker syndrome
H/ABI	Hypoxic/anoxic brain injury
HSA	Human serum albumin
iCJD	Iatrogenic Creutzfeldt-Jakob disease
mQH_20	Milli-Q water

MRI	Magnetic resonance imagining
MSA	Multiple system atrophy
MWCO	Molecular weight cut-off
NAC	Non-amyloid-β component
ND-A	Non-dementia alcoholism
Ni-NTA	Nickel-nitrilotriacetic acid
OND	Other neurodegenerative diseases
OPRI	Octapeptide repeats insertion
ORF	Open reading frame
PAF	Pure autonomic failure
PB	Phosphate buffer (sodium)
PBS	Phosphate buffered saline
PD	Parkinson disease
PDD	Parkinson disease with dementia
PK	Proteinase K
PMCA	Protein Misfolding Cyclic Amplification
PMSF	Phenylmethylsulfonyl fluoride
PrP^{C}	Cellular prion protein
PrP^{TSE}	Pathological prion protein
PTM	Posttranslational modifications
QC	Quality control
rα-Syn (WT)	Recombinant alpha-synuclein wild-type
rBVPrP	Recombinant bank vole prion protein
rHAPrP23-231	Recombinant hamster prion protein
rHAPrP90-231	Short recombinant hamster prion protein
RML	Rocky mountain laboratories (prion strain)
rPrP	Recombinant prion protein
RT	Room temperature
RT-QuIC	Real-Time Quacking-Induced Conversion assay
SAA	Seeding Amplification Assay
sCJD	Sporadic Creutzfeldt-Jakob disease
SD	Standard deviation
SD_{50}	Seeding dose 50%
SDS	Sodium dodecyl sulfate

SDS-PAGE	Sodium dodecyl sulfate – polyacrylamide gel electrophoresis
Syn	Synucleinopathy
TBS	Tris buffered saline
TBS-T	Tris buffered saline with Tween 20
ThT	Thioflavin T
Tris	Trisaminomethane
TSE	Transmissible spongiform encephalopathies
TTT	Time to threshold
VaD	Vascular dementia
vCJD	Variant Creutzfeldt-Jakob disease
VPSPr	Variably protease-sensitive prionopathy
WB	Western blot

1 Literature overview

1.1 Prion protein and its structure

Cellular prion protein (PrP^C) is a highly conserved protein found on the outer cell plasma membrane attached with glycosylphosphatidylinositol (GPI) anchor. PrP^C is continuously expressed from early stage of the embryogenesis in most vertebrates, mostly in the central nervous system, specifically in neocortical and hippocampal neurons, Purkinje cells in cerebellum and motor neurons in spine. (Westergard *et al*., 2007; Sarnataro, Pepe and Zurzolo 2017). Low amount of PrP^C was also found in the cells of internal organs such as heart, skeletal muscles, intestine, uterus, or testis (Brown *et al*., 1990; Smith *et al*., 2011; Morrel *et al*., 2004; Tanji *et al.,* 1995). Moreover, PrP^C can be expressed in the immune system in mature lymphoid tissues (Isaacs, Jackson and Altmann, 2006). The function of PrP^C in the organisms remains unclear, however many biological functions such as anti-apoptotic activity, copper binding, cell adhesion or transmembrane signaling were assigned to the protein (Legname 2017; Zhu *et al.,* 2021).

In humans, the PrP^C is encoded by the *PRNP* gene which is localized on the short arm of chromosome 20. The human *PRNP* gene contains 3 exons within open reading frame (ORF) lying on the last, third exon. This prevents alternative splicing of the mRNA during gene expression (Colby and Prusiner, 2011). The mRNA transcript is around 2.1 – 2.5 kb.

The translated nascent protein contains around 250 amino acids (aa) before all posttranslational modifications (PTM). The N-terminal domain (23 – 124 aa) is flexible and unstructured with octapeptide repeats region with PHGGGWGQ aa pattern that binds monovalent (e.g. Cu^+) or bivalent cations (e.g. Cu^{2+}) binding to histidine residues located at this region. Well-structured C-terminus (125 – 230 aa) contains one disulfide bond between cysteine 179 and 214 residues which stabilized the overall structure of the protein. Moreover, two glycosylation sites can be found on C-terminus at 181 and 197 asparagine residues. The C-terminus is structured with three antiparallel β-sheets and three α-helices (Fig. 1) (Kupfer *et al*., 2009; Legname 2017). After PTM in endoplasmic reticulum, signal peptide (1 – 22 aa) at N-terminus is cleaved and GPI anchor is attached to C-terminus (Baral *et al*., 2019). Additional PTM can include glycosylation of asparagine residues (Asn 181, Asn 197) with N-glycosidic bond leading to different isoforms which can be either glycosylated on both residues, only at one residue or unglycosylated at all. These isoforms can be distinguished on western blot (WB) as a typical three band pattern (Parchi *et al*., 2009).

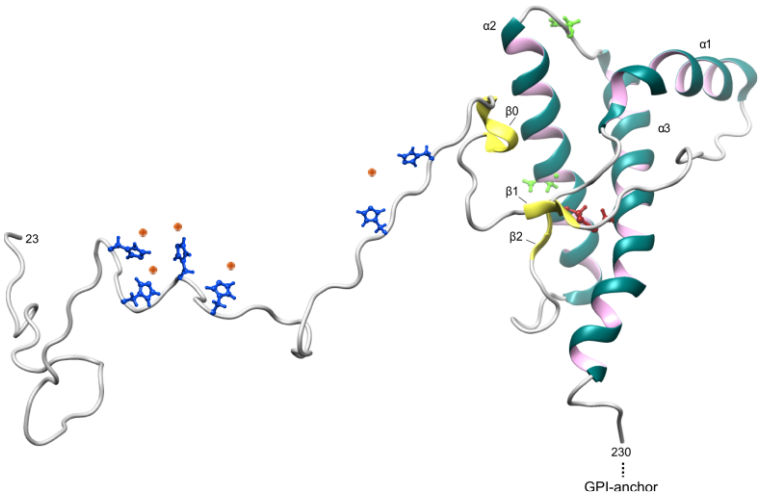

Figure 1. Schematic representation of cellular human prion protein (PrP^C). Unstructured N-terminus (grey) contains an octapeptide repeats region with histidine residues (blue) able to bind monovalent or bivalent cations (orange dots). Well-structured and conserved C-terminus contains three α-helices (green) that are stabilized with single disulfide bond (red) and three β-sheets (yellow) and two asparagine residues (light green) that undergoes glycosylation during posttranslational modifications. The PrP^C is attached to the outer plasma membrane by glycophosphatidylinositol (GPI) anchor on C-terminus. The figure was adopted from Legname 2017.

1.2 Misfolding of PrP^C to its pathogenic form

In the late 1960s, the 'protein-only' hypothesis proposed for the first time that the infectious particle can consist only of misfolded protein without the involvement of DNA or RNA (Alper *et al.,* 1967; Griffith 1967). Since 1990s, the propensity of PrP^C to undergo transition from monomeric structure to its pathogenic, misfolded infectious isoform rich in β-sheets called prion became widely accepted. The infectious prion causing transmissible spongiform encephalopathy (PrP^{TSE}) serves as a template during the conversion of PrP^C and requires direct physical contact with PrP^C. Later, small PrP^{TSE} oligomers are formed which are considered as the most infectious particles that can spread through the cell or organism. Oligomers turn into larger protofibrils. As the final step, long mature amyloid fibrils are formed within the cell that are the hallmarks of the prion diseases (Fig. 2) (Collinge, 2016). Moreover, it was proposed that the misfolding is chaperoned by so called 'protein X' (Telling *et al.,* 1995), but by nature of this protein remains elusive.

The PrP^{TSE} was chemically characterized by its insolubility in detergents and its partially resistant core to digestion with proteinase K (PK). The PK resistant PrP^{TSE} was associated with prion diseases as the only pathogenic form for a long time. Later, the presence of PK sensitive forms of PrP^{TSE} was found to be involved in the prion diseases pathogenesis although these forms remained poorly characterized (Cronier *et al.*, 2008). Therefore, a theory about a cloud of different prion conformers that coexists within one organism and only dominant conformer can propagate to proteinase K resistant fibrils was formed. This theory is supported by the existence of transmission species barrier, where one prion conformer or 'strain' is unable to invade different species (Collinge

2016). Even though PrP^{TSE} infectious particles lack specific DNA sequence, mammalian prions exist as numerous strains, that can be propagated in animals and transfer to a new host without altering the PrP^{TSE} conformation. Different prion strains are causing distinct disease patterns characterized by length of incubation period, clinical symptoms, and neuropathological findings (Morales *et al*., 2007). For example, in humans, polymorphism at codon 129 in the *PRNP* gene affects the strain selection and influences the susceptibility to prion diseases (Mead *et al*., 2003). However, the first high-resolution structures of infectious prion strains (hamster 263K, mouse wild-type and anchorless RML) were solved only recently utilizing cryo-electron microscopy in the laboratory of Dr. Caughey (Kraus *et al*., 2021, Caughey *et al*., 2022) and further studies are needed to better understand the structural diversity of prion strains.

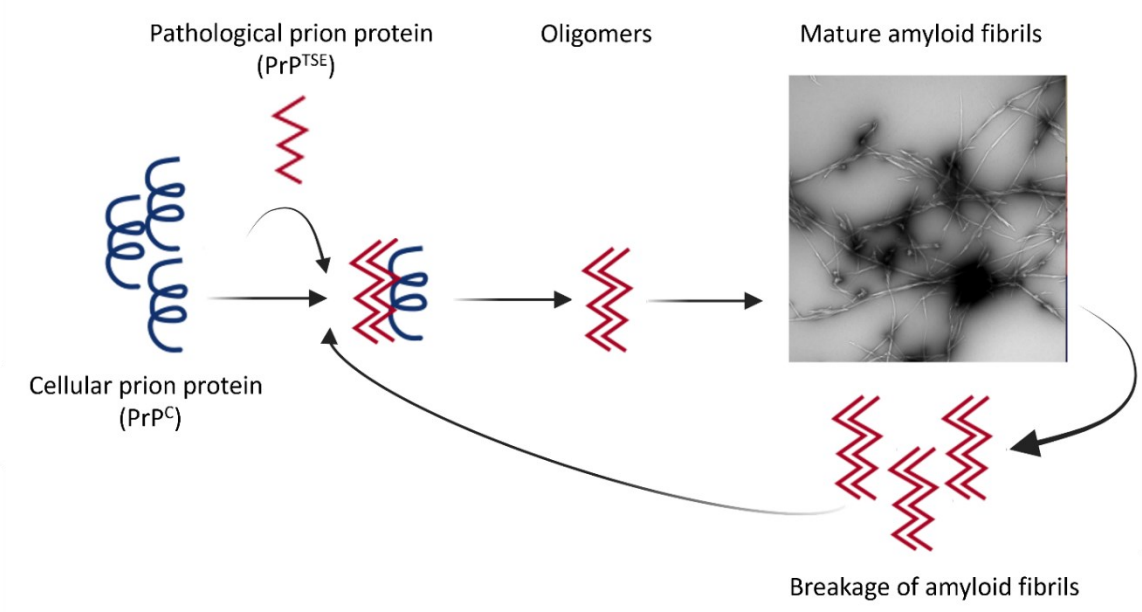

Figure 2. Schematic representation of prion propagation. Pathological prion protein (PrP^{TSE}) physically binds to its cellular monomeric form (PrP^{C}) serving as a template for misfolding. Later, small infectious particles (oligomers) and mature amyloid fibrils are formed. Amyloid fibrils can be disrupted and broken, creating another infectious oligomers that can spread within the cell or tissues.

1.3 Prion diseases

Human prion diseases or transmissible spongiform encephalopathies (TSE) are progressive and fatal neurodegenerative disorders that are caused by the spread of misfolded PrP^{TSE} within central and peripheral nervous system. The annual incidence of prion diseases is around 1 – 2 cases per million inhabitants (Zerr *et al*., 2024).

TSEs are clinically characterized by long incubation period without any visible symptoms and often very short clinical period with rapid cognitive decline leading within few months to death. Neuropathologically, they are characterized by the PrP^{TSE} aggregates presence, spongiform changes, astrogliosis and neuronal loss within the brain (Ironside, Ritchie and Head, 2018). Based on the

etiology, human prion diseases occur in three different forms. The first is sporadic Creutzfeldt-Jakob disease (sCJD) with unknown origin that accounts for 85 – 90% of all human prion diseases. The second, genetic prion diseases account for 10 – 15% of all human TSE cases. The last group with only <1% of all cases is acquired or transmitted form of prion diseases (Bernardi and Bruni, 2019).

1.3.1 Sporadic prion diseases

Sporadic CJD is the most prevalent prion diseases in humans. While the origin or cause of the disease remains unknown, it is assumed that sCJD emerges spontaneously within the organism, either due to somatic mutation or because of *de novo* misfolding of PrPC. sCJD also include variably protease-sensitive prionopathy (VPSPr) which differs from typical sCJD cases by its susceptibility to PK digestion (Gambetti *et al*., 2008, Head et al., 2013).

Classification of sCJD is based on the polymorphism in the *PRNP* gene at codon 129 which can be methionine (M) or valine (V) and on different WB profile after the digestion with PK which causes type 1 or type 2 PrP fragments. While the type one has molecular weight around 21 kDa with the cleavage site at residue 82, type 2 has molecular size around 19 kDa and the cleavage site at residue 97 (Parchi and Saverioni, 2012). Therefore, we recognize six types (MM1, MM2, MV1, MV2, VV1 and VV2) of sCJD. However, based on the clinical representation and neuropathological findings, MM1/MV1, VV1, VV2, MV2, MM2C (cortical) and MM2T (thalamic) phenotypes were proposed (Geschwind, 2015). The most common MM1/MV1, account about 65% of sCJD cases and have almost identical clinical features of the disease. Subtypes VV1, MM2T and MM2C are the least common in the population comparing to the rest (Franceschini *et al*., 2018).

1.3.2 Genetic prion diseases

Genetic prion diseases (gCJD) are conditioned by the presence of mutation in *PRNP* gene with autosomal dominant inheritance and variable penetrance. Most of genetic prion diseases are caused by the missense mutation within the gene, however a number octapeptide repeats insertions/deletions and stop codon mutations have been recognized (Mead *et al*., 2007; Takada *et al*., 2017). To this days, more than 50 genetic mutations associated with prion diseases have been discovered (Zerr *et al*., 2024). Based on the clinical and neuropathological heterogeneity they are historically dived into three groups - genetic form of Creutzfeldt-Jakob disease (gCJD), Gerstmann-Sträussler-Scheinker syndrome (GSS) and Fatal familial insomnia (FFI). Moreover, the phenotype of the diseases is also influenced by the polymorphism at codon 129. For example, mutation D178N (substitution of aspartic acid with asparagine) is associated with both gCJD and FFI phenotype (Kovács *et al*., 2005) depending on co-segregation with M (gCJD) or V (FFI) at codon 129.

The incidence of gCJD and frequency of *PRNP* mutation varies among different countries and varies between Caucasian and East Asia races (Ladogana and Kovacs, 2018). In the Europe, the most common mutations are E200K (substitution of glutamate with lysine) and V210I (substitution of valine with isoleucine). Especially family clusters with E200K mutation have been recognized in Slovakia, Israel, and Italy (Kovacs *et al*., 2011; Minickel *et al*., 2016). In Slovakia this mutation accounts for 65% of all prionopathies cases (Mitrová *et al*., 2011). On the other hand, only 7 people in a 10-year period were detected with rare GSS syndrome associated mostly with P102L (substitution of proline with leucine) mutation in Czech Republic (Tesar *et al*., 2019).

1.3.3 Acquired prion diseases

Acquired prion diseases are caused by exogenous transmission of PrP^{TSE} during the surgery or other invasive procedure (iatrogenic, iCJD) or by consumption of prion infected meal. The first transmission of PrP^{TSE} during the corneal transplantation surgery was detected in 1974 (Duffy *et al*., 1974). Other surgeries like transplantation of dura mater grafts from cadavers or administration of human growth hormone from pituitary gland are recognized as high-risk sources of iCJD (Brown *et al*., 2012). Although, both epidemics peaked in the 1990s, some individuals with a long incubation period are being still diagnosed (NCJDRSU, 2024).

Variant Creutzfeldt-Jakob disease (vCJD) was first reported in 1996 in the United Kingdom it is believed that the disease was transmitted by prion contaminated food. It was proven that vCJD is caused by the same prion strain that causes bovine spongiform encephalopathy (BSE) in cattle (Watson *et al*., 2021). All patients diagnosed with vCJD were homozygotes (MM) in polymorphic codon 129, except MV case (Zerr *et al*., 2024). However, the first human prionopathy proven to be transmissible was endemic disease known as kuru described by Dr. Gajdušek in Papua New Guinea (Gajdusek, Gibbs and Alpers, 1966). Nowadays, it its considered eradicated.

1.4 Alpha-synuclein and its structure

Similarly to prion protein, cellular alpha-synuclein (α-syn) is well conserved intracellular protein mostly expressed in the central nervous system in neocortex, substantia nigra (SN), hippocampus, thalamus, and cerebellum (Emamzadeh 2016). On cellular level, α-syn can be found in synaptic terminals, mitochondria, and other cell organelles. However, the expression of α-syn was also detected in the periphery in muscles, kidney, lung, red blood cells, plasma, or lymphocytes (Hashimoto *et al*., 1997; Askanas et al., 2000; Shin *et al*., 2000; Baltic *et al*., 2004). Still, its function of α-syn is unknown although many functions connected to cells physiology has been assigned to

the protein. Among the most significant functions belong the role in synaptic plasticity, dopamine metabolism, neurotransmitter release, membrane regulation and the last research also highlights its role in immune system (Ferreira and Romero-Ramos, 2018; Balestrino and Schapira, 2020; Grozdanov and Danzer, 2020).

In humans, the α-syn is encoded by the *SNCA* gene localized on the long arm of chromosome 4 containing 114 kb. *SNCA* gene is composed of six exons, with open reading frame (ORF) in the last five exons (Xu *et al.,* 2015). Because of this, at least three different isoforms due to alternative splicing occurs during the transcription of the gene. The first isoform αsyn-126 lacks exon 3, the second αsyn-112 lacks exon 5 and the last and the shortest isoform, αsyn-98 lacks exon 3 and 5 (Beyer *et al.,* 2008; Röntgen *et al*., 2024). Although, it is not clear if all mRNA isoforms are translated. For now, only α-syn112 isoform was detected in blood or brain tissue of individuals with synucleinopathy (Toby *et al*., 2017; Fuchler *et al*., 2021).

Mature cellular α-syn with 140 aa is intrinsically disordered protein, and its monomeric form is characterized by three main domains. The first domain at N-terminus (1 – 60 aa) contains four repeats with the KTKGEV motif, which allows to form two α-helices binding negatively charged lipids. The second domain consist of non-amyloid-β component (NAC, 61 – 95 aa). The NAC is able to form hydrophobic core of α-syn fibrils which drives aggregation of the protein (Jha *et al*., 2018; Stephens *et al*., 2019). The last negatively charged domain (94 – 140 aa) at C-terminus binds positively charged ions (e.g. Ca^{2+}), small molecules or membranes (Binolfi *et al*., 2006). The α-syn undergoes PTMs mostly within its C-terminus like phosphorylation, ubiquitination, glycation, or glycosylation. This changes lead to alternations in protein charge, influencing binding of metal ions, lipids, and other proteins (Gonzáles *et al*., 2019). Especially, phosphorylation at S129 (pS129) has been shown to play a key role in the pathology of α-syn. Under normal conditions, only 4% of α-syn is constitutively phosphorylated, whereas in the synucleinopathy brain it is 90% (Fujiwara *et al*., 2002; Oueslati *et al*. 2016).

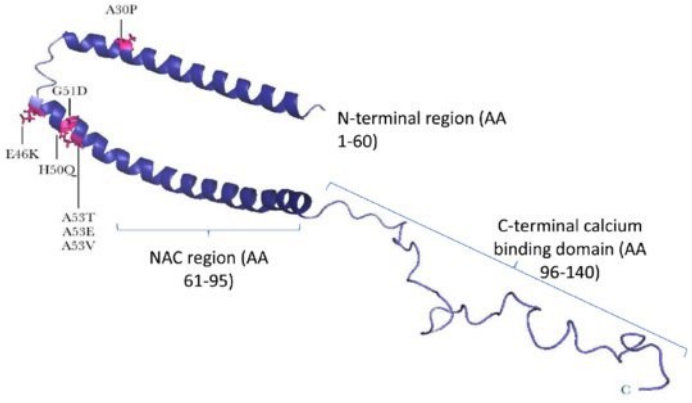

Figure 3. The schema of cellular alpha-synuclein (α-syn). The protein consists of three main domains. Positively charged N-terminus contains two α-helices. The second domain, known as non-amyloid-β (NAC) component contains four repeats

with the KTKGEV motif. The last negatively charged third domain is at C-terminus with a binding site for positively charged ions. Point mutations leading to synucleinopathies are marked with pink.
The figure was adopted from Whittaker *et al*., (2017).

1.5 'Prion-like' misfolding of α-synuclein

Hypothesis of 'prion-like' misfolding of α-syn was recently supported by emerging evidence from different studies observing the spread of pathological alpha-synuclein (α-syn^{D}) between cells (Luk *et al*., 2009; Luk *et al*., 2012; Elfarrash *et al*., 2019). However earlier, Braak with colleagues already observed and described different stages of α-syn^{D} propagation from the brain stem to other areas in the brain connecting them with clinical symptoms and pathology of patients (Fig. 4) (Braak *et al*., 2003). Later, the most significant spread of α-syn^{D} aggregates supporting 'prion-like' hypothesis was described from the host to the graft from fetal mesencephalic progenitor neurons (Li *et al*., 2008).

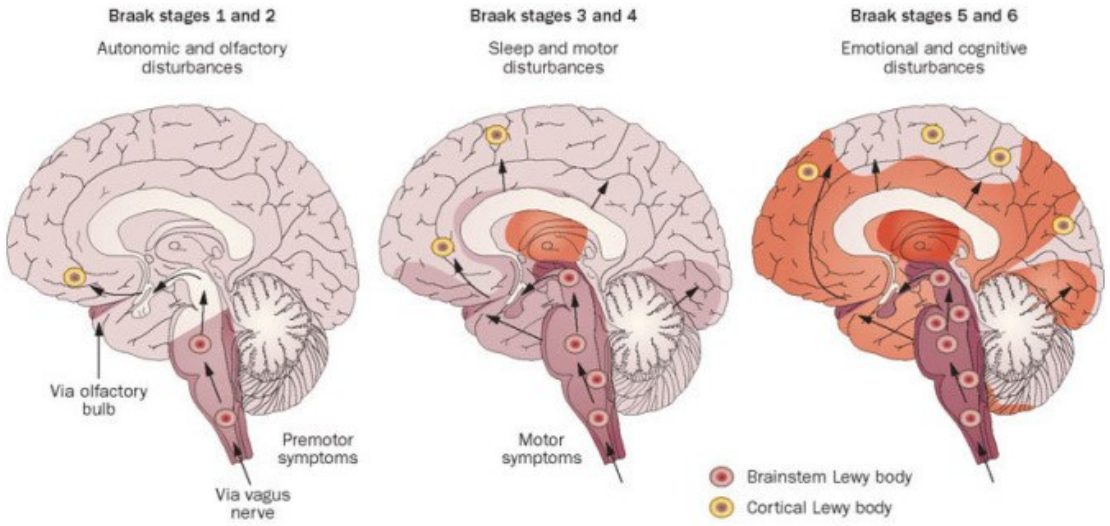

Figure 4. Schematic representation of Braak staging system for synucleinopathies. Spread of Lewy bodies from brain stem and the olfactory system to substantia nigra and later to mesocortex and allocortex. Every stage is characterized by clinical symptoms from mild premotor symptoms in early stages to more severe motor and cognitive symptoms in the final stages of disease.
The figure was adopted from Ramesh and Arachchige, 2023

Misfolding of the protein is described by the same process as it was described for prions. During the lag phase monomeric proteins physically bind to a pathologically folded protein, creating aggregation center. During the elongation stage, newly formed oligomers spread and turn into mature amyloid fibrils with typical cross β-sheet architecture. In the last, stationary phase the lack of monomeric α-syn leads to decreasing the growth rate (Villar-Piqué *et al*., 2016). Similarly to PrP^{TSE}, misfolded α-syn^{D} is rich in β-sheets forming long amyloid fibrils not only in the neurons but also in neighboring astroglial cells. Aggregation of α-syn^{D} was connected not only to many

environment conditions such as acidic pH, increased temperature, molecular crowding, or the presence of pesticides (Uversky *et al*., 2001; Uversky *et al*., 2001; Shtilerman *et al*., 2002) but also to genetic mutations in the *SNCA* gene (Fig. 3). Moreover, the influence of carboxy terminal truncation on aggregation has been described recently (Hass *et al*., 2021).

Different morphotypes of α-syn^{D} fibrils isolated from patients were resolved by cryo-EM underlying the similarities with prion protein strains. These structural studies discovered differences between classical Parkinson disease (PD) fibrils that consist only of one protofilament and multiple system atrophy (MSA) fibrils that consist of two protofilaments (Schweighauser *et al*., 2020; Yang *et al*., 2022). Moreover, it was shown that these two morphotypes differ in the localization of salt bridges that stabilize their structure (Holec *et al*., 2022).

1.6 Synucleinopathies

Synucleinopathies, just like prion diseases, are progressive and fatal neurodegenerative diseases with long incubation period and heterogenous clinical symptoms. The first group, primary synucleinopathies, are characterized by the aggregation of α-syn^{D} either within the cell known as Lewy bodies or Lewy neurites in Parkinson disease (PD), Parkinson disease with dementia (PDD), Dementia with Lewy bodies (DLB), and pure autonomic failure (PAF) or as a cytoplasmic inclusion in oligodendrocytes known as Papp-Lantos bodies in multiple system atrophy (MSA) (Coon and Singer, 2020). However, α-syn^{D} aggregates are commonly observed also in patients with other primary neurodegenerations such as Alzheimer disease (AD), frontotemporal dementia (FTLD), corticobasal degeneration (CBD) or prionopathies as secondary comorbidity synucleinopathy (Visanji *et al*., 2019). Highest frequency of concomitant Lewy pathology was reportedly observed in around 40% cases of AD (Rahim and Kovacs, 2014). On the other hand, in CJD it is only 9 – 23%, depending on the study (Vital *et al*., 2009; Grau-Rivera *et al*., 2015).

Parkinson disease is the second most common neurodegeneration after AD with estimated annual incidence of 11 – 19 cases per 100 000 inhabitants. However, in elderly people, above 60 years this incidence increases rapidly (Lindgren *et al*., 2005). It is characterized by the loss of dopaminergic neurons in substantia nigra pars compacta. The origin of the disease is not known, although genetic mutation has been accounted for 5 – 10% of PD cases (Balestrino and Schapira, 2020). On the other hand, the second most common dementia, Dementia with Lewy bodies has annual incidence of 3.5 cases per 100 000 people (Coo and Singer, 2020). DLB is often associated with concomitant AD where it can be manifested as a rare Lewy pathology observed only in amygdala resulting in AD with Amygdala Lewy bodies (ALB) comorbidity (Uchikado *et al*., 2006). It was shown that the majority of α-syn^{D} in amygdala is truncated at C-terminus resulting in large Lewy

body inclusion. Sorrentino suggested that a new more sequenced and less pathogenic α-syn^{D} strain can be present in amygdala (Sorrentino *et al*., 2019).

1.7 Seeding amplification assays

Early and reliable *ante-mortem* diagnosis of neurodegenerative diseases is crucial not only for patients and their families in order to not misdiagnose treatable diseases, but also for the management of prevention of secondary transmission, especially in prion diseases. However, a*nte-mortem* diagnosis of neurodegenerative diseases often relies predominantly on the evaluation of clinical symptoms such as rapid progressive dementia, cognitive decline, myoclonus, and ataxia in CJD (Green, 2016) and tremor, bradykinesia, rigidity, loss of movement or cognitive decline in synucleinopathies (Grinberg *et al.*, 2010). Clinical findings are often supported by familial history, and evaluation of protein levels such as 14-3-3, *p*-tau and *t*-tau in cerebrospinal fluid (CSF), magnetic resonance imagining (MRI), and electroencephalogram (EEG) (Chatzikonstantinou *et al*., 2021). However, the concerns about the sensitivity and specificity of these tests arise naturally as symptoms are overlapping with other neurodegenerations and the levels of proteins in CSF is low in the preclinical and early stages of the disease (Chohan *et al*., 2010; Panigaj *et al*., 2011). Moreover, the assignment of probable *ante-mortem* diagnosis depends largely on the experience of examining clinical doctor. Therefore, only probable diagnosis can be made during patient´s lifetime. The gold standard for definite diagnosis remains direct detection of aggregated PrP^{TSE} or α-syn^{D} in brain by immunohistochemistry during the autopsy (Fiorini *et al.*, 2020). For CJD, autopsy findings are complemented with WB analysis of PK resistant PrP^{TSE} in brain.

In the last decade, new ultra-sensitive methods exploiting the seeding prion-like ability of misfolded proteins emerged as a new diagnostic tool to improve *ante-mortem* diagnosis. Collectively named as seeding amplification assays (SAAs) these assays include protein misfolding cyclic amplification (PMCA) (Soto, Saborio and Anderes, 2002) and Real-Time Quaking-Induced Conversion (RT-QuIC) assay (Atarashi *et al*., 2007; Wilham *et al*., 2010).

1.7.1 Protein misfolding cyclic amplification

PMCA was first established in the laboratory of Dr. Claudio Soto in 2002 using normal brain homogenates or cell extracts as a source of PrP^{C} in the reaction mix (Yokoyama *et al*., 2011). The reaction was successfully seeded with various tissues like brain, spleen (Rubenstein and Chang, 2013) or with fluids such as urine (Moda *et al*., 2014), or blood as a source of PrP^{TSE} (Bougard *et al*., 2016). The PMCA assay utilizes cycles of sonication to increase the number of PrP^{TSE} seed by

breaking the fibrils. The final amplified product is analyzed, after digestion with PK, by WB. After the optimization, the assay was able to detect as low as 1 ag of PrP^{TSE} in the brain tissue (Rubenstein and Chang, 2013). However, the biggest limitation of PMCA is its poor reproducibility and the infectivity of final product, as the structure or the strain of the prion seed is preserved during the amplification (Weber *et al*., 2007; Castilla *et al*., 2008).

1.7.2 Real-Time Quaking-Induced Conversion

RT-QuIC assay, developed by the laboratory of Dr. Byron Caughey, utilize recombinant prion protein (rPrP) as a source of monomeric PrP substrate instead of brain tissue PrP^{C} as in PMCA (Atarashi *et al*., 2007). The reaction mix containing fluorescent dye Thioflavin T (ThT) and rPrP is typically seeded with patient's samples such as brain homogenate, CSF, skin, or olfactory mucosa swab in quadruplicates using 96-well plate (Bongianni *et al*., 2017; Moško *et al*., 2021; Baranová *et al*., 2024). The samples undergo cycles of intermitting shaking, which breaks newly formed fibrils and incubation period during which amyloid aggregates can grow. During the reaction, ThT binds to the formed aggregates and the increase of the fluorescence is detected in real time using fluorescence reader (Fig. 5).

One of the most critical components in the assay is the rPrP used as a reaction substrate which should be stable enough to not aggregate spontaneously during run of the assay. In the first generation of RT-QuIC assay, full-length rPrP from hamster (rHAPrP23-231) was used as a substrate, however, the reaction time was longer and the sensitivity lower (Peden *et al*., 2012). To increase the sensitivity and improve the overall outcome of the reaction many optimization steps such as increase of temperature or inclusion of small amount of sodium dodecyl sulfate (SDS) were included in the development (Orrú and Caughey, 2011). However, the best results with the detection limit of ~1 fg (10-15 g) of PrP^{TSE} were achieved by the second-generation RT-QuIC assay utilizing shortened rHAPrP90-231 and higher temperature (Orrú *et al*., 2015). Improved RT-QuIC assay was shown to provide rapid and ultra-sensitive tool for highly sensitive (82 – 97%) and specific (99 – 100%) diagnosis of prion diseases (Lattanzio *et al*., 2017, Orrú *et al*., 2020).

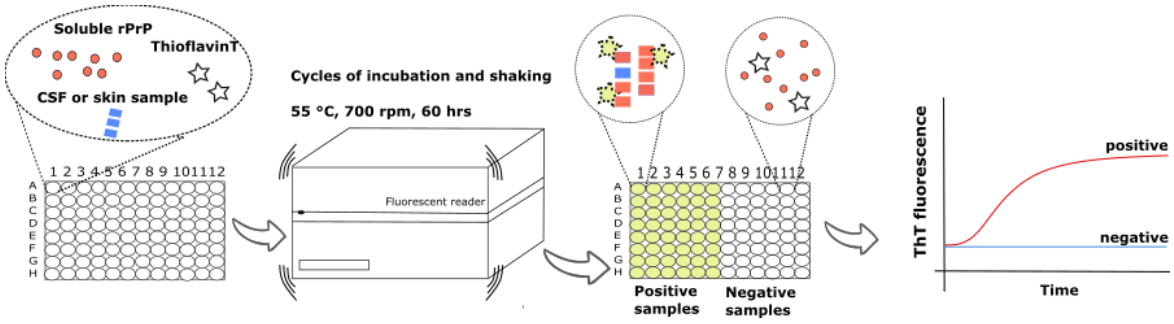

Figure 5. Overview of Real-Time Quacking-Induced Conversion (RT-QuIC) assay. The reaction mix containing patients' sample, soluble recombinant prion protein (rPrP) and fluorescent dye Thioflavin T (ThT) is added into 96-well plate in quadruplicates. The samples undergo cycles of double-orbital shaking (1 min, 700 rpm) and incubation period (1 min) during 48 or 60 hrs. If PrP^{TSE} is present in the sample, it will aggregate monomeric rPrP into amyloid fibrils which have high affinity to ThT. The amyloid formation is detected in real-time and observed as the fluorescence increase.

Recently, RT-QuIC for prion diseases was adapted for other neurodegenerative diseases, including synucleinopathies. The assay utilizes monomeric recombinant alpha-synuclein (rα-Syn) either wild-type (WT) or K23Q mutant as a substrate for *in vitro* conversion. Mutation (K23Q) within rα-syn. should lower the rate of spontaneous aggregation in the assay (Koo *et al*., 2008). However, in contrast with prion RT-QuIC assay, the conversion of α-syn is usually promoted by the addition of mixing beads (silica, glass, or zinc) into the reaction mix. For the first time, Fairfoul *et al*., (2016) utilized 'prion-like' seeding activity to detect $\alpha\text{-syn}^{D}$ in brain and CSF from patients with PD and DLB with 95% sensitivity and 92 – 100% specificity. Later, many adaptations of the assay emerged in diagnosis of synucleinopathies with reported high sensitivity and specificity. The presence of $\alpha\text{-syn}^{D}$ seeding activity was confirmed not only in various types of symptomatic patient samples including CSF, skin (Donadio *et al*., 2021) and olfactory mucosa (Kuzkina *et al*., 2022) but also in prodromal stages of DLB and PD (Zerr *et al*., 2021; Iranzo *et al*., 2021). Despite the number of reported successful studies, the $\alpha\text{-syn}^{D}$ RT-QuIC assay remains much less developed than its prion version and more studies are needed to better understand its real diagnostic potential.

2 Aims

Early and sensitive detection of misfolded proteins is crucial for the prognosis and the treatment management of neurodegenerative diseases. However, *intra-vitam* diagnosis is still challenging as many neurodegenerations overlap symptoms, particularly at clinical onset, leading to misdiagnosis. For that reason, direct pathological examination of amyloid aggregates in brain remains the gold standard for definite diagnosis. Ultra-sensitive Real-Time Quaking-Induced Conversion (RT-QuIC) assay exploits the ability of misfolded proteins (prion, α-synuclein) in patient's samples to convert soluble monomeric substrate into amyloid fibrils which are detected by fluorescent dye Thioflavin T.

Therefore, our main aim was to validate the diagnostics potential of RT-QuIC assay analyzing different patient's samples with definite diagnosis of prionopathy or synucleinopathy in our laboratory.

Our partial aims were:

1. Purification of recombinant rHAPrP90-231 and rBVPrP (full-length) for prion RT-QuIC and rα-Syn (WT) for α-syn RT-QuIC assay.
2. Validation of prion RT-QuIC utilizing corresponding *post-mortem* cerebrospinal fluid (CSF), skin, and archive formalin-fixed paraffin-embedded brain samples.
3. Assessment of the RT-QuIC sensitivity with skin samples and usefulness of the assay during the asymptomatic stage utilizing mouse model.
4. Validation of prion RT-QuIC in patients with a rare genetic form of prion disease.
5. Validation of α-syn RT-QuIC in *post-mortem* brain and CSF samples.

3 Materials and Methods

3.1 Purification of recombinant proteins for RT-QuIC assay

3.1.1 Preparation of recombinant prion protein (rPrP)

For RT-QuIC analysis, recombinant short Syrian hamster prion protein (rHAPrP90-231) and full-length recombinant Bank vole prion protein (rBVPrP) were used as a substrate. Expression plasmids (pET41) were kindly provided to our laboratory by Professor Jiří Šafář (Departments of Pathology and Neurology at Case Western Reserve University, OH, USA). Protein was expressed in *E. coli* (Rosetta™,(DE3)), Novagen, Merck KGaA, Germany) under inducible T7 promotor. Protein was purified according to published protocol by Foutz *et al*. (2017).

Four cultivation, tubes with 2 ml of LB Broth (Luria/Miller) medium were inoculated with a bacterial glycerol stock culture and incubated at 300 rpm, 5-6 hrs, 37°C. 1 L of LB medium, supplemented with 50 µg/ml of kanamycin (Fisher Scientific), 34 µg/ml of chloramphenicol (Sigma-Aldrich), and Overnight Express™ Autoinduction System 1 (Novagen, Merck, KGaA, Germany) was split into four Erlenmeyer flask. Every flask was inoculated with one prepared mini culture and incubated overnight at 300 rpm, 37°C.

Next day, the cells were pelleted by centrifugation at 3 500 x g, 20 min, 4°C into four 50 ml centrifuge tubes (TPP). The centrifugation was repeated until the whole culture was harvested. Supernatant was discarded, and bacterial mass was weighted.

Next, the pellets were lysed using 0.1x BugBuster master mix (BBMM) (Merck Millipore) prepared from 1x stock solution. 12 ml of 0.1x BBMM was added into each tube and cells were resuspended with tissue homogenizer (Benchmark Scientific, NJ, USA) and incubated for 20 min at RT on a rotating mixer (Biosan, Latvia). Subsequently, the suspension was centrifugated at 13 000 x g, 20 min, 4°C and supernatant was discarded. Pellets were resuspended in 1x BBMM with tissue homogenizer and suspension was again incubated 15 min at RT on rotating mixer. The volume was then adjusted up to 40 ml by 0.1x BBMM, mixed by inversion and centrifuged at 7 900 x g, 15 min, 4°C. Again, supernatant was discarded, and pellet resuspended in 40 ml of 0.1 BBMM using tissue homogenizer. Suspension was centrifuged at 13 000 x g, 15 min, 4°C, supernatant was discarded, and pelleted inclusion bodies were frozen at -20°C until the next day.

The washed inclusion bodies were thawed at RT and 10.5 ml of 8 M guanidine hydrochloride (GndHCl) was added to every tube. Pellets were resuspended using tissue homogenizer and suspensions were poured together, so at the end only 3 tubes remained which were incubated 50 min at RT on a rotating mixer. During the incubation, Ni-NTA Fast Flow resin beads (NiSepharose® 6

Fast Flow, Cytiva, Merck, KGaA, Germany) were washed with 100 ml of mQH_2O and 18 g of beads were added to each of three new 50 ml centrifuge tubes with 5 ml of denaturing buffer (100 mM phosphate buffer (PB), pH 8.0; 10 mM trisaminomethane (Tris), 6 M GndHCl). Volume was adjusted to 30 ml and Ni-NTA beads were equilibrated for 50 min on rotating mixer. Solutions of dissolved inclusion bodies were centrifuged at 13 000 x g, 5 min, 4°C and supernatants were transferred to the tubes with Ni-NTA beads and incubated 40 min on rotating mixer. After, the Ni-NTA beads with bound protein were loaded onto the 100 ml column (GE Healthcare XK chromatography columns, KGaA, Germany).

Protein was purified using a BioLogic LP Low-Pressure Liquid Chromatography System (BioRad, Czech Republic). First, column was washed with denaturing buffer at flow rate 2.3 ml, 30 min. Protein refolding step was carried out on the column by slowly replacing denaturation condition with physiological using linear gradient of refolding buffer (100 mM PB, pH 8.0; 10 mM Tris) at flow rate 2.3 ml/min during 240 min. The protein was eluted by linear gradient of 0 – 500 mM imidazole in elution buffer (100 mM PB, pH 8.0; 10 mM Tris) at flow rate 6 ml/min, 50 min. The protein was collected into 50 ml tube with 10 ml of dialysis buffer (10 mM PB, pH 5.8) on ice after absorbance at 280 reached 0.2 AU.

Purified protein was filtered through 0.22 µm syringe filter and dialyzed overnight at 4°C against 4 L of dialysis buffer using 10K MWCO SnakeSkin^{TM} Dialysis Tubing (Thermo Fischer Scientific, Czech Republic). The next day, protein was transferred to beaker with a fresh dialysis buffer for 3 hours at 4°C. After 3 hours, this step was repeated. At the end, protein was filtered through 0.22 µm syringe filter into a new tube kept on ice.

Absorbance of the protein was measured three times using UV cuvette (Brand GmbH+CO, Germany) with an optical length of 10 mm at 280 nm using spectrometer (Eppendorf BioSpectrometer® kinetic, Germany). Concentration was determined by dividing an average absorbance, from three read-outs, with theoretical extinction coefficient of 1.4 $mg/ml^{-1}cm^{-1}$ for rHaPrP90-231 and 2.7 $mg/ml^{-1}cm^{-1}$ for rBVPrP. Protein was aliquoted into 2 ml tubes with a screw cap and stored at -80°C.

The purity and quality of every batch of purified rPrP was analyzed by Coomassie blue staining on 15% polyacrylamide gel and by the quality control assay using Real-Time Quaking-Induced Conversion assay.

3.1.2 Preparation of recombinant α-synuclein (rα-Syn)

For the analysis of the seeding activity of pathological α-synuclein (α-syn^{D}) recombinant α-synuclein wild-type (rα-Syn WT) with 6x His-Tag on N-terminal was used as a substrate. Expression

plasmids (pET24) were generous gift to our laboratory by Dr. Byron Caughey (National Institute of Allergy and Infectious Diseases, MT, USA). Protein was expressed in *E.coli* BL21 (DE3) (Sigma-Aldrich, MO, USA) under inducible T7 promotor. Protein was purified according to Groveman *et al*., 2018 with some modifications.

The protein was expressed in bacteria the same was as described previously for prion protein, using Overnight Express™ Autoinduction System I in the presence of 50 µg/ml of kanamycin. After harvesting bacterial cells next day, the pellets were gently resuspended in 25 ml of osmotic shock buffer (30 mM Tris-HCl, pH 7.2; 40% saccharose) using serological pipette and incubated 15 min on rotating mixer. Suspensions were then centrifuged at 9 000 x g, 20 min, 20°C and the pellets were quickly resuspended on the ice again this time in 25 ml of ice-cold mQH_2O. The suspensions were pooled together to final volume of 50 ml. 50 µl of saturated $MgCl_2$ were added into every tube followed by incubation on a tube rocker for 3 min. Subsequently, suspensions were centrifuged at 9 000 x g, 30 min, 4°C and the supernatant was transferred into a new clean glass beaker. The pH was reduced to 3.5 by adding approx. 700 – 1 000 µl of 1 M HCl while continuously stirring the lysate without introducing bubbles and monitoring pH using pH indicator strips. Lysate was then incubated another 10 min at RT while gently stirring. After, the lysate was centrifuged for the last time at 9 000 x g, 30 min, 4°C and the supernatant was collected into a new glass beaker. The pH was adjusted to 7.5 by adding approx. 700 – 1 000 µl of 1 M NaOH while stirring. Finally, the bacterial lysate was filtered through 0.45 µm syringe filter before loading onto a column.

In the first step, the protein was purified using nickel affinity chromatography using NGC Chromatography System (BioRad, Czech Republic). Bacterial lysate was loaded onto 5 ml HisTrap™ FastFlow (Cytiva, WA, USA) nickel column and washed with washing buffer (20 mM Tris-HCl, pH 7.5) at flow rate 5 ml/min for 15 min. The loosely bound proteins were washed out with buffer composed of 50 mM imidazole in 20 mM Tris-HCl, pH 7.5 at the same flow rate until the peak containing contaminants was eluted. At final step, the protein was eluted using linear gradient of 50 – 500 mM imidazole in 20 mM Tris-HCl, pH 7.5 at flow rate 5 ml/min and the peak containing rα-Syn (WT) was collected. In the second step, the protein was purified and concentrated on 5 ml HiTrap® Q HP by anion exchange chromatography. The protein was loaded onto the column at flow rate 4 ml/min and equilibrated with washing buffer at 5 ml/min for 5 min and further washed with buffer containing 20 mM Tris-HCl, pH 7.5 / 100 mM NaCl. The rα-Syn (WT) was then eluted in linear gradient of 100 mM – 500 mM NaCl and the generated peak was collected.

The purified protein was filtered through 0.22 µm syringe filter and dialyzed overnight at 4°C against 5 L of mQH_2O or 40 mM phosphate buffer, pH 8.0 using 3.5K MWCO SnakeSkin™ Dialysis Tubing. The next day, protein was transferred into a new buffer and dialyzed at 4°C for 4 hours.

Absorbance was measured at 280 nm and the concentration was determined using theoretical extinction coefficient of 0.36 $mg/ml^{-1}cm^{-1}$. Protein was aliquoted and stored at -80°C.

The quality of the protein was determined by Coomassie blue staining on 15% polyacrylamide gel and by the quality control assay using RT-QuIC.

3.2 Determination of RT-QuIC ability to detect prions before the occurrence of the disease symptoms – Animal study

To determine the sensitivity of RT-QuIC assay using "*in vivo*" model, we have decided to follow the course of the disease using the mouse model. The animal experiment was approved by The Ministry of Education, Youth and Sports of Czech Republic (approval number 70030/2013-MZE-17214 granted 26.11.2018) and performed following Czech and European Union Legislation. 80 healthy female mice (*Mus musculus*, CD-1, 16 – 18 g) where purchased from Charles River Laboratories (MA, USA). The mice were acclimatized for 14 days in the infectious laboratory before the start of the experimental study. During the whole experiment, mice were controlled daily and weighted once a week.

3.2.1 Mice experiment

Animals were divided into two groups according to the site of inoculation. Within the first group, 18 mice were inoculated intracerebrally (i.c.) with 30 µl of 0.1% brain homogenate with RML prion strain adapted to mice and 17 mice were inoculated intracerebrally with phosphate buffered saline (PBS), pH 7.4 as controls. In the second group, 27 mice were inoculated subcutaneously (s.c.) with 500 µl of 0.2% brain homogenate with RML prion strain and 18 mice were subcutaneously inoculated with PBS, pH 7.4 as controls. Inoculum was prepared from brain homogenate of terminally ill mouse inoculated with RML prions. Before the inoculation, the mice were anesthetized with sevoflurane. During the whole inoculation process animals were closely observed and did not show any signs of pain or discomfort. The mice were divided into cages according to the inoculation route. In every cage, three mice inoculated with RML prions, and two control mice inoculated with PBS were housed together. Five control mice inoculated intracerebrally with PBS were placed in one additional cage.

One cage of animals (n=5) from the first group subjected to intracerebral inoculation was sacrificed every 28 days while those from the second groups with subcutaneous inoculation were initially sacrificed every 42 days, later every 28 days. However, any mouse showing symptoms of terminal neurodegeneration was sacrificed immediately. At autopsy, ten organs from each mouse,

specifically blood, skin from the head apex, both ears, tail, liver, spleen, both kidneys, and brain were harvested and weighted. Skin from the head apex, ear lobes and tail were harvested before opening the skull using sterile instruments to avoid cross-contamination. All organs were frozen and stored at -80°C until further analysis.

3.2.2 Preparation of 10% brain homogenates

Brains from mice were thawed on ice and half of the brain was weighted in a new tube. First, 1 ml of buffer containing PBS, pH 7.4; 2 mM ethylenediamine tetraacetic acid (EDTA) and 1 mM phenylmethylsulfonyl fluoride (PMSF) was added to the brain. 10% brain homogenates (BH) were prepared by 3 x 30 s homogenization cycles using ~1ml of 1.0 mm glass beads (BioSpec Products, OK, USA) in Mini-BeadBeater-8 (BioSpec Products, OK, USA). At the end, the remaining calculated volume of the buffer was added into every tube to prepare exactly 10% BHs. Samples were frozen and stored at -80°C.

3.2.3 Detection of PrP^{Sc} by SDS-PAGE and Western blot

Mice BHs were lysed by 0.5% sodium deoxycholate with 0.5% triton X-100. One half of the sample was digested with 50 µg/ml PK (Merck KGaA, Germany) for 30 min at 37°C. Digestion was terminated by addition of 2 mM PMSF into the sample. The other half of the sample was analyzed untreated. The samples were denaturated in 1x sample buffer (125 mM Tris, pH 6.8; 2% SDS; 20% glycerol and 0.01% bromophenol blue) for 5 min at 95°C before loading onto a gel.

Proteins were separated based on their molecular weight by SDS-PAGE (105 V, 90 min) in 12% or 15% polyacrylamide gel buffered in running buffer (0.025 M Tris base, 0.192 M glycine and 0.1% SDS). After that, the separated proteins in gel were transferred to a 0.2 µm nitrocellulose membrane (Bio-Rad Laboratories, CA, USA) by WB (200 mA, 120 min) buffered in transfer buffer (0.025 M Tris base, 0.192 M glycine and 1% methanol).

The, membrane was washed in tris buffered saline (TBS) supplemented with tween 20 (TBS-T; 20 mM Tris, 150 mM NaCl, pH 7.5, 0.05% Tween 20) followed by 30 min blocking by 5% (w/v) non-fat dry milk in TBS-T. Proteins were immunodetected by incubation with mix of mouse monoclonal primary antibodies AH6 (TSE Resource Center, UK) and 6D11 (BioLegend, CA, USA) diluted in 1% (w/v) non-fat dry milk in TBS-T for 2 hrs at RT. After washing, the membrane was incubated for 1 hr at RT with mice polyclonal secondary antibody conjugated with alkaline phosphatase (F(ab)´2donkey anti-mouse IgG (H+L); Jackson ImmunoResearch, PA, USA) which was diluted 1:2,000 in 1% (w/v) milk in TBS-T. Unbound antibodies were washed by TBS. Alkaline phosphatase was developed using chromogenic substrate 5-bromo-4-chloro-3-indolylphosphate

toluidine salt/nitro-blue tetrazolium chloride (BCIP/NBT, Merck Millipore, MA, USA). Membrane was digitalized using scanner (CanonScan LiDE 220, Canon, Tokio, Japan).

3.3 Determination of total protein concentration in CSF and skin samples

The concentration of proteins in samples was determined using commercial kit Pierce™ BCA Protein Assay (Thermo Scientific, Prague, Czech Republic). The assay is based on reduction of Cu^{2+} to Cu^{1+} by protein peptide bonds in alkaline medium. Subsequently, Cu^{1+} ions are detected by colorimetric reaction with bicinchoninic acid (BCA).

For the reaction, 25 µl of sample was added into 200 µl of BCA solution, mixed and incubated in the dark at 37°C, 30 min. The absorbance was measured at 562 nm using spectrofluorometer (Perkin Elmer 1420 Victor3 (model 1420-012), MA, USA). Serially diluted bovine serum albumin (fraction V, Carl Roth GmbH, Germany) was used to create calibration curve for determination of the concentration of total protein in sample.

3.4 Preparation of samples for RT-QuIC analysis

All *post-mortem* samples were obtained at autopsy and provided to our laboratory by National Reference Laboratory (NRL) for Human Prion Diseases (Thomayer University Hospital, Prague, Czech Republic). The study was approved by ethical committee of the Institute for Clinical and Experimental Medicine and Thomayer University Hospital in Prague (G-16-06-39).

3.4.1 Brain homogenates

10% BH were all prepared in the NRL for Human Prion Diseases by their standardized protocol. Before the RT-QuIC analyses, aliquots were thawed and serially diluted according to protocol.

For the prion RT-QuIC, samples were tested in end-point dilution $5x10^{-6}$ – $5x10^{-12}$ in a dilution buffer (PBS, pH 7.4; 1x N-2 supplement (Gibco) and 0.1% SDS). For the α-syn RT-QuIC, BH samples were tested in end-point dilution 10^{-2} – 10^{-8} diluted both in a buffer containing PBS, pH 7.4; 1x N-2 supplement and 0.025% SDS or only in PBS, pH 7.4.

3.4.2 Cerebrospinal fluid

Cerebrospinal fluid (CSF) was carefully drawn out from a lateral ventricle avoiding cross-contamination using a sterile needle and immediately frozen at -80°C.

The CSF samples were thawed and centrifuged at 2 000 x g, 2 min, RT (MiniSpin Plus, Eppendorf, Germany) before seeding the reaction. CSF was tested both undiluted and 10x diluted in PBS, pH 7.4 for both prion and α-syn RT-QuIC.

3.4.3 Skin

Skin was taken from the area behind the ear using a sterile scalpel before opening a skull to prevent cross-contamination and frozen at -80°C until further analysis. 10% skin homogenates were prepared fresh at the day of the analysis by previously published protocol (Orrú *et al*., 2017).

Skin was thawed at RT and cut into a small piece about 30 – 60 mg containing all three layers. Samples were then 3x washed with ice-cold PBS, pH 7.4. Skin 10% homogenate was prepared by tissue lysis with a buffer containing 0.25% collagenase (Roche, Basilea, Switzerland), TBS, pH 7.4, and 2 mM $CaCl_2$ over 4 hrs at 37°C, 300 rpm using thermomixer (Eppendorf, Germany). Subsequently, the samples were sonicated (30% amplitude, 20 kHz, Cup Horn probe, CPX750 sonicator, Cole-Parmer, Ilm USA) for 30 s and centrifuged at 500 x g, 7 min, RT. The supernatant was transferred into a new 1.5 ml tube and centrifuged again at 2 000 x g, 2 min, RT before 10x or 100x diluted in a buffer containing PBS, pH 7.4; 1x N-2 supplement and 0.1% SDS.

3.4.4 Formalin-fixed paraffin-embedded brain tissue

Formalin-fixed paraffin embedded (FFPE) brain samples (n=30) were prepared for RT-QuIC according to previously published method (Hoover *et al*., 2016). Ten 4 µm thick paraffine-embedded tissue wax curls were obtained from National Reference Laboratory (NRL) for Human Prion Diseases (Thomayer hospital, Prague, Czech Republic) from the same patients as CSF/skin samples. To remove paraffin, wax curls were firstly washed in 500 µl xylene. After, the tissue was rehydrated with graded ethanol washes (100%, 95% and 70%) and then washed with PBS, pH 7.4. After every wash, samples were centrifugated at 13 000 x g, 7 min, RT. Rehydrated tissue was dried out, weighted and 10% homogenates (w/v) in PBS, pH 7.4 were prepared using 60 s sonication. Samples were diluted in buffer containing PBS, pH 7.4, 1x N-2 supplement (Gibco) and 0.1% SDS and analyzed in end-point dilution 10^{-2} – 10^{-8} utilizing RT-QuIC protocol for brain homogenates.

3.5 Real-Time Quaking-Induced Conversion (RT-QuIC) assay

3.5.1 Detection of prion seeding activity

Prion seeding activity was analyzed using a second-generation Real-Time Quaking-Induced Conversion (RT-QuIC) assay established by Dr. Byron Caughey ´s lab (National Institute of Allergy and Infectious Diseases, MT, USA).

All reagents were filtered through 0.22 µm syringe filter prior to use. Reaction mix was prepared, containing 119 mM PB, pH 7.4; 1 mM EDTA; 130 mM sodium chloride (NaCl); 10 µM Thioflavin T (ThT); 0.1 mg/ml rHAPrP90-231 or rBVPrP and for CSF analysis also 0.002% SDS. Aliquot of recombinant protein was thawed and immediately filtered through 100 kDa centrifuge filter with Omega membrane (Cytiva, WA, USA) at 7 000 x g, 5 min, RT before slowly adding into the reaction mix. 98µl or 85 µl of reaction mix was then loaded into Nunc™ non-treated 96-well plate with optical bottom (Thermo Fischer Scientific, Prague, Czech Republic) and seeded with either 2 µl of brain/skin or 15 µl of CSF sample into a final volume 100 µl in quadruplicates. As a positive control, 2 µl of 10% BH with CJD (MM1) diluted to $5x10^{-6}$ was used in every reaction.

The plate was tightly sealed with Nunc™ Sealing Tape and incubated in FLUOstar Omega plate reader (BMG Labtech GmbH, Germany) undergoing repeating cycles of shaking (1 min, 700 rpm, double orbital) and incubation (1 min) at 42°C (rBVPrP) or at 55°C (rHAPrP90-231) over 48 or 60 hrs. The gain of the reader was set to 1 900 and fluorescence was read from bottom every 15 minutes. Each RT-QuIC plate was analyzed by Mars Software (BMG Labtech GmbH, Ortenberg, Germany).

3.5.2 Detection of seeding activity of pathological α-synuclein

Seeding activity of pathological α-synuclein ($\alpha\text{-syn}^D$) was analyzed by RT-QuIC assay utilizing protocol that was first established by Groveman *et al*. (2018) with minor modifications. 10% BH samples were analyzed both in the absence and presence of SDS and N-2 supplement.

All buffers were filtered through 0.22 µm syringe filter prior to use. The reaction mixture was composed of 40 mM PB, pH 8.0 (prepared in the laboratory); 170 mM NaCl; 10 µM ThT; 0.1 mg/ml rα-Syn (WT) and 0.0015% for the analysis of *post-mortem* CSF samples. Before adding calculated volume of rα-Syn (WT), the aliquot was thawed and filtered through 100 kDa centrifugation filters at 7 000 x g, 5 min, RT. After, 98 or 85 µl of the mixture was added into 96-well plate that was supplemented with six 0.8-micron silica beads (OPS Diagnostics, NJ, USA) in every well. The reaction was seeded with 2 µl of BH sample or 15 µl of CSF sample in quadruplicates.

The plate was sealed and incubated in fluorescent reader (FLUOstar Omega) undergoing repeating cycles of shaking (1 min, 400 rpm, double orbital) and incubation (1 min) at 42°C over 48 or 60 hrs. The gain was set at 1900 with the fluorescence reading every 15 min. Data were analyzed using the same software as for the prions.

3.5.3 Quality control assay

Every batch of rPrP and rα-Syn (WT) was tested by quality control (QC) assay utilizing RT-QuIC as described earlier. In the QC assay for rPrP, 10% brain homogenate with CJD (MM1) was analyzed in serial dilution $5x10^{-6}$ – $5x10^{-9}$ as a positive control. 2 µl of sample and 13 µl of PBS, pH 7.4 were added into designated wells for positive control. As negative control, 15 µl of 0.035 mg/ml human serum albumin (HSA) and PBS, pH 7.4 were used as a seed for the reaction.

In the QC assay for rα-Syn (WT), 10% brain homogenate with definite synucleinopathy and 10% brain homogenate from corneal donor without any neurodegenerations were used as a positive and negative control, respectively. BHs were analyzed in serial dilution 10^{-2} – 10^{-7} diluted in both PBS, pH 7.4 and in a buffer containing PBS, pH 7.4; 1x N-2 supplement and 0.1% SDS. 98 µl of reaction mix was seeded with 2 µl of the BH sample.

Purified rPrP and rα-Syn (WT) was considered suitable for RT-QuIC when no more than four spontaneous aggregations out of 80 wells for prion and 48 wells for α-syn occurred during the assay.

3.5.4 Analysis of RT-QuIC data

To analyze data from RT-QuIC assay, we evaluated four parameters – max ThT fluorescence, time to threshold (TTT), lag time, and area under the curve (AUC). Max ThT fluorescence was determined from the mean of four wells of tested sample. TTT was characterized as a time point when the signal crosses the calculated threshold. This correlates with lag time of the sample which is characterized by the time when the ThT fluorescence at one time point is 6% higher from the previous one. Therefore, the lag time marks the start of protein substrate aggregation. The AUC was calculated from the time course of mean ThT fluorescence.

To determine the outcome of the RT-QuIC assay, we established the threshold for every type of the sample separately. Threshold represents a cut off value for the positive outcome of the RT-QuIC assay. Threshold for prion RT-QuIC in our laboratory was calculated as mean max ThT fluorescence of all tested non-TSE samples plus five times standard deviation (SD). For FFPE brain samples analysis, the threshold was calculated from 10^{-4} sample dilution. For α-syn BH samples, the threshold was calculated separately for 10^{-4} dilution.

To estimate the seeding dose 50% (SD_{50}), Spearman-Kärber analysis was used as previously described (Wilham *et al*., 2010). Every well was evaluated separately and considered positive for prion seeding activity only when ThT fluorescence was >200% of the mean ThT fluorescence of the negative control. The SD_{50} was calculated using following formula:

$$log_{10}SD_{50} = x_{p=1} + \frac{1}{2}d - d\sum_{x_{p=1}}^{x_{min}} px.$$

$x_{p=1}$= highest dilution with all four wells positive

d= log_{10} dilution factor

$x_{min=}$ the most diluted dilution

The results from α-syn RT-QuIC assay were plotted and statistically analyzed using GraphPad Prism 5 (GraphPad Software Inc.). Data were analyzed by nonparametric t-test. The difference was assumed significant for *P* value < 0.05.

4 Results

4.1 Purification of recombinant proteins for the RT-QuIC assay

4.1.1 Recombinant prion protein

For the second-generation RT-QuIC assay either rHAPrP90-231 or rBVPrP used as substrates were purified as previously described (Foutz et al., 2017) with minor modifications. rPrP was isolated from inclusion bodies and then purified on Ni-NTA column. Protein was first denaturated using high concentrations of GndHCl. After, the refolding step was carried out for 240 min on the column by slowly replacing denaturation conditions by physiological. During this step, the peak with contaminants is generated that is not collected (Fig. 6A, arrow). The protein was then eluted by the linear gradient of imidazole. The peak was collected when the absorbance at 280 nm increased above the 0.2 AU (Fig. 6B). Ater, the purified protein was dialyzed, and absorbance of the protein was measured at 280 nm. The concentration was determined using extinction coefficient either 1.4 $mg/ml^{-1}cm^{-1}$ for rHaPrP90-231 or 2.7 $mg/ml^{-1}cm^{-1}$ for rBVPrP. The standard yield of the rPrP from 1 l of bacterial culture was 45 – 60 mg per batch. The quality of protein was confirmed by Coomassie blue staining (Fig. 7) and quality control assay (Fig. 10).

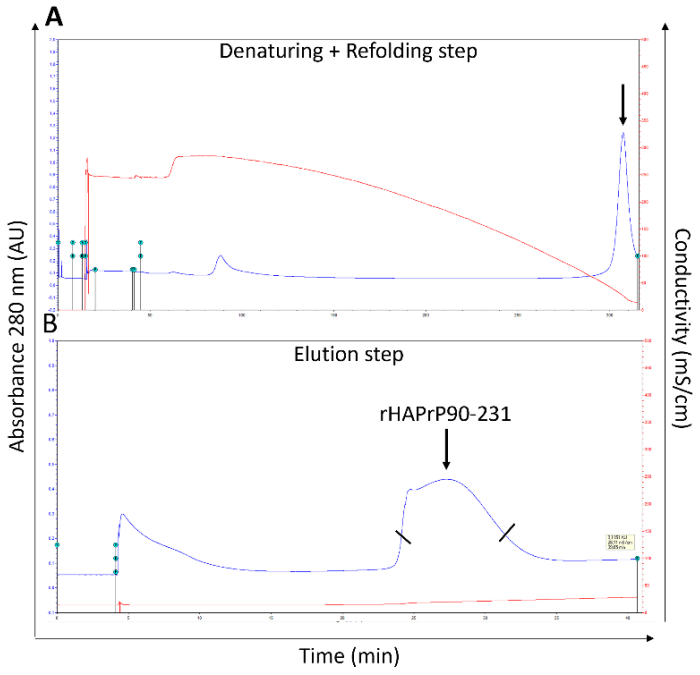

Figure 6. Chromatograms of purification of recombinant prion protein (rHAPrP90-231) carried out on Ni-NTA column by BioLogic LP Low-Pressure Liquid Chromatography System. (A) At the beginning, the protein was shortly washed with buffer at denaturing conditions. After, the refolding step was carried out on the column over 240 min, slowly replacing denaturing conditions by physiological. During this step, the peak which was not collected was generated (arrow). (B) The elution step was carried out by linear gradient of imidazole. The peak was collected when absorbance measured at 280 nm exceeded 0.2 AU. AU- absorbance units

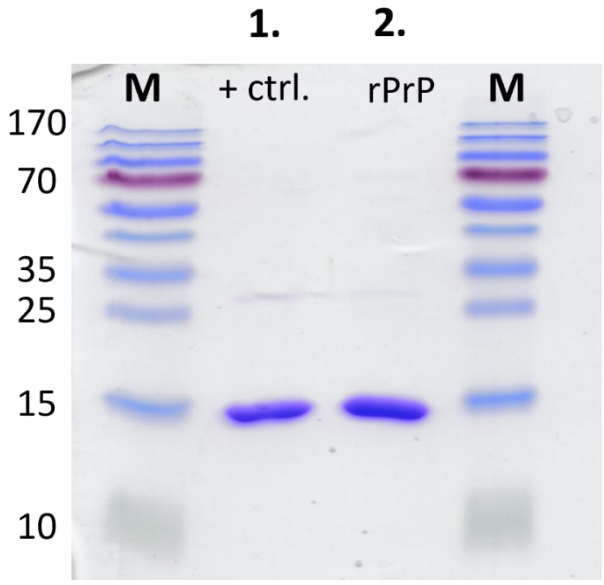

Figure 7. Coomassie blue staining of purified recombinant prion protein (rHAPrP90-231). Purified rPrP (line 2) was compared to the positive control (+ ctrl., line 1) on 15% gel. The bands show rPrP at ~15 kDa.
M – molecular weight standard (kDa)

4.1.2 Recombinant alpha-synuclein (WT)

Recombinant α-synuclein (WT) was isolated from bacterial periplasm by osmotic shock and purified using two step chromatography protocol. During the first step, protein was purified using Ni-NTA column by affinity chromatography. In this step, contaminants were washed away, and the generated peak was not collected (Fig. 8A, arrow). The peak containing rα-Syn (WT) was eluted between 150 – 375 mM of imidazole linear gradient. During the second step, which was carried out on the anion exchange column, the protein was further purified and concentrated. The peak containing rα-Syn (WT) was eluted in a linear gradient of NaCl, between 300 - 350 mM (Fig. 8B). The protein was dialyzed in mQH_2O or 40 mM PB, pH 8.0 according to a protocol. The concentration of rα-Syn (WT) was determined by spectrophotometry at 280 nm using theoretical extinction coefficient 0.36 mg/ml^{-1}cm^{-1}. The average yield of the rα-Syn (WT) from 1 l of bacterial culture was 20 mg. The purity and quality were confirmed by Coomassie blue staining (Fig. 9) and RT-QuIC quality control assay (Fig. 11).

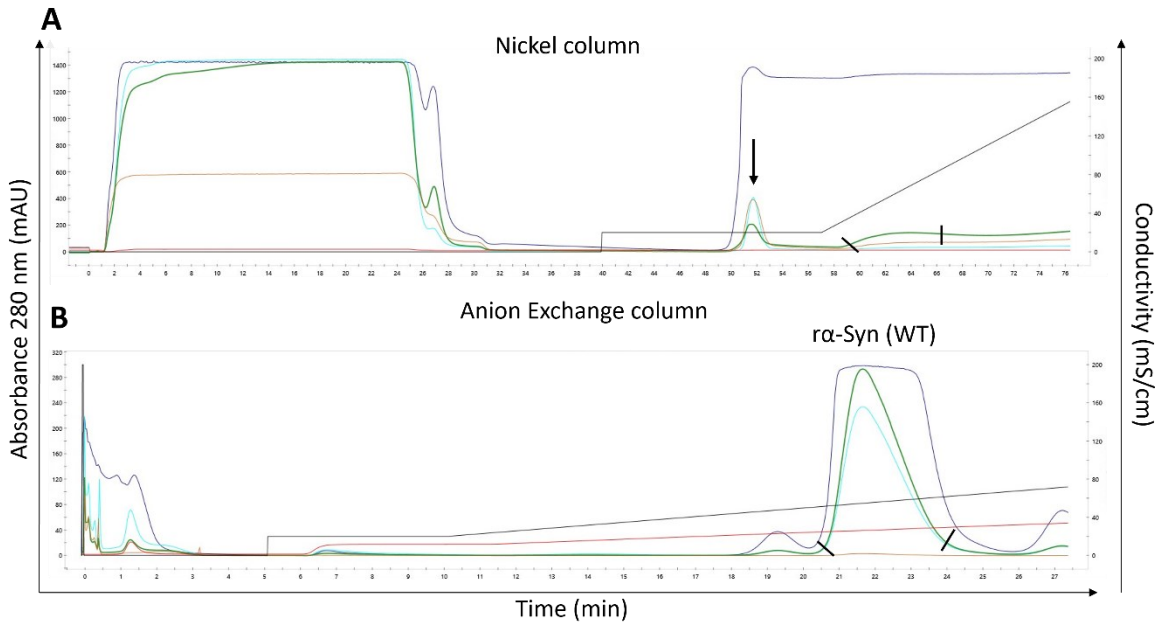

Figure 8. Chromatograms of purification of recombinant alpha-synuclein (WT) carried out on Ni-NTA and anion exchange column by NGC Chromatography System. (A) Affinity chromatography on Ni-NTA column. The bound proteins were eluted using a linear gradient of imidazole. The arrow points to non-collected peak of contaminants. (B) During the second step, protein was further purified and concentrated on anion exchange column and eluted by a linear gradient of NaCl.
mAU – milli absorbance units

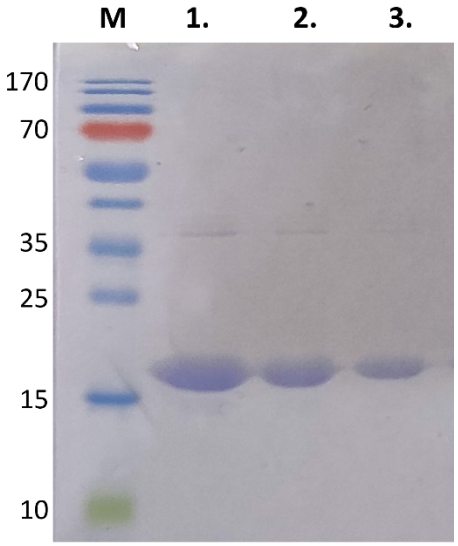

Figure 9. Coomassie blue staining of purified recombinant alpha-synuclein (rα-Syn (WT)). The purity of a new batch of rα-Syn (WT) (1. line) was confirmed on 15% acrylamide gel. The protein was analyzed in 1:2 dilution (2. and 3. line). The bands show purified protein at ~16 kDa.
M – molecular weight standard (kDa)

4.1.3 Quality control assay of the purified recombinant proteins

Every batch of purified rPrP and rα-Syn (WT) was analyzed by standardized quality control RT-QuIC. A new batch of prion protein substrate was considered acceptable for RT-QuIC when no more than four wells from out of 84 well of no seed controls (PBS, pH 7.4; HSA) showed spontaneous

aggregation. As a positive control, standard 10% BH with sCJD MM1 phenotype was analyzed in end-point dilution to examine the aggregation competence of the purified protein (Fig. 10).

New batch of rα-Syn (WT) was tested using 10% BH from corneal donor without any definite neurodegeneration and 10% BH from patient with definite Dementia with Lewy body (DLB) in the final stage of the disease. The protein was considered acceptable for RT-QuIC analysis when no more than four wells out of 48 with negative control gave positive ThT fluorescent signal (Fig. 11).

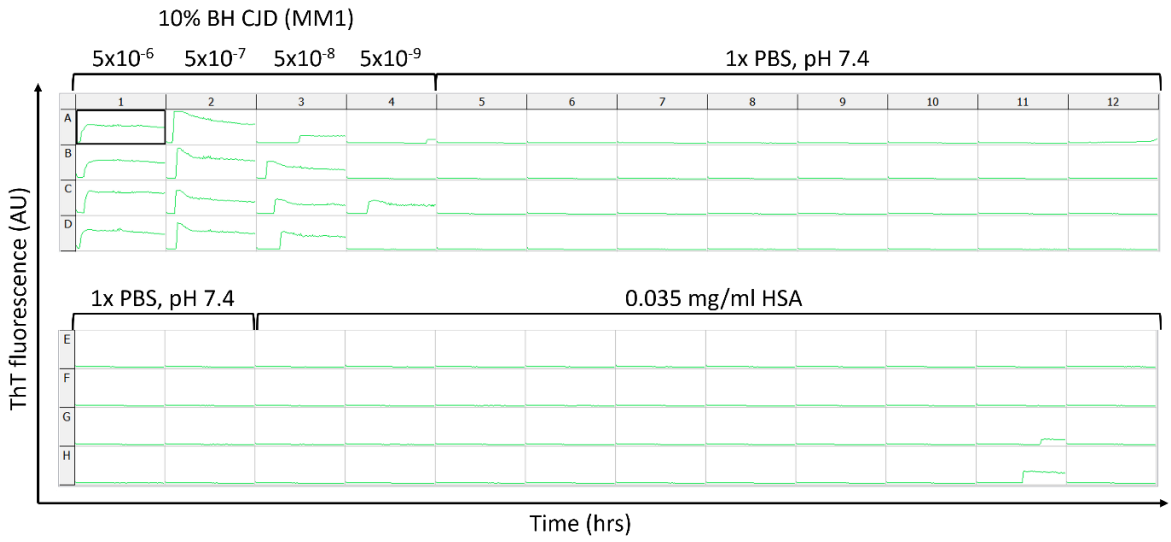

Figure 10. Quality control assay of recombinant prion protein (rHAPrP90-231) substrate by RT-QuIC assay. Every batch of the purified protein was analyzed to examine the occurrence of spontaneous aggregates during the RT-QuIC run. The protein was considered suitable when no more than four control wells exhibited spontaneous aggregation. 10% BH with sCJD (MM1) was used as positive control and wells seeded with PBS and with HSA served as negative controls. Two wells (G11, H11) have demonstrated spontaneous aggregation.
PBS – phosphate buffer saline, HSA – human serum albumin, BH – brain homogenate, sCJD – sporadic Creutzfeldt-Jakob disease, AU – arbitrary units

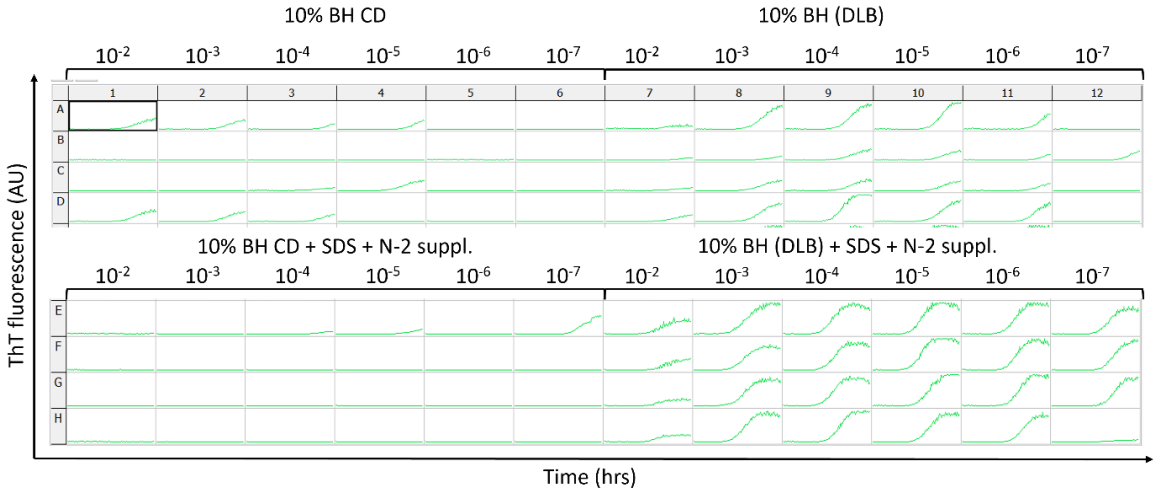

Figure 11. Quality control assay of recombinant α-synuclein (WT) by RT-QuIC assay. Each batch of the purified protein was analyzed to assess the presence of spontaneous aggregations during the assay run. The protein was considered acceptable when no more than four wells gave positive ThT signal either in the presence or absence of SDS and N-2 supplement. 10% BH from CD was used as a negative control, and 10% BH with final stage of DLB as a positive control. This batch of the rα-Syn (WT) has provided 8 nonspecific aggregations with 10% BH CD, but only two in the presence of SDS and N-2 supplement.
BH – brain homogenate, CD – corneal donor, DLB – Dementia with Lewy body, AU – arbitrary units

4.2 Patients' cohort analyzed in retrospective analysis of CSF and skin samples

In total, 38 *post-mortem* skin and CSF samples were obtained from patients with definite diagnosis of prionopathy. Majority of the patients were diagnosed with sCJD (n= 34), mostly with MM1 phenotype (n=16). Other types of sCJD were represented by two to four cases including one case of rare variably protease-sensitive prionopathy (VPSPr). Cases with gCJD included E200K mutation (n=2) and GSS syndrome with P102L mutation (n=2). The control cohort consisted of 30 *post-mortem* samples of patients with other neurodegenerative diseases (n=24) or without confirmed neurodegeneration (n=6).

Definitive prionopathy diagnosis was confirmed by standard neuropathological assessment of brain tissue and Western blotting in NRL for Human Prion diseases. Definitive diagnosis and patients' demographic information are provided in the Table 1 and 2.

Table 1. Characteristics of RT-QuIC analysis of patient´s cohort with prionopathies. The definite diagnosis of prionopathy was confirmed by neuropathological examination of brain by immunohistochemistry and western blot during the autopsy.

	n	mean age ± SD	male (n)/ female (n)	CSF/skin mean max. ThT ± SD (AU) x10^4	CSF/skin lag time ± SD (hrs)	CSF/skin mean AUC (AU) x10^8
Sporadic TSEs	**34**	**69 ± 10**	**18/16**	**24±3.8/14.3±4.8**	**6±2.3/4.8±3.5**	**9.63/4.65**
CJD MM1	16	75 ± 8	12/4	25.4±1.4/13.4±4.8	5.4±2/5.5±4.3	11.1/4.4
CJD MM2	2	56, 59	0/2	26; 24/12; 12	5; 7.5/ 3.75; 5	11.8; 9/3.6; 3.7
CJD VV1	3	59 ± 10	1/2	24.8±2.1/15±7.8	5.3±2/3.25±0.4	10.5/4.9
CJD VV2	4	68 ±11	2/2	24.4±1.7/15.5±3.7	7.1±3.23/4.1±2.4	10.6/5.2
CJD MV1	3	70 ± 4	1/2	21±8.3/13.2±5.2	5.2±1.7/5.25±2.1	8.1/4.4
CJD MV2	3	57 ± 12	1/2	23±2.7/19.7±1.8	6±1.4/2.4±0.3	10/6
CJD MM1+2	2	63, 70	0/2	26; 20/13.7; 22	5.5; 6.5/ 2.25; 2.8	9.2; 12.8/6.6; 4.5
CJD VPSPr	1	73	1/0	10/9	13/11.5	3.2/3.2
Genetic TSEs	**4**	**62 ± 16**	**1/3**	**20.3±7.6/16.4±5.2**	**8.1±3/8±12.7**	**8.8/5.45**
gCJD E200K	2	65,75	1/1	26; 10/19.3; 20.3	12; 5/2; 2.75	3.1; 12.7/7.2; 5.6
GSS P102L	2	38, 69	0/2	26; 18.1/8.8; 17.4	7.3; 8.3/ 22.5; 4.5	12.4; 7/3.1; 5.9

CJD – Creutzfeldt-Jakob disease, VPSPr – variably protease-sensitive prionopathy, gCJD – genetic CJD, GSS – Gerstmann-Sträussler-Scheinker syndrome.

Table 2. Characteristics of RT-QuIC analysis of non-TSE patients control cohort. The definite diagnosis of non-TSE was confirmed at neuropathological examination of brain by immunohistochemistry and western blot during the autopsy.

	n	mean age ± SD	male (n)/ female (n)	skin mean max. ThT ± SD (AU) $x10^4$	CSF $10^0/10^{-1}$ mean max. ThT ±SD (AU) $x10^4$	skin mean AUC (AU) $x10^6$	CSF $10^0/10^{-1}$ mean AUC (AU) $x10^6$
non-TSEs	**30**	**72 ±14**	**18/12**	**2.6±2.2**	**2±0.8/2.4±2.1**	**1.2**	**0.9/0.8**
AD	12	79 ± 8	8/4	2.1±1.3	2.3±1.3/2.4±2.2	0.8	1.1/1
DLB	2	89, 78	2/0	7.2; 1.4	1.7; 1.8/1.6; 1.6	2.8; 0.6	0.8; 1/0.7;0.8
FTLD*	8	74 ± 6	5/3	2.3±2.1	1.9±0.3/4.1±2.7	1	0.9/1.2
VaD	1	94	0/1	1.5	1.8/1.6	0.7	0.9/0.8
Syn	1	56	1/0	6.5	1.7/1.6	2	0.7/0.8
ND-A	1	56	1/0	1.7	1.7/1.6	0.7	0.8/0.7
lymphoma infiltration	1	54	0/1	1.6	1.7/1.5	0.7	0.9/0.7
H/ABI	3	43 ± 8	1/2	4.6±3.8	2.2±0.4/1.6±0.01	1.6	1.1/0.7
encephalitis, DLBCL	1	66	0/1	1.6	1.7/1.6	0.7	0.8/0.7

AD – Alzheimer disease, DLB – dementia with Lewy´s bodies, FTLD – frontotemporal lobar degeneration, VaD – vascular dementia, Syn – synucleinopathy, ND-A – non-dementia-alcoholism, H/ABI – hypoxic/anoxic brain injury, DLBCL – diffuse large B-cell lymphoma. *FTLD includes FTLD-UPS, FTLD-tau, FTLD-TDP, FTLD-U+TDP-43 and progressive supranuclear palsy

4.3 Concentration of total protein in *post-mortem* CSF and skin

The protein concentration of samples was determined using commercial kit Pierce™ BCA Protein Assay. The average protein content in TSE CSF (n=38) was 4.27±2.27 mg/ml and in non-TSE CSF (n=30) it was 5.38±4.57 mg/ml. The range of the concentrations was between 1.37 and 9.70 mg/ml excluding one outlier (Fig. 12A). The protein concentration of the undiluted CSF TSE samples that gave negative result at the beginning (n=8) was higher (5.69±2.50 mg/ml) than of the rest of TSE samples (3.39±2.09 mg/ml), but the difference was not significant (P=0.082).

The average protein content in 10% TSE skin samples treated with collagenase A was 4.4±0.7 mg/ml and for 10% non-TSE samples it was 4.36±1.36 mg/ml. The range of the concentration was from 2.05 and 7.97 mg/ml (Fig. 12B). The protein content in skin TSE samples that gave negative signal (4.08±0.6 mg/ml; n=7) was similar as in TSE samples (4.48±0.7 mg/ml) that were positive in RT-QuIC assay.

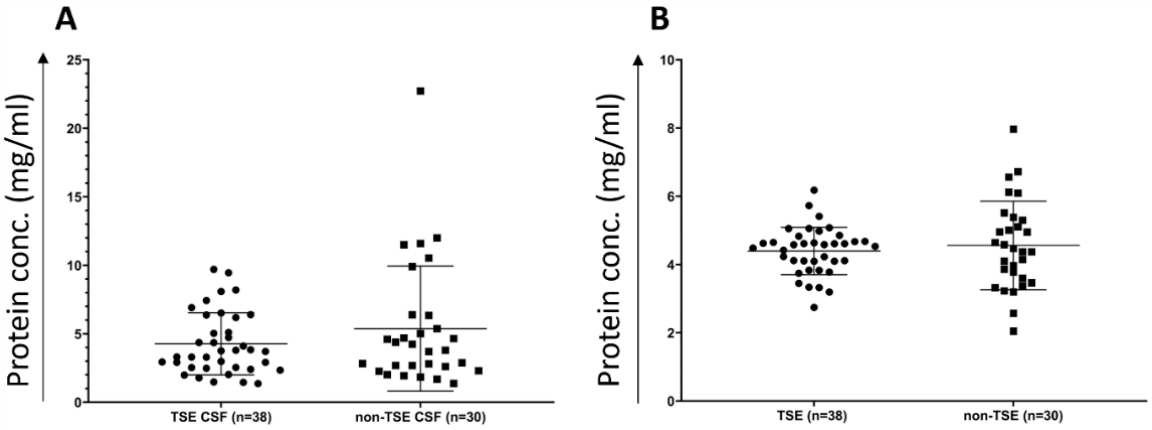

Figure 12. Protein concentration for individual TSE and non-TSE samples. The concentration was determined using BCA protein assay. Bars show mean ± standard deviation (SD) (A) The protein concentration of TSE and non-TSE CSF samples for every individual patient. (B) The protein concentration of TSE and non-TSE skin samples for every individual patient. TSE – transmissible spongiform encephalopathy

4.4 Detection of prion seeding activity in *post-mortem* ventricular CSF

All *post-mortem* CSF samples (n=68) were analyzed utilizing previously published RT-QuIC protocol (Orrú *et al*., 2015) for *ante-mortem* CSF using rHAPrP90-231 substrate. When tested undiluted, 7 *post-mortem* TSE CSF samples, specifically one VV1, VV2, MV1, VPSPr, GSS, and two MM1, gave negative result, and one sample with sCJD (MM1) was just borderline positive corresponding to the 81.6% sensitivity of the assay. However, after 10x dilution with PBS, pH 7.4 these samples gave clearly positive result, hitting the detection limit of the fluorescence reader, therefore suggesting the presence of RT-QuIC reaction inhibitors in *post-mortem* CSF. When analyzing CSF from control group, non were classified as positive, suggesting 100% assay specificity. Although, after they were diluted, higher fluorescence was observed in one well within three patient samples which resulted in calculation of notably higher threshold. For non-TSEs, cases where higher ThT fluorescence was observed in one well, RT-QuIC analysis was repeated and the measured max ThT fluorescence dropped (Fig. 13A). The threshold for undiluted CSF samples was 58,736 AU which was notable lower than for diluted CSF where the threshold was 94,607 AU.

The mean max ThT fluorescence, of all undiluted TSE CSF (n=30) samples, was $23\pm5x10^4$ which was comparable to that of diluted CSF (n=8) samples, $21\pm6x10^4$. Two undiluted CSF samples with gCJD (E200K) mutation and sCJD (MV1), and one diluted CSF VPSPr sample provided noticeably lower ThT signal in comparison to the other samples (Fig. 14B). The specific aggregation of rPrP started very quickly, before 10 hrs of the assay. The corresponding time to threshold was 7.0±5.3 hrs for undiluted and 5.4±4.1 for diluted samples (Fig. 13B). The longest lag time (780 min ~ 13 hrs) was observed for VPSPr case (Fig. 14C). The normalized area under the curve (AUC) for undiluted samples was $9.6x10^6$ and for diluted it was $8.4x10^6$. Similarly to a lag time, the mean AUC among

TSEs phenotypes was very similar, except for VPSPr case and one case with gCJD E200K phenotype where the AUC was the smallest (Fig. 14D).

The mean max. ThT fluorescence of all undiluted samples in non-TSEs CSF (n=30) control group was 19±5x10^3. After the dilution, three samples (one AD and two FTLD) gave higher ThT fluorescent response in one or two wells. The RT-QuIC analysis for these samples (n=3) was repeated, and their signal dropped (Fig 13A). However, all the control samples remained negative. Total AUC for undiluted non-TSEs was 7.6x10^4 and for diluted it was 14x10^4.

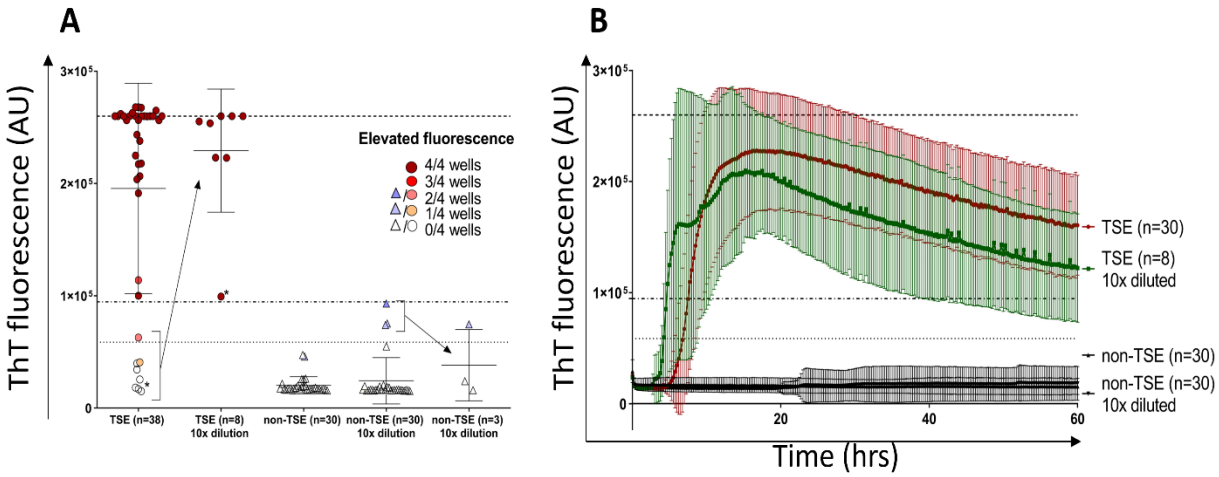

Figure 13. Detection of prion seeding activity in *post-mortem* cerebrospinal fluid (CSF) samples. (A) Dot plot of max. ThT fluorescence intensity of TSEs and non-TSEs CSF. Samples were tested in quadruplicates and were considered positive when at least two out of four wells showed elevated ThT signal and the max average ThT fluorescence exceed the threshold (dotted line for undiluted and dash dotted line for diluted samples). Every dot represents the mean of four wells of tested samples. Number of a wells with elevated ThT signal is represented by color intensity. Eight TSEs samples gave negative signal but became positive after dilution. None of control non-TSEs sample was positive. Bars show mean ± standard deviation (SD). Dotted line represents detection limit of a reader. (B) The mean kinetics of undiluted TSE CSF samples (n=30, red), diluted TSE CSF samples (n=8, green), undiluted non-TSE CSF samples (n=30, black) and diluted non-TSE samples (n=30, grey) over 60 hrs. Bars represents standard deviation (SD) at a specific time point.
AU – arbitrary units, TSE – transmissible spongiform encephalopathy,
*Variably proteinase-sensitive prionopathy (VPSPr)

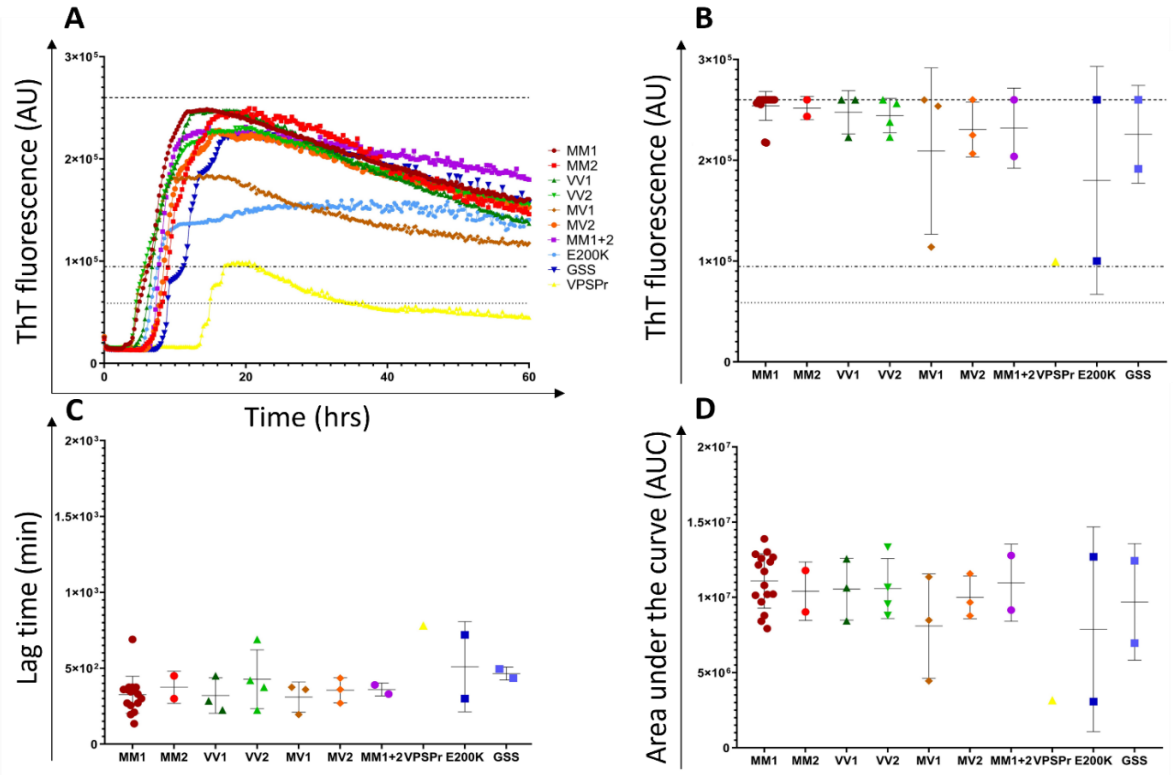

Figure 14. Analysis of TSE cerebrospinal fluid (CSF) samples according to the disease type. *Post-mortem* CSF samples were analyzed utilizing RT-QuIC assay. The size of the groups varies from n= 16 for CJD (MM1) to one sample with VPSPr. CSF samples were analyzed using the mean values of undiluted CSF samples (n=30) and of diluted (n=8) samples that were classified as negative when undiluted. Every sample was tested in quadruplicates. The dotted line represents threshold for undiluted and dot-dashed line for diluted CSF samples. The upper dashed line represents detection limit of fluorescence reader. Bars show mean ± standard deviation (SD). (A) The mean ThT fluorescence for each CSF TSE type over 60 hrs. (B) Analysis of max. ThT fluorescence for individual patients in every group. Every dot shows the mean max ThT fluorescence from four wells. (C) Analysis of lag time which represents the time when aggregation started for every sample. (D) Comparison of area under the curve (AUC) for every TSE phenotype. AUC was analyzed from the traces in a graph A using GraphPad Prism software.
AU – arbitrary units, VPSPr – variably protease-sensitive prionopathy, GSS – Gerstmann-Sträussler-Scheinker syndrome

4.5 Detection of prion seeding activity in *post-mortem* skin utilizing protocol for CSF samples

Because the concentration of PrP^{TSE} in skin is presumably very low, we first utilized the same RT-QuIC protocol for analysis of corresponding skins (n=68) as for the CSF. We reasoned that using 15 µl of the samples to seed the 85 µl of reaction would increase the sensitivity of the assay.

The mean max. ThT signal of TSE skin samples (n=38) was $15\pm4.2x10^4$ which was three times higher than in non-TSE (n=30) control samples which was $5\pm5x10^4$. However, six non-TSE samples, specifically cases with FTLD-U, syn., H/ABI, FTLD-UPS and two cases with AD, gave high false-positive signal which overlapped with TSE signal (Fig. 15A). To assess if the false-positive signal is reproducible caused by the nature of a samples, newly prepared 10% skin homogenates were tested utilizing the same protocol. The mean max signal, for a newly prepared control, samples was

6.7±4.5x10^4. Still, five samples gave high false-positive signal, which was overlapping with the TSE positive samples (Fig. 15A). However, only two samples with H/ABI and syn. gave repeatedly high ThT signal suggesting that the false-positive result could be caused by technical problems arising during the preparation of skin homogenates. Interestingly, the skin sample with H/ABI diagnosis gave constantly high ThT signal in all four wells and during repeated RT-QuIC analysis. Insufficiently separated RT-QuIC signal of skin samples is also shown at mean kinetics curves over the 60 hrs (Fig. 15B).

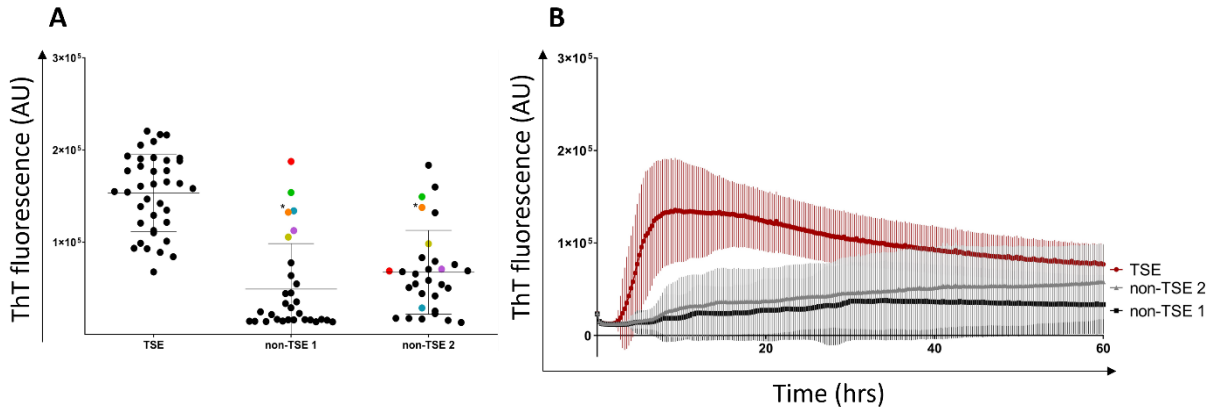

Figure 15. Detection of prion seeding activity in skin samples utilizing the same RT-QuIC protocol for cerebrospinal fluid (CSF) samples. (A) Dot plot of max. ThT fluorescence intensity in 10% skin homogenates. Samples were analyzed in quadruplicates and every dot represents the average max. of four wells. Portion of non-TSE1 samples (n=6, colorful dots) gave higher ThT signal, overlapping with TSE cases (n=38). After, RT-QuIC analysis was repeated with newly prepared homogenates (non-TSE2). Still, five samples gave higher ThT signal, although only two correlates with non-TSE1. Asterisk (*) represents a sample with hypoxic/anoxic brain injury which gave repeatedly high ThT signal. Bars show mean ± standard deviation (SD). (B) The mean kinetics of TSE skin (n=38, red), non-TSE1 skin (n=30, black) and non-TSE2 skin (n=38, grey) homogenates over 60 hrs. Bars represents standard deviation (SD) at a specific time point.
AU – arbitrary units, TSE – transmissible spongiform encephalopathy

4.5.1 RT-QuIC analysis of *post-mortem* skin samples utilizing the CSF protocol with addition of N-2 supplement

We have attempted to decrease the false-positive signal in non-TSE skin samples, and at the same time to increase the ThT signal in TSE samples with addition of N-2 supplement in a buffer used for the skin homogenate dilution.

This approach led to a better separation of TSE and non-TSE samples comparing to the assay without the N-2 supplement (Fig. 16). The mean max. ThT signal, 19.3±3.9x10^4, in TSE skin (n=38) was little bit higher, while mean max. ThT signal, 5.6±4.6x10^4, in control non-TSE skin (n=30) samples remained the same. Only one sample with H/ABI again gave high false-positive signal (Fig. 16A). However, the high dispersion of values of non-TSE skin did not allow to establish a practical threshold for the positive samples. The overlap of two groups is again shown at the mean signal kinetics of the reaction over 60 hrs (Fig. 16B).

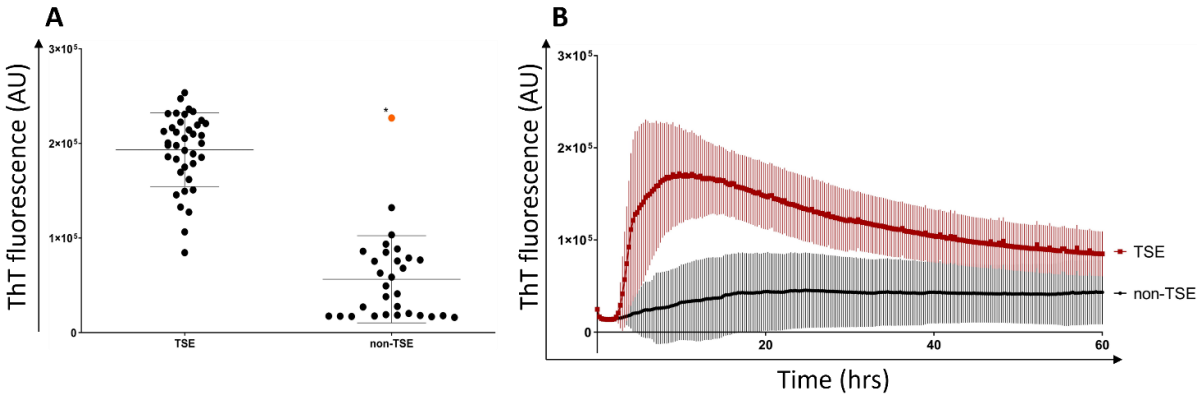

Figure 16. Detection of prion seeding activity in skin samples using RT-QuIC protocol for cerebrospinal fluid (CSF) samples with N-2 supplement addition. (A) Dot plot of max. ThT fluorescence intensity in 10% skin homogenates. Samples were analyzed in quadruplicates and every dot represents the average max. of four wells. Mean max. ThT signal in TSE samples was almost four times higher than in non-TSE samples, however, the dispersion of data did not allow to establish a threshold. Again, sample with hypoxic/anoxic brain injury gave high false-positive signal (marked with asterisk). Bars show mean ± standard deviation (SD). (B) The mean kinetics of TSE (n=38, red) and non-TSE (n=30, black) over 60 hrs. Bars represent standard deviation (SD) at a specific time point.
AU- arbitrary unit, TSE – transmissible spongiform encephalopathy

4.6 Detection of prion seeding activity in *post-mortem* skin samples utilizing protocol for brain homogenates

Employment of protocol for brain homogenates utilizing 2 µl of ten times diluted skin homogenates led to a suppression of false-positive signals in majority of non-TSE samples while maintaining ThT signal in TSE samples. Also, the separation of the two groups was sufficient to set the threshold for the positive outcome of the reaction (Fig. 17). Out of 38 skin samples, 31 were classified as positive suggesting 81.6% assay sensitivity. Seven TSE skin samples, specifically with MM1 (n=4), MV1 (n=1), VV1 (n=1) phenotype and gCJD with GSS (n=1), provided signal in two or more wells, but did not reach the threshold and were classified as negative (Fig. 17A). Therefore, their RT-QuIC analysis was repeated, and three samples gave positive ThT signal improving the assay sensitivity to 89.5%. Similarly to CSF, skin sample of VPSPr patient gave borderline positive signal (Fig.17A). In contrary, skin samples of sCJD MV2 and gCJD E200K phenotypes gave the highest mean max. ThT signal (Fig. 18A and B). Analysis of non-TSE skin (n=30) samples gave negative signal below the established threshold suggesting the 100% assay specificity. However, five control samples, specifically FTLD-UPS, DLB, syn., AD and H/ABI cases, gave higher ThT signal above the SD (Fig. 17A). Four of them showed elevated fluorescence only in one well. Interestingly, the sample with H/ABI diagnosis gave again stable increases ThT signal in all four wells, similarly as in previous analyses using different assay protocols. Samples, that gave higher ThT signal in at least one well, were reanalyzed by RT-QuIC assay. Overall ThT fluorescence of these samples (n=6) decreased (Fig. 17A), although the sample with H/ABI still gave elevated ThT signal in three wells and other three samples

in one well. Two samples were negative in all four wells, without any elevated ThT signal. The threshold for the skin samples was determined at 91,459 AU.

The max ThT value from mean of all TSE skin samples was $12\pm5.7x10^4$ with the mean time to threshold of 5.5±4.8 hrs. In one GSS case very long lag time (1350 min ~ 22.5 hrs) was observed suggesting the possible presence of inhibitors in skin homogenate or lower sensitivity of the assay for GSS prions (Fig. 18C). For non-TSE skin samples, the mean max value from the mean ThT fluorescence was $20\pm21x10^3$ which was six times lower than for positive skin (Fig. 17B). The mean AUC of all samples was normalized to the baseline value which was the second measurement (after 30 min of the assay). For TSE samples the mean AUC was $3.9x10^6$ while for non-TSE samples it was $2.7x10^5$. The biggest mean AUC was observed in TSE phenotypes with sCJD MV2 and gCJD E200K (Fig. 18D).

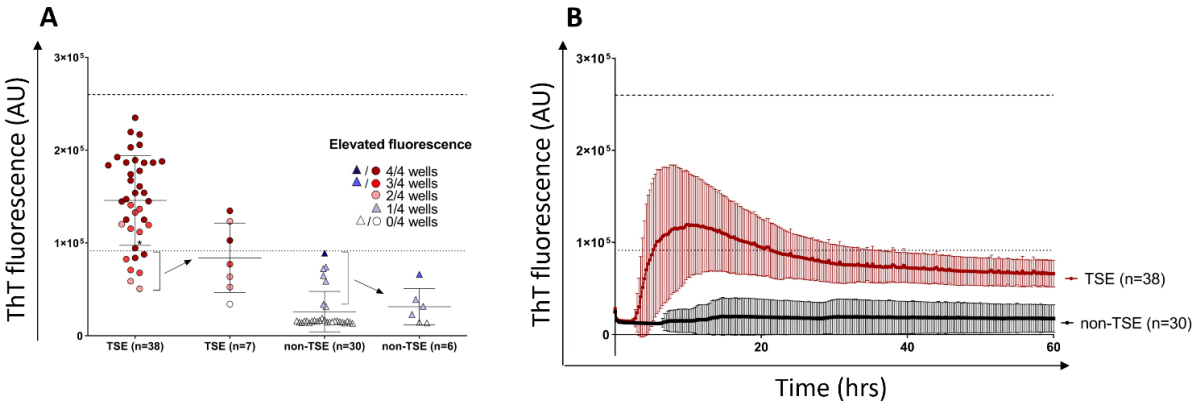

Figure 17. Detection of prion seeding activity in skin samples utilizing RT-QuIC protocol for brain homogenates. (A) Dot plot of max. ThT fluorescence intensity in 10% skin homogenates. Samples were analyzed in quadruplicates and every dot represents the average max, of four wells. Seven out of 38 TSE skin samples gave negative ThT fluorescence under established threshold (dotted line) and were reanalyzed (arrow up). None of non-TSE skin samples gave false-positive signal, however, samples (n= 6) with higher ThT signal in at least one well were reanalyzed (arrow down). Number of wells with elevated ThT fluorescence signal is represented by color intensity. The detection limit of fluorescence reader is represented by dashed line. Bars show mean ± standard deviation (SD). Asterisk (*) shows a sample with VPSPr. (B) The mean kinetics of TSE (n=38, red) and non-TSE (n=30, black) skin samples over 60 hrs. Bars represents standard deviations (SD) at a specific time point.
AU- arbitrary units, TSE – transmissible spongiform encephalopathy
*Variably proteinase-sensitive prionopathy (VPSPr)

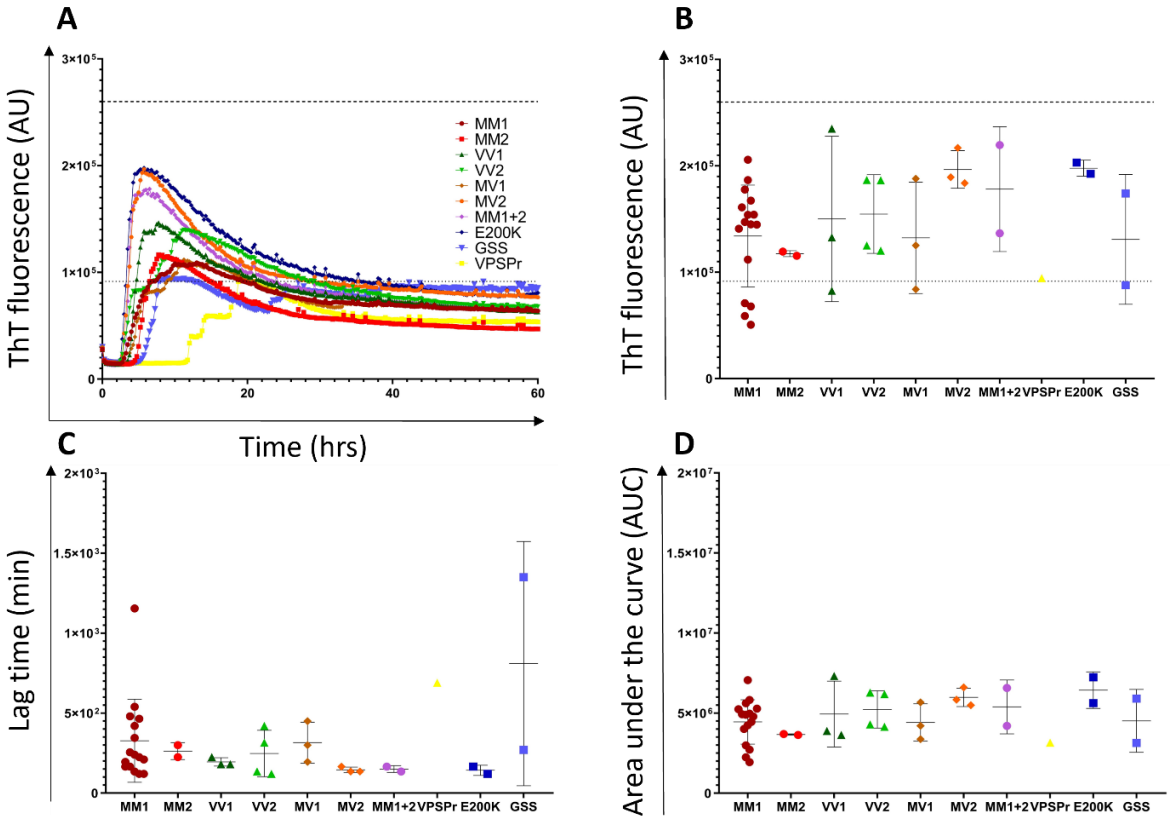

Figure 18. Analysis of skin TSE samples RT-QuIC results according to their phenotype. *Post-mortem* skin samples were analyzed utilizing RT-QuIC assay. The size of the groups varies from n= 16 for CJD (MM1) to one sample with VPSPr. Every sample was tested in quadruplicates. The dotted line represents threshold for skin samples. The samples with the mean ThT fluorescence below the threshold were classified as negative. The dashed line represents detection limit of fluorescence reader. Bars show mean ± standard deviation (SD). (A) The mean ThT signal kinetics of skin samples for every TSE phenotype group over 60 hrs. (B) Analysis of max. ThT fluorescence for individual patients in every group. Every dot shows the mean max ThT fluorescence from four wells. (C) Analysis of lag time which represents the time when the substrate aggregation started for every sample. (D) Comparison of area under the curve (AUC) for every TSE phenotype. AUC was analyzed from the traces in a graph A using GraphPad Prism software.
AU- arbitrary units, VPSPr – variably protease-sensitive prionopathy, GSS – Gerstmann-Sträussler-Scheinker syndrome

4.7 Analysis of seeding dose 50% of patient's CSF and skin samples

To determine the seeding dose of 50% (SD_{50}) in *post-mortem* CSF and skin, equal aliquots of samples with sCJD MM1 (n=16), VV2 (n=4), MV1 (n=3), MV2 (n=3) were mixed to create representative mixed samples according to TSE phenotype. Only the tissue of single case with VPSPr was tested unmixed. The samples were analyzed in end-point dilution 10^{-3} – 10^{-6}. CSF mixed samples were diluted in PBS, pH 7.4. and mixed skin samples were diluted in PBS, pH 7.4, 1x N-2 supplement and 0.1% SDS.

When analyzing CSF samples in end-point dilution, mixed sCJD MV1 and MV2 gave negative signal at 10^{-5} dilution. The samples with sCJD MM1, VV2 and VPSPr lost the signal in tenfold higher dilution of 10^{-6} (Table 3). The highest SD_{50} in 1 ml of CSF, specifically $10^{7.1}$, was calculated for sCJD

VV2 phenotype. TSE phenotypes sCJD MV1, MV2 and VPSPr all showed very similar SD_{50} with $10^{5.6-5.8}$ (Table 5).

When analyzing skin homogenates, all samples became negative after at 10^{-6} dilution (Table 4). Interestingly, the highest SD_{50} of $10^{7.7}$ in 1 g of skin was observed in sCJD MM1 and VPSPr cases. Samples with sCJD VV2 and MV2 showed the same SD_{50} of $10^{7.4}$ and sCJD MV1 gave the lowest SD_{50} of $10^{6.9}$.

Table 3. Number of replicates that were RT-QuIC positive for prion seeding activity in cerebrospinal fluid (CSF) at serial dilutions. Samples were tested utilizing RT-QuIC protocol for CSF in quadruplicates. Seeding dose 50% (SD_{50}) present in the CSF of different TSE phenotypes was tested by mixing all patient samples within the specific phenotype. Every well was evaluated separately and was considered positive only when the ThT signal exceeded 200% of mean negative control wells.

	no. of replicates	no. of positives at 10^{-3}	no. of positives at 10^{-4}	no. of positives at 10^{-5}	no. of positives at 10^{-6}
sCJD MM1	4	4	3	2	0
sCJD VV2	4	4	4	3	0
sCJD MV1	4	4	2	0	0
sCJD MV2	4	4	1	0	0
sCJD VPSPr	4	4	4	1	0

sCJD – sporadic Creutzfeldt-Jakob disease

Table 4: Number of replicates that were positive for prion seeding activity in representative skin samples utilizing RT-QuIC after their serial dilution. Samples were tested utilizing RT-QuIC protocol for brain in quadruplicates. Seeding dose 50% (SD_{50}) present in skin of different TSE phenotypes was tested by mixing all patient samples within the specific phenotype. Every well was evaluated separately and was considered positive only when ThT signal exceeded 200% of mean negative control wells.

	no. of replicates	no. of positives at 10^{-3}	no. of positives at 10^{-4}	no. of positives at 10^{-5}	no. of positives at 10^{-6}
sCJD MM1	4	4	4	2	0
sCJD VV2	4	4	4	1	0
sCJD MV1	4	4	2	1	0
sCJD MV2	4	4	4	1	0
sCJD VPSPr	4	4	4	2	0

sCJD – sporadic Creutzfeldt-Jakob disease

Table 5. Seeding dose 50% (SD_{50}) determined in cerebrospinal fluid (CSF) and skin utilizing RT-QuIC. The SD_{50} was calculated as described previously (Wilham *et al*., 2010).

	log_{10} SD_{50} / 15 µl of CSF	log_{10} SD_{50} / ml of CSF	log_{10} SD_{50} / 2 µl of skin	log_{10} SD_{50} / g of skin
sCJD MM1	4.75	6.6	5	7.7
sCJD VV2	5.25	7.1	4.75	7.4
sCJD MV1	4	5.8	4.25	6.9
sCJD MV2	3.75	5.6	4.75	7.4
VPSPr	4	5.8	5	7.7

4.8 Determination of RT-QuIC ability to detect prions before the occurrence of the disease symptoms in animal model

All mice (n=80) were closely observed after the inoculation and subsequently divided into cages of five mice (3 infected and 2 controls). One cage consisted only of five control mice that were sacrificed at the end of the experiment. Intracerebrally inoculated mice displayed more rapid course of the disease when the first mice displayed symptoms 140 dpi (Fig. 19). The last five mice were sacrificed 8 days earlier (160 dpi) after the onset of symptoms. Subcutaneously inoculated mice started displaying symptoms later (180 dpi) and, the variability among the mice was higher. Mice from cage no. 14, 15, and 16 had to be sacrificed earlier than was planned because of the onset of symptoms (Fig. 20).

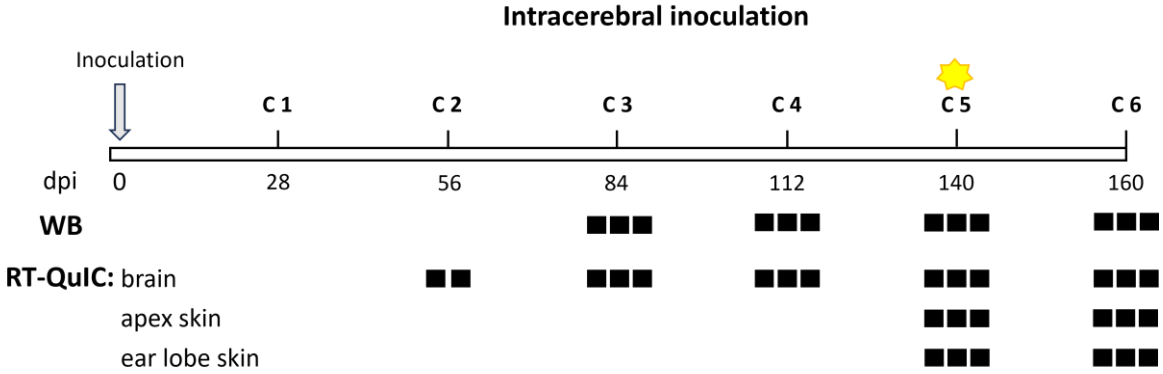

Figure 19. Schematic diagram of time points with detectable PrP^{TSE} by WB and RT-QuIC positive prion seeding. Intracerebrally inoculated mice were sacrificed every 28 days, except the last cage (C6) where the mice were sacrificed after 20 days. Prion seeding activity was analyzed in brain, skin from head apex and ear lobe. Every black square represents one mouse that showed positive result. The onset of visible symptoms is marked in yellow asterisk.

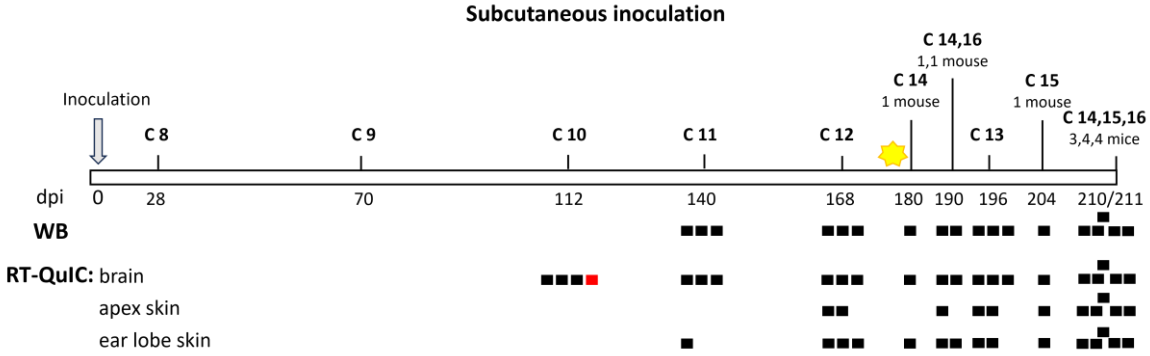

Figure 20. Schematic diagram of time points with detectable PrP^{TSE} by WB and RT-QuIC positive prion seeding activity. Subcutaneously inoculated mice were sacrificed every 42 days at the beginning and every 28 days later in the course of disease. Mice that started showing symptom earlier were sacrificed at different time (marked with longer bars). Prion seeding activity was analyzed in brain, skin from head apex and ear lobe. The onset of symptoms in the first mouse is marked with yellow asterisk. Every black square represents one mouse that displayed positive result. One control mouse (red square) gave positive RT-QuIC result 112 dpi.
dpi – days post inoculation

4.8.1 Detection of PrP^{TSE} in mice brains by Western blot

The presence of PK resistant PrP^{TSE} in the brain was analyzed by WB. In mice that were inoculated intracerebrally, the positive signal for PrP^{TSE} was first detected 84 days post inoculation (dpi) although the signal was weak. At this time mice still did not show any visible onset of symptoms. Subsequently, the concentration of PrP^{TSE} increased within brain over time with the strongest signal at 140 dpi and 160 dpi (Fig. 21). In mice, that were inoculated subcutaneously, the positive PK resistant PrP^{TSE} signal was first observed 140 dpi. Similarly to the first group, the mice did not present any visible symptoms or weight loss and the PrP^{TSE} signal grew stronger over time. Two control mice from both groups in each cage remained negative for PK resistant PrP^{TSE} (Fig. 22). All mice from the control group PrP^{TSE} remained negative at any experimental time point (Supplementary Fig. 1).

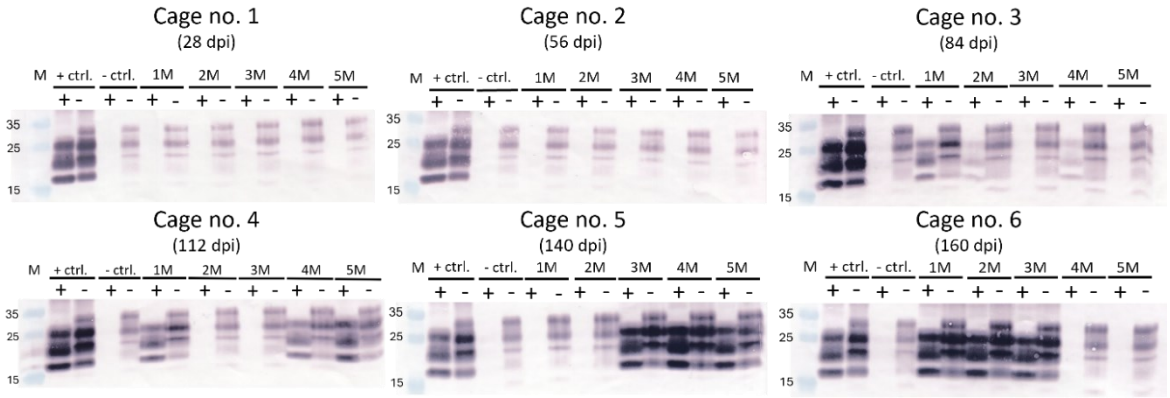

Figure 21. Western blot detection of pathogenic prion protein (PrP^{TSE}) in brain from mice with intracerebral inoculation of 0.1% brain with RML prion strain. Samples were analyzed either untreated (-) or treated (+) with proteinase K (PK). After, they were immunostained with the mixture of AH6 and 6D11 primary mice antibodies. Archive 10% brain homogenate (BH) from CD-1 mouse infected with RML prion strain was used as a positive control (+ctrl.) while 10% BH from healthy CD-1 mouse as a negative control (-ctrl.). PrP^{TSE} was first detected 84 dpi in mouse number 1 (M1), 2 (2M) and 4 (4M). Two control mice housed together with inoculated mice remained PrP^{TSE} negative at all experimental time points.
M – molecular weight standard (kDa)

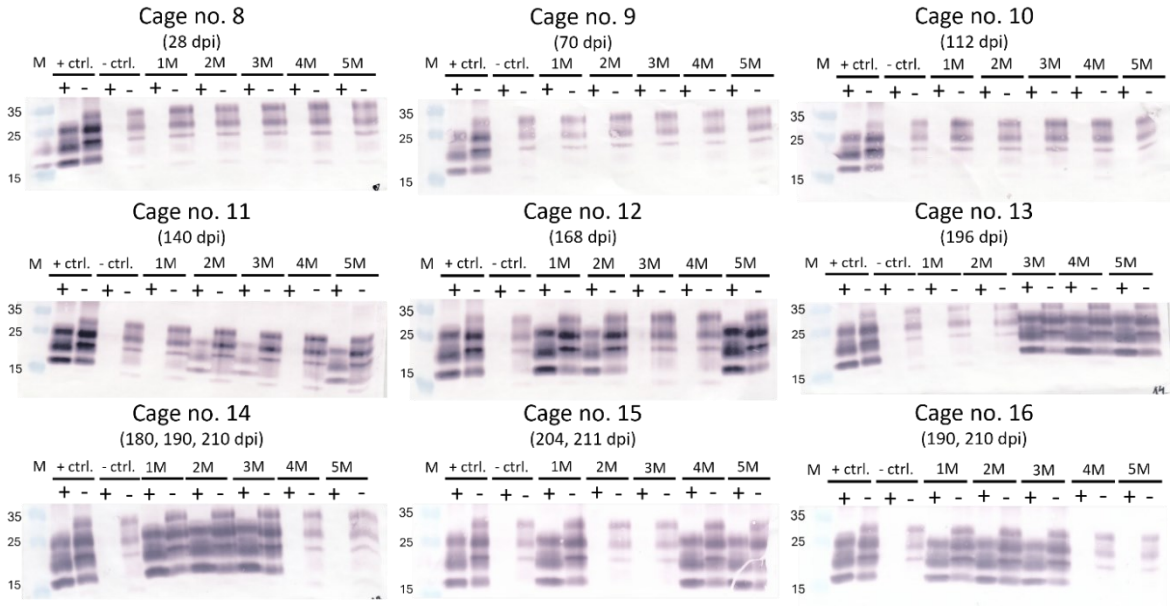

Figure 22. Western blot detection of pathogenic prion protein (PrP^{TSE}) in brain from mice with subcutaneous inoculation with RML prions. Samples were analyzed either untreated (-) or treated (+) with proteinase K (PK). After blotting, they were immunostained with the mixture of AH6 and 6D11 prion monoclonal antibodies. Archive 10% brain homogenate (BH) from CD-1 mouse infected with RML prion strain was used as a positive control (+ctrl.) while 10% BH from healthy CD-1 mouse as a negative control (-ctrl.). PrP^{TSE} was first detected 140 dpi in mouse number 2 (M2), 3 (3M) and 5 (5M). Two control mice housed together with inoculated mice from every cage remained PrP^{TSE} negative at all experimental time points.
M – molecular weight standard (kDa)

4.8.2 Detection of prion seeding activity in mice brains by RT-QuIC assay

All 10% brain homogenates from mice were analyzed in end-point dilution $5x10^{-6}$ - $5x10^{-10}$ by the second-generation RT-QuIC assay using rHAPrP90-231 as a substrate. As dilution for the RT-QuIC positive outcome, we have decided to use the lowest dilution of $5x10^{-6}$. The threshold (18,615 AU) was determined as mean max ThT fluorescence values from the mice control group plus five standard deviations (SD).

When analyzing the first group of mice that were subjected to intracerebral inoculation (n=30), all mice gave negative ThT fluorescence signal 28 dpi. At 56 dpi, two out of three RML inoculated mice showed positive ThT signal with max fluorescence of $5.3x10^4$ and $3.9x10^4$ (Fig. 23A). The corresponding time to threshold was 11 and 26.75 hrs, respectively. After 84 dpi, all three RML inoculated mice in each cage gave clearly positive ThT signal (Fig. 23). The highest max ThT fluorescence ($10.3x10^4$ and $10.7x10^4$) was detected in two mice 160 dpi with corresponding time to threshold of 8.5 and 10.5 hrs (Fig. 24). The mice inoculated with normal brain homogenate which were housed in the cages together with RML infected mice remained RT-QuIC negative at all experimental points. Similarly, the separately housed control mice (n=5) gave ThT signal below the established threshold and were classified as negative (Supplementary Fig. 2).

In the second group, where mice were subjected to subcutaneous inoculation (n=45), three mice showed low prion seeding activity 70 dpi, however it was just above the threshold ($2x10^4$, $2.1x10^4$ and $2.2x10^4$). However, at 112 dpi all three RML inoculated mice gave positive ThT signal ($5.3x10^4$, $6.6x10^4$ and $8.7x10^4$) (Fig. 23B) with time to threshold of 20.5, 16.25 and 10.5 hrs, respectively. Curiously, one control mouse also displayed positive signal, although it was lower ($3x10^4$) with long time to threshold of 21.75 hrs. The highest max ThT signal ($13.1x10^4$) was achieved 210 dpi with time to threshold of 10.75 hrs. Interestingly, one control mouse showed higher background ThT signal ($2.5x10^4$) at 210 dpi that gave false-positive RT-QuIC result (Fig. 25).

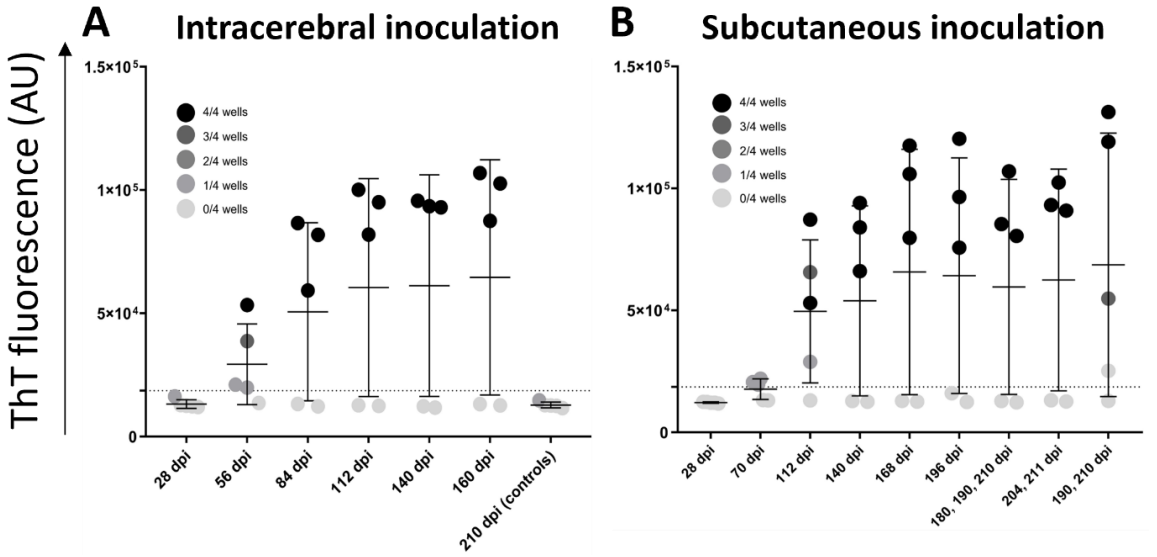

Figure 23. RT-QuIC detection of prion seeding activity in brain at $5x10^{-6}$ dilution from mice inoculated with RML prions and from control group. Dot plots of max ThT fluorescence for every mouse that was sacrificed at given time. Every dot represents the mean of four wells. Bars show the mean ± SD. The dotted line shows the threshold for the RT-QuIC positivity. The sample was classified as positive when the ThT signal exceed the calculated threshold. Intensity of the color shows number positive wells in the sample. (A) Max ThT fluorescence from mice with intracerebral inoculation. 56 dpi two mice showed clear positive signal and one mouse gave higher false-positive ThT signal just above the threshold. Mice from the control group sacrificed 210 dpi (n=5) were inoculated only with PBS, pH 7.4. and all remained negative (B) Max ThT fluorescence from mice with subcutaneous RML inoculation. 112 dpi mice showed positive ThT fluorescence. One mouse gave false-positive signal at 112 dpi and one showed higher background signal at 210 dpi.
AU – arbitrary units, dpi – days post inoculation

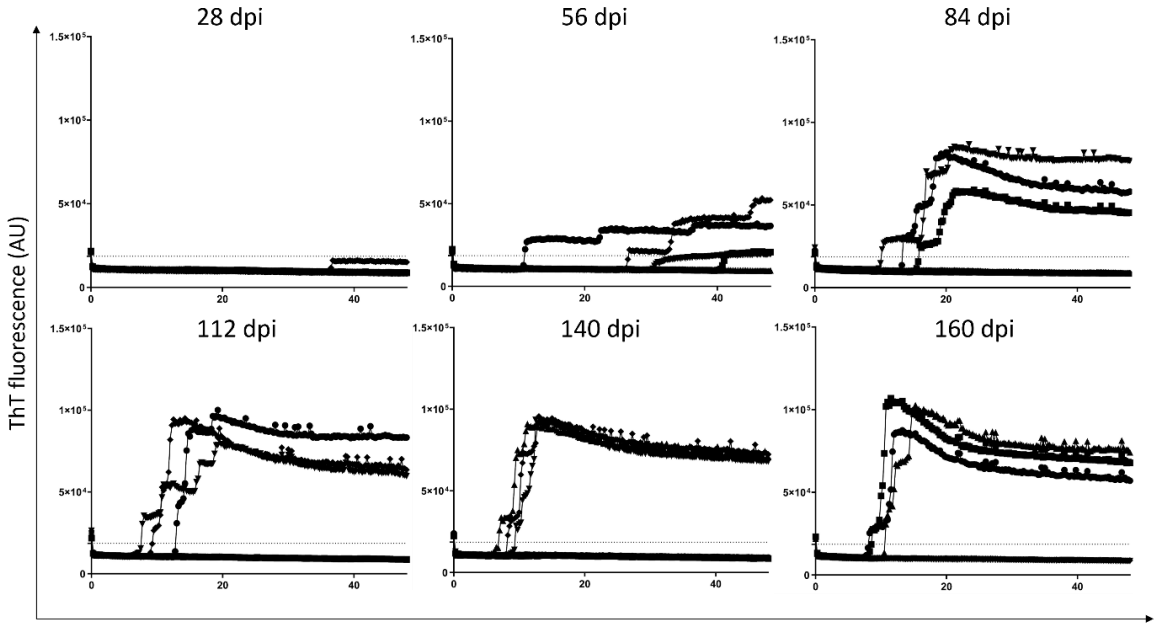

Figure 24. RT-QuIC detection of prion seeding activity in brain at 5x10^{-6} dilution from mice with intracerebral inoculation with RML prions. Samples were analyzed in quadruplicates over 48 hrs utilizing rHAPrP90-231 as a substrate. Traces in every graph show the mean of four wells for every mouse (n=5) that was sacrificed at given time. The dotted line represents threshold for the RT-QuIC positivity. The clear positive seeding activity for all three RML mice was detected 84 dpi. Some low positive seeding activity with long lag phase was detected also 56 dpi, however the signal was lower. Two mice in every cage gave ThT signal that was considered as negative.
AU - arbitrary units, dpi – days post inoculation

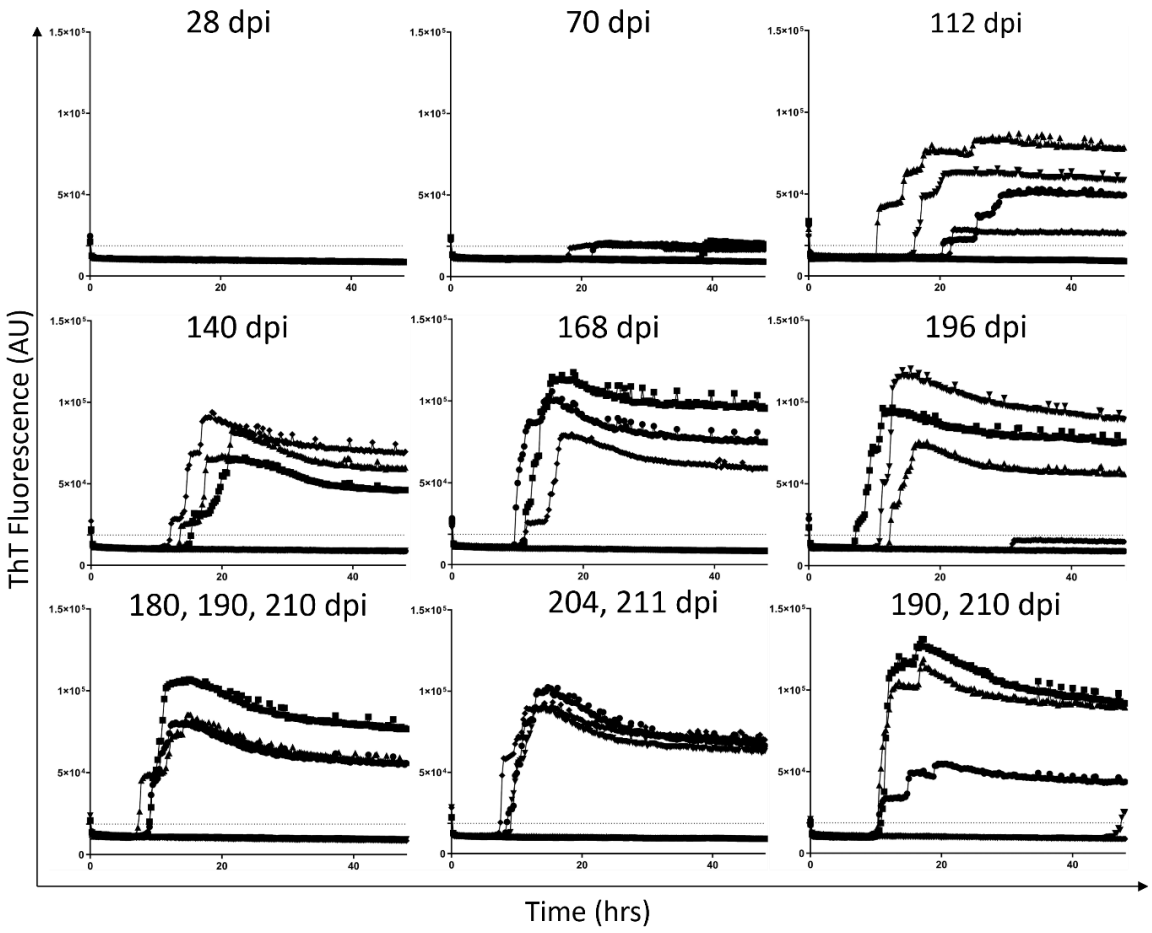

Figure 25. RT-QuIC detection of prion seeding activity in brain at 5x10^{-6} dilution from mice with subcutaneous inoculation with RML prions. Samples were analyzed in quadruplicates over 48 hrs utilizing rHAPrP90-231 as a substrate. Traces in every graph show mean of four wells for every mouse (n=5) that was sacrificed at given time. The dotted line represents threshold for the RT-QuIC positivity. Positive seeding activity in all three RML inoculated mice was detected 112 dpi. Some low seeding positivity was also detected 70 dpi, however the signal was just above the threshold. One control mouse inoculated with normal brain homogenate gave positive signal in one well at 112 dpi.
AU – arbitrary units, dpi – days post inoculation

4.8.3 Detection of prion seeding activity in mouse skin tissue by RT-QuIC

Analysis of prion seeding activity in skin samples of mice was, as expected, more complex when compared to the brain tissue. Skin was analyzed 1000x diluted using rHAPrP90-231 as a substrate for the RT-QuIC reaction. Samples that exhibited prion seeding activity only in one well or gave unclear ThT signal were reanalyzed and the mean signal from all 8 wells was calculated and used for the analysis. The threshold (51,073 AU) was determined from the mean max ThT values of all mice (n=5) in control group plus five SD.

In the first group, within mice inoculated intracerebrally, the positive ThT fluorescence signal was detected 140 dpi with the highest max ThT fluorescence (10.7x10^4) (Fig. 26A). The corresponding time to threshold was 12.5 hrs. At this time, first mice already started showing symptoms, but were not at the terminal stage of disease. Interestingly, mice that were sacrificed

160 dpi gave lower ThT signal although still RT-QuIC positive. Before the 140th day, some mice displayed low prion seeding activity that was below the established threshold (Fig. 27). Three mice showed elevated ThT fluorescent signal ($3x10^4$, $3.9x10^4$, and $4x10^4$) 28 dpi and one mouse gave higher ThT signal ($4.5x10^4$) 84 dpi, but all signals were below the threshold. The RT-QuIC analysis in two control PBS inoculated mice was repeated and confirmed their negative status (Fig. 26A and Supplementary Fig. 2).

Mice with subcutaneous inoculation gave first positive ThT fluorescent signal ($6.9x10^4$ and $10.3x10^4$) in two mice 168 dpi (Fig. 26B), 12 days before the first mouse started showing the clinical symptoms. Corresponding time to threshold was 12.5 and 9 hrs, respectively. All three RML inoculated mice were classified as positive only in cage from which mice were sacrificed 204 dpi and 210 dpi. The highest ThT signal ($13x10^4$) with time to threshold of 11.25 hrs was detected in mouse sacrificed 210 dpi. Some low ThT fluorescence was detected also in other mice, however, signal did not reach the threshold (Fig. 28).

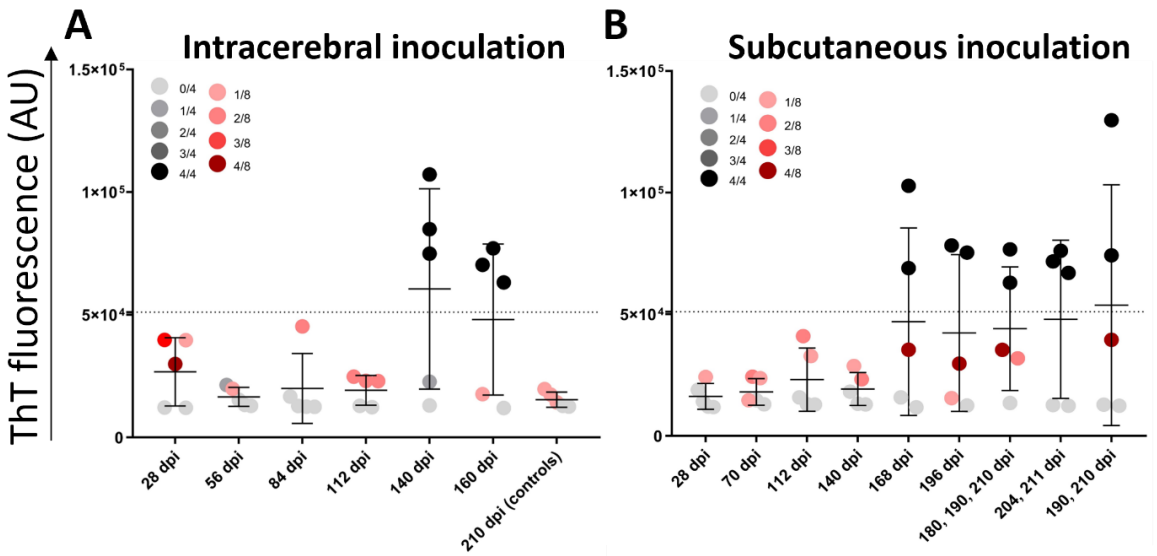

Figure 26. RT-QuIC detection of prion seeding activity in skin samples from mice inoculated with RML prions and from control mice inoculated with PBS, pH 7.4. Dot plot of max ThT fluorescence for every mouse that was sacrificed at given time. Every dot represents the mean max ThT fluorescence from four wells. Bars show the mean ± SD. The dotted line represents the calculated threshold for the RT-QuIC positivity. Intensity of colors shows how many wells were positive for prion seeding activity. Red shades demonstrate samples that were reanalyzed in RT-QuIC. (A) Max ThT fluorescence in skin from mice with intracerebral inoculation. All three RML inoculated mice gave positive result 140 dpi. All control PBS inoculated mice (n=5) remained negative. (B) Max ThT fluorescence in skin from mice with subcutaneous inoculation. RT-QuIC positivity was detected in two mice at 168 dpi. All three mice were positive only in the group sacrificed 204 and 211 dpi.
AU – arbitrary units, dpi – days post inoculation

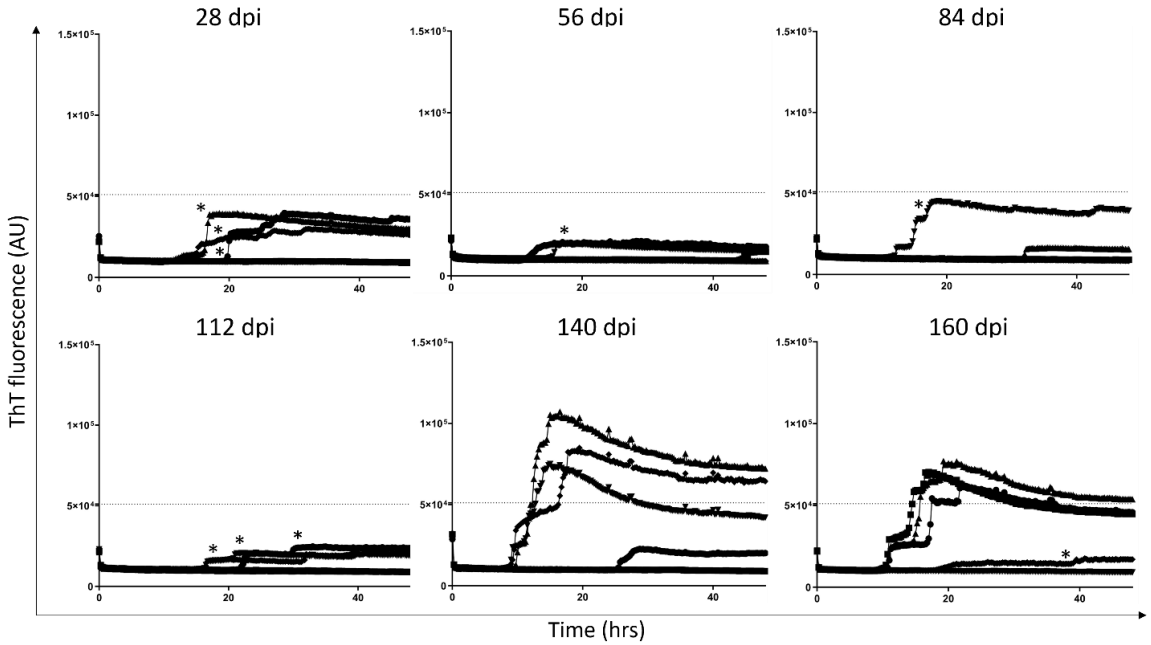

Figure 27. RT-QuIC detection of prion seeding activity in 1000x diluted skin from mice with intracerebral inoculation with RML prions. Samples were analyzed in quadruplicates over 48 hrs utilizing rHAPrP90-231 as a substrate. Traces show the mean from four wells for every mouse (n=5) sacrificed at given time. Samples with only one well positive for prion seeding activity or samples with unclear ThT signal (marked with asterisk) were reanalyzed and the mean from 8 wells was plotted in the graph. The dotted line represents established threshold for the positive outcome of RT-QuIC reaction. All three RML inoculated mice gave positive signal 140 and 160 dpi. Some low prion seeding activity was detected also in other samples, but signal did not reach the threshold.
AU – arbitrary units, dpi – days post inoculation

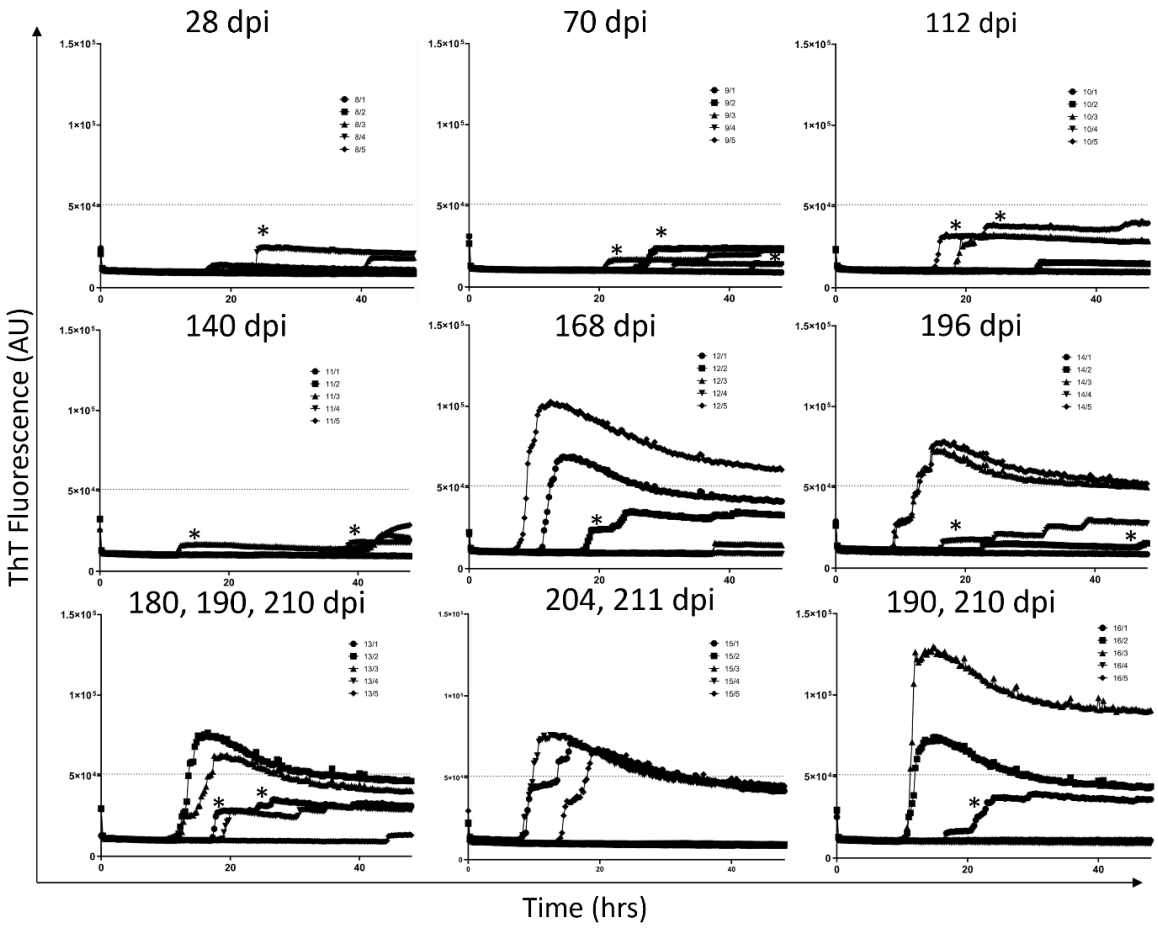

Figure 28. RT-QuIC detection of prion seeding activity in apex head skin samples from mice with subcutaneous inoculation with RML prions. Samples were analyzed in quadruplicates over 48 hrs utilizing rHAPrP90-231 as a substrate. Traces show the mean from four wells for every mouse (n=5) sacrificed at given time. Samples with only one well positive for prion seeding activity or samples with unclear ThT signal were reanalyzed and the mean from 8 wells was plotted in the graph (marked with asterisk). The dotted line represents calculated threshold for the positive outcome of RT-QuIC reaction. First two mice positive for prion seeding activity were detected 168 dpi. All three RML inoculated mice were detected only 204 and 211 dpi.
AU – arbitrary units, dpi – days post inoculation

4.8.4 Detection of prion seeding activity in the skin from the right ear lobule by RT-QuIC

Skin from the right ear lobule was chosen as the second area for the analysis of prion seeding activity, because of its connection to peripheral nervous system. Ear tissue was analyzed in the same manner as the apex head skin. Similarly to the skin, some ear samples gave only one well positive for the seeding activity or very unclear fluorescent signal and were reanalyzed. The mean of 8 wells was determined and used for further analysis in these samples. The threshold (50,182 AU) was calculated from mouse control group (n=5) plus five SD.

Intracerebrally inoculated mice gave positive ThT fluorescent signal in all three RML inoculated mice 140 and 160 dpi (Fig. 29A). The max ThT fluorescent signal ($8.6x10^4$) was detected 140 dpi, similarly to skin samples. The corresponding time to threshold was 9.25 hrs. Two control

mice inoculated with normal brain homogenate remained negative in each group. Mice that were sacrificed earlier than 140 dpi, showed very low prion seeding activity with very long lag phases with more than 20 hrs (Fig. 30). Again, all control mice inoculated with PBS (n=5) gave negative RT-QuIC result (Fig. 29A and Supplementary Fig. 2).

When analyzing mice with subcutaneous inoculation of RML prions, one mouse showed positive ThT signal 140 dpi (Fig. 29B), 20 days before the first mouse started showing symptoms. However, the signal was lower with just threshold RT-QuIC positivity with the max ThT fluorescence of $5.2x10^4$ and prolonged time to threshold of 30 hrs. All three RML inoculated mice displayed positive signal 168 dpi with the max ThT fluorescence of $9.4x10^4$ and the corresponding time to threshold of 9 hrs. Although, the overall max ThT fluorescence ($10.8x10^4$) was detected in mice from last cage that was sacrificed 190 dpi. The corresponding time to threshold was 7.5 hrs. Mice that were sacrificed earlier displayed low prion seeding activity that was below the calculated threshold (Fig. 31).

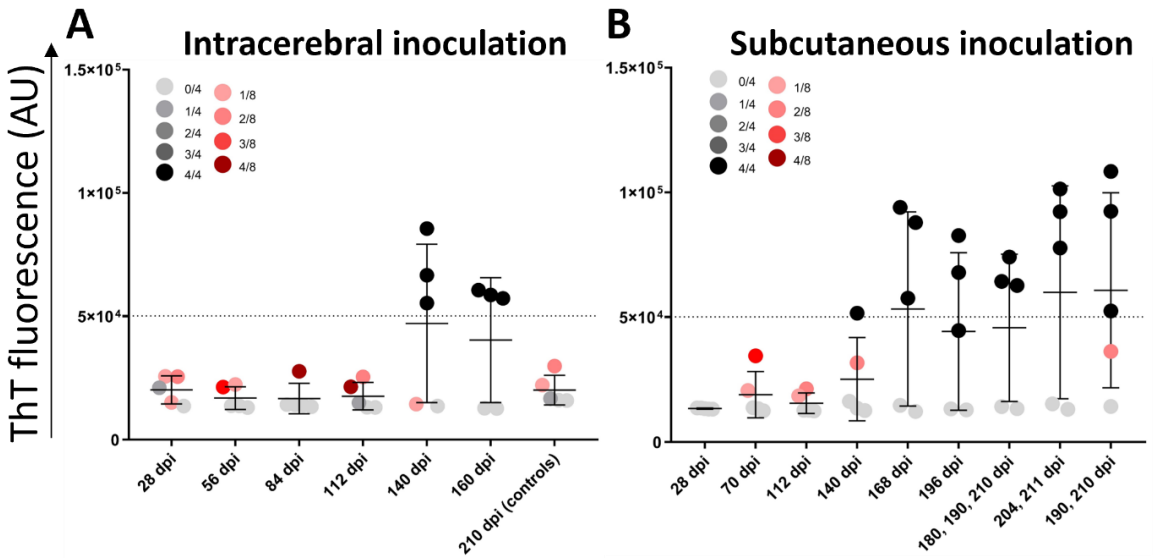

Figure 29. RT-QuIC detection of prion seeding activity in the skin from ear lobule from mice inoculated with RML prion strain and from PBS inoculated control mice. Dot plot of max ThT fluorescence for every mouse that was sacrificed at given time. Every dot represents the mean max ThT fluorescence from four wells. Bars show the mean ± SD. The dotted line represents threshold for the RT-QuIC positivity. Intensity of colors shows how many wells were positive for prion seeding activity. Red shades demonstrate samples that were reanalyzed in RT-QuIC. (A) Max ThT fluorescence in ear lobule from RML intracerebrally inoculated mice. The max ThT signal that was classified as positive was detected 140 dpi and 160 dpi. All control mice (n=5) gave only negative ThT signal. (B) Max ThT fluorescence in ear lobule from subcutaneously inoculated mice. All three RML inoculated mice displayed positive signal after 168 dpi.
AU – arbitrary unit, dpi – days post inoculation

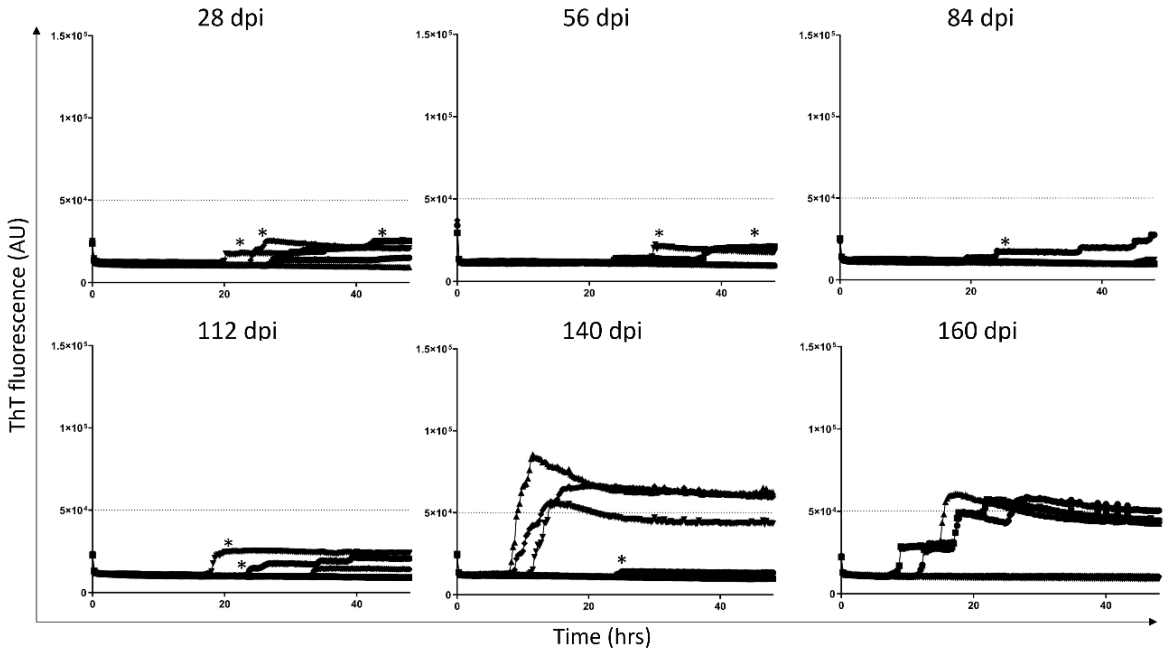

Figure 30. RT-QuIC detection of prion seeding activity in skin from ear lobe from mice intracerebrally inoculated with RML prions. The ear skin **s**amples were examined in quadruplicates utilizing rHAPrP90-231 as a substrate. Each trace represents the mean ThT fluorescence from four wells for every mouse (n=5) sacrificed at the given specific time. Samples with only one well positive for prion seeding activity or samples with unclear ThT signal (marked with asterisk) were reanalyzed and the mean from 8 wells was plotted in the graph. The dotted line shows the calculated threshold. The RML inoculated mice were classified positive only 140 and 160 dpi.
AU – arbitrary units, dpi – days post inoculation

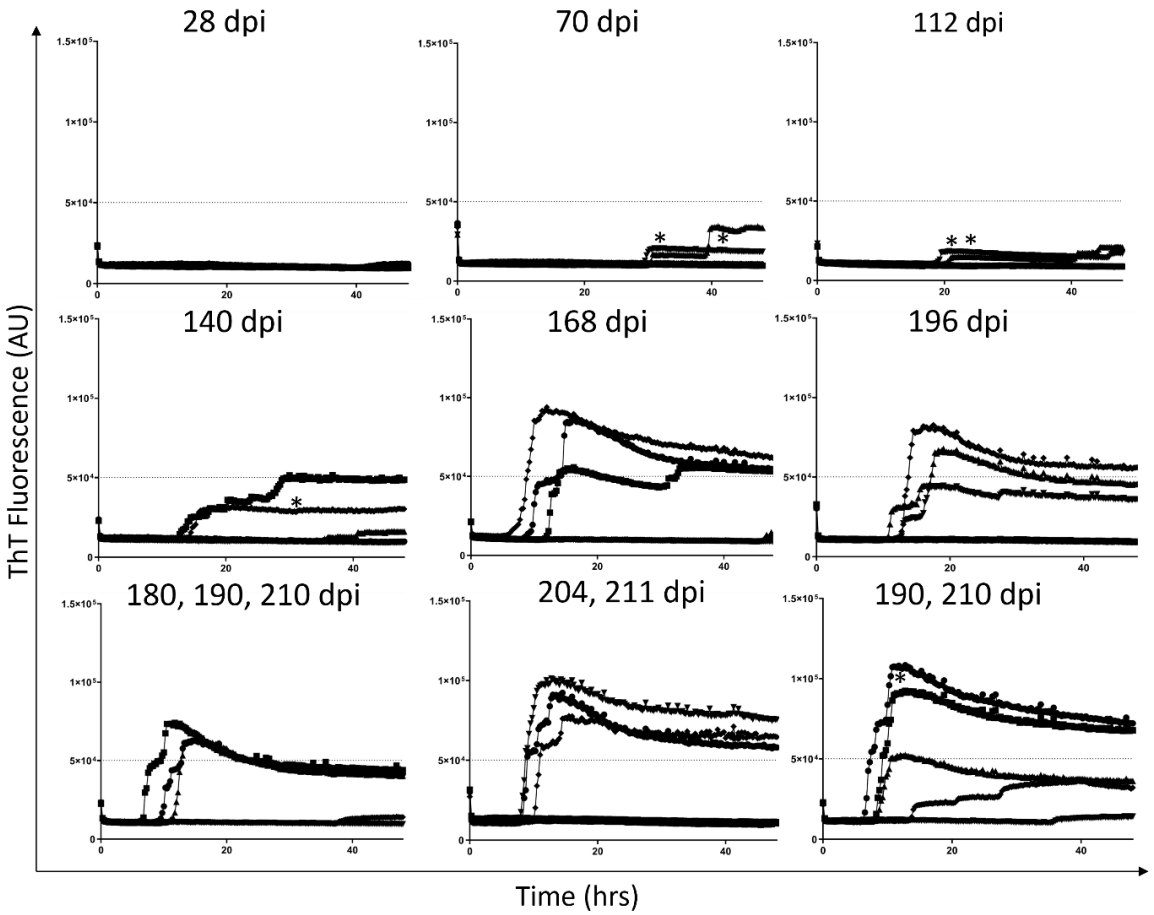

Figure 31. RT-QuIC detection of prion seeding activity in skin from ear lobe from mice subcutaneously inoculated with RML prions. The ear skin samples were examined in quadruplicates over 48 hrs utilizing rHAPrP90-231 as a substrate. Each trace represents the mean ThT fluorescence from four wells for every mouse (n=5) sacrificed at the given specific time. Samples with only one well positive for prion seeding activity or samples with unclear ThT signal (marked with asterisk) were reanalyzed and the mean from 8 wells was plotted in the graph. The dotted line shows the calculated threshold. Mice inoculated with RML were classified positive 168 dpi and later.
AU – arbitrary units, dpi – days post inoculation

4.9 Detection of prion seeding activity in archive formalin-fixed paraffin-embedded brain tissue

To assess the prion seeding activity within archive formalin-fixed paraffin-embedded (FFPE) brain tissue from frontal lobe, a total of 30 TSE and 30 non-TSE FFPE tissue samples were analyzed using RT-QuIC assay protocol for brain homogenates. Samples for the analysis were chosen from individuals that were included in the CSF and skin retrospective study. Characteristics of TSE phenotypes are shown in Table 6. Non-TSE control samples are closely characterized in Supplementary Table 1.

Table 6. Characteristics of analyzed archive FFPE samples from with TSE. The definitive diagnosis of TSE was confirmed by neuropathological examination of brain by immunohistochemistry and western blot during the autopsy.

	n	mean age ± SD	male (n)/ female (n)	mean max. ThT ± SD (AU) x10^4	mean lag time ± SD (hrs)	mean AUC (AU) x10^6
Sporadic TSEs	**27**	**65±7**	**14/13**	**12 ± 2.9**	**4.3 ± 1.7**	**3.8**
MM1	11	75 ± 5	9/2	13 ± 1.7	3.7 ± 1.1	4.1
MM2	2	56, 59	0/2	10; 11	3.25; 7.5	3.3; 3.3
VV1	2	65, 65	0/2	9; 17	2.5; 5.5	3.3; 5.9
VV2	4	68 ± 11	2/2	10 ± 5.3	6.1 ± 2.9	3.2
MV1	3	70 ± 4	1/2	11 ± 3	4 ± 1	3.6
MV2	3	57 ± 12	1/2	12 ± 1.4	3.8 ± 1	3.8
MM1+2	1	63	0/1	8.4	3.75	2.5
VPSPr	1	73	1/0	15	4.5	5
Genetic TSEs	**3**	**70 ± 5**	**1/2**	**9.5 ± 7.1**	**2.75; 3.25**	**2.8**
E200K	2	65, 75	1/1	14; 13	2.75; 3.25	3.6; 4.2
GSS P102L	1	69	0/1	1.5	-	0.6
controls**	**30**	**72 ± 14**	**18/12**	**2.2 ± 1.4**	-	**0.7**

VPSPr – variably protease sensitive prionopathy, GSS – Gerstmann-Sträussle-Scheinker syndrome, AU – arbitrary units
** includes Alzheimer disease (AD), Dementia with Lewy bodies (DLB), frontotemporal dementia (FTLD), vascular dementia (VaD), synucleinopathy (Syn), non-dementia alcoholism (ND-A), lymphoma infiltration, hypoxic/anoxic brain injury (H/ABI), encephalitis/ diffuse large B-cell lymphoma (DLBCL)

10% homogenates from rehydrated tissues were analyzed in end-point dilution 10^{-2} – 10^{-8} (Fig. 32A-G). Prion seeding activity was detected in all FFPE samples from TSE patients up to 10^{-3} dilution, however after that, the seeding activity noticeably decreased. At 10^{-8} dilution, none of the samples exhibited the specific aggregation (Fig. 32G, 33A). Also, the samples showed lower seeding activity at 10^{-2} dilution comparing to 10^{-3}, which could be caused by the presence of inhibitors in the brain tissue. Some of control non-TSE FFPE brain samples showed higher ThT fluorescence signal at 10^{-2} and 10^{-3} dilution, but the signal decreased at higher dilutions (Fig. 33B).

The lowest overlap between the TSE and control groups was seen at 10^{-4} dilution which was chosen for the of RT-QuIC outcome analysis. At 10^{-4}, two TSE (sCJD VV2 and GSS) cases gave ThT fluorescence signal below the threshold while conversely four non-TSE (FTLD-UPS, FTLD-tau, AD and ND-A) cases gave higher ThT fluorescence signal above the SD of the control group and were reanalyzed. After repeating RT-QuIC analysis, the ThT signal increased above the threshold for one TSE sample and in four control samples the signal significantly decreased (as shown in inserted graphs Fig. 33A and B). The mean of eight wells of the reanalyzed non-TSE samples (n=4) was plotted in a graph and the threshold of 71,405 AU was subsequently calculated utilizing all measurements for control group samples. Therefore, the assay demonstrated the sensitivity of 93.3% and specificity of 100%.

At 10^{-4} dilution, the mean max ThT fluorescence for TSE samples was $12\pm3.3x10^4$ with time to threshold 6.3±2.5 hrs. However, the lag time started earlier, after 252 min ~ 4.4 hrs. The mean max ThT fluorescence for non-TSE samples was $2.2\pm1x10^4$ which was six times lower than for TSE cases. The mean AUC for TSE and non-TSE was $3.7x10^6$ and $0.7x10^6$, respectively (Fig. 32C).

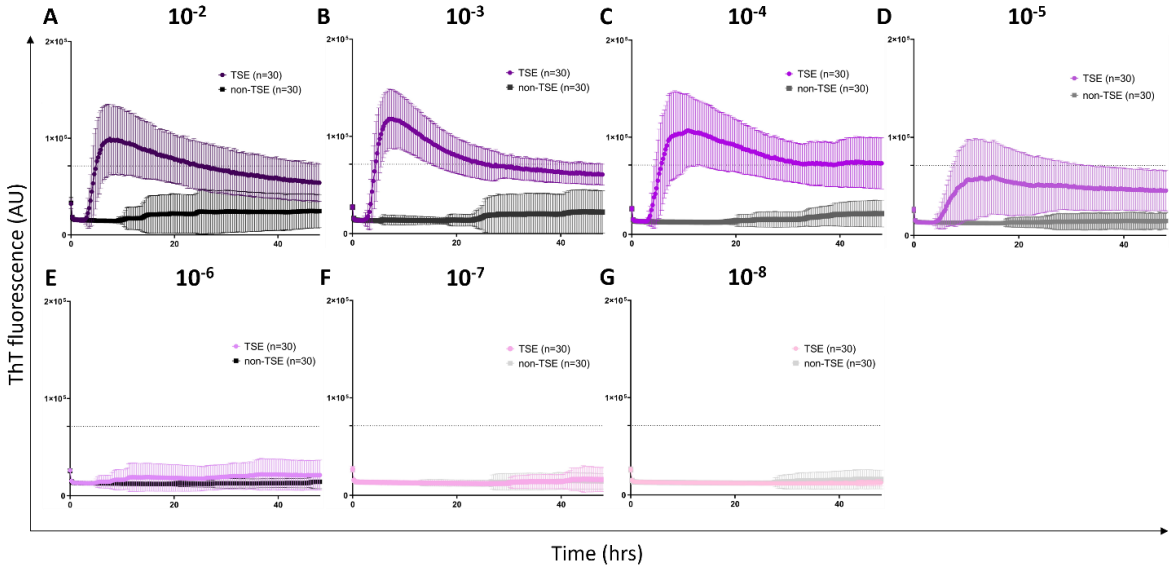

Figure 32. Detection of prion seeding activity in archive formalin-fixed paraffin-embedded (FFPE) brain samples utilizing RT-QuIC. (A-G) Samples were analyzed in end-point dilution 10^{-2} – 10^{-8} in quadruplicates over 48 hrs. Each trace shows the mean ThT fluorescence over the time for TSE (purple, n=30) and non-TSE (black, n=30) samples. The intensity of color signifies the dilution. The dotted line represents the threshold for the positive outcome of the assay. Bars show the standard deviation (SD) for every specific time point.
AU- arbitrary units, TSE – transmissible spongiform encephalopathies

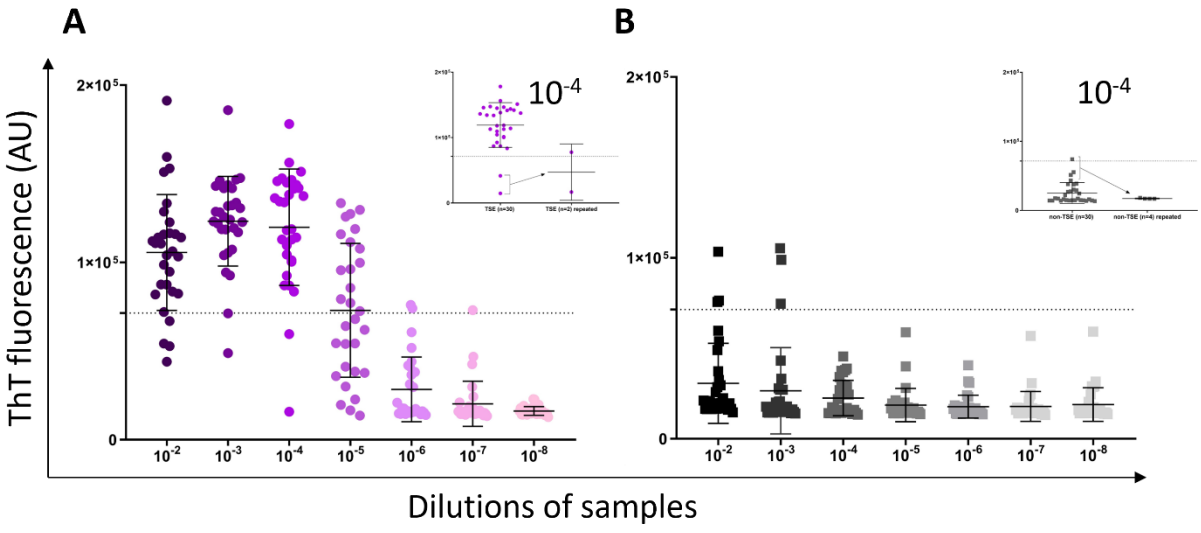

Figure 33. Detection of prion seeding activity in archive formalin-fixed paraffin-embedded (FFPE) brain samples utilizing RT-QuIC. Dot plots of max ThT fluorescence intensity for every sample. Every dot represents the mean max ThT signal from four or eight wells. The sample was considered positive when the signal exceeded the threshold (dotted line). The intensity of color represents decreasing dilution (10^{-2} to 10^{-8}) of the samples. Bars show the mean ± standard deviation (SD) (A) Max ThT fluorescence for TSE (n=30) samples. Best resolution was achieved at 10-4 dilution. Two samples at 10^{-4} gave negative signal and were reanalyzed. The signal for one sample has increased (inserted graph,

left upper corner). The mean of eight wells for these cases (n=2) was plotted in the main graph. (B) Max ThT fluorescence for control non-TSE (n=30) samples. Four samples at 10^{-4} dilution gave higher ThT signal, above the standard deviation (SD). After the RT-QuIC reanalysis, their signal significantly decreased (inserted graph, left upper corner) and the mean of eight wells was plotted in the main graph.

4.10 Retrospective RT-QuIC analysis of samples from patients with rare genetic Creutzfeldt-Jakob disease

Post-mortem samples from two siblings (Table 7) with gCJD and a specific genetic mutation of five octapeptide repeats insertions (5-OPRI, R1-R2-R2-R3-R4-**R2-R2-R3-R3-R4**) in the *PRNP* gene encoding the prion protein were examined for prion seeding activity by RT-QuIC. The analysis was carried out on BH samples from the frontal lobe, ventricular cerebrospinal fluids (CSFs), skin samples, and formalin-fixed paraffin-embedded (FFPE) cerebellum tissues.

Table 7. Characteristics of two siblings with 5-OPRI mutation in PRNP gene. The mutation was confirmed by genotyping and the definite diagnosis was established *post-mortem* at autopsy by immunohistochemistry and western blot.

	Sex	Age	Disease duration	129 codon polymorphisms	Levels of tau and B-amyloid in CSF
Case no. 1	F	54	15 years	MM	normal*
Case no. 2	M	65	12 years	MM	normal*

*tau – <450 pg/ml; B-amyloid – >580 pg/ml (case 1) and >430 pg/ml (case 2) (National Reference Laboratory for Prion Diseases, Thomayer Hospital, Prague)

Firstly, 10% brain homogenates from frontal lobes were analyzed in end-point dilution $5x10^{-6}$ – $5x10^{-12}$ using rHAPrP90-231 as substrate. Sample from the first case gave positive ThT signal, up to $5x10^{-7}$ dilution. The seeding activity was detected also at $5x10^{-8}$ dilution; however, the signal did not achieve the threshold for the positivity. The max. ThT fluorescence was $12x10^{4}$ at $5x10^{-6}$ dilution, which was noticeably lower comparing to the positive control with sCJD MM1 phenotype (Fig. 34A). The time to threshold at the same dilution was 3.5 hrs and the AUC was $3.3x10^{6}$. On the contrary, the sample of the case no. 2 gave no ThT response when analyzed by RT-QuIC assay (Fig. 34B). We repeated RT-QuIC analysis, this time with rBVPrP as a substrate which is supposed to be a universal substrate for gCJD. The sample from the first case showed higher aggregation response when the prion seeding activity was detectable even at $5x10^{-9}$ (Fig. 34C). The max ThT fluorescence $18x10^{4}$ at $5x10^{-6}$ dilution and the AUC was $6.1x10^{6}$. Again, the sample from the second case did not show any specific aggregation (Fig. 34D).

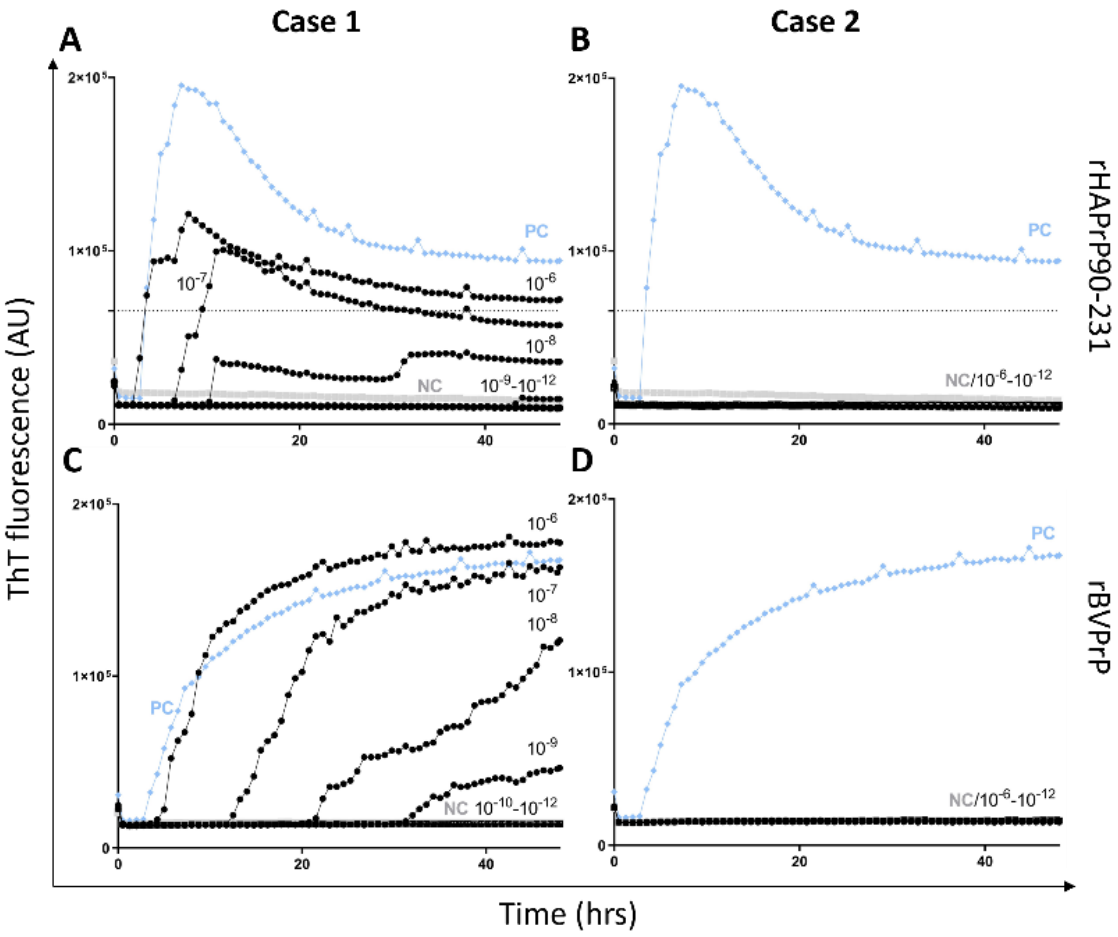

Figure 34. Detection of prion seeding activity in *post-mortem* brain homogenates of sibling patients with gCJD with 5-OPRI in *PRNP* gene. Samples, showed in black, were analyzed in end-point dilution $5x10^{-6}$ – $5x10^{-12}$ in quadruplicates. The traces represent the mean of four wells at every time point. Blue trace shows positive control (PC) sCJD MM1 brain homogenate at $5x10^{-6}$ dilution. Grey trace represents negative control seeded by buffer. The dotted line represents the calculated threshold for the positive RT-QuIC outcome. (A) Prion seeding activity in the brain from the 1st case using rHAPrP90-231 as a substrate. The seeding activity was observed up to $5x10^{-8}$ dilution. (B) Analysis of brain sample from the 2nd case using rHAPrP90-231. No ThT fluorescent signal was observed at any sample dilution. (C) Prion seeding activity in brain sample from the 1st case using rBVPrP as a substrate. The seeding activity was observed up to $5x10^{-9}$ dilution. (D) Analysis of brain sample from the 2nd case using rBVPrP. No ThT fluorescent signal was observed at any sample dilution. rHAPrP90-231 – recombinant prion protein from Syrian hamster (90 – 231 amino acids residues), rBVPrP – recombinant prion protein from (Bank vole full-length), AU – arbitrary units

To confirm the results, we examined archive FFPE of cerebellum tissue, where PrP^{TSE} aggregates were most abundant by immunohistochemistry in both siblings 5-OPRI cases. Rehydrated 10% homogenates were analyzed in end-point dilution 10^{-3} – 10^{-5}. In the first case, the RT-QuIC positivity was observed up to 10^{-4} dilution. At 10^{-5} dilution, some low prion seeding activity was detected, although it did not cross the threshold (Fig. 35A). The max ThT fluorescence at 10^{-3} was $11x10^4$ with TTT corresponding to 5 hrs and the AUC to $3.1x10^6$. For the second case, we were able to confirm negative result without any seeding activity (Fig. 35B).

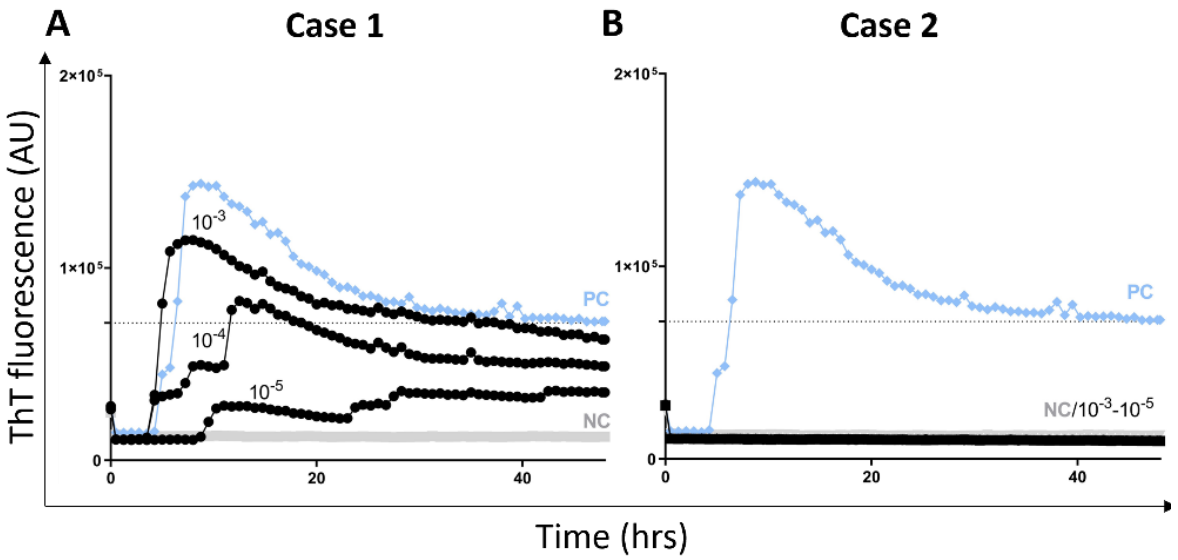

Figure 35. Detection of prion seeding activity in archive FFPE cerebellum samples from sibling gCJD patients with 5-OPRI in *PRNP* gene. Samples, showed in black, were analyzed in dilution 10^{-3} – 10^{-5} in quadruplicates. using rHAPrP90-231 as a substrate. The traces represent the mean of four wells at every time point. Blue trace shows representative positive control at 10^{-3} dilution from FFPE brain homogenate with sCJD MM1 phenotype. Grey trace represents negative control seeded by dilution buffer (PBS, pH 7.4, 1x N-2 supplement, 0.1% SDS). The dotted line represents the calculated threshold for the positive RT-QuIC outcome. (A) Kinetics of prion seeding activity in cerebellum from 1st case. The seeding activity was detected up to 10^{-5} sample dilution. (B) No prion seeding activity was detected in the sample from 2nd case at any dilution.
AU – arbitrary units

Next, ventricular CSF was analyzed either undiluted or 10x diluted using rHAPrP90-231 as a substrate. When analyzing the 1st case, both diluted and undiluted CSF samples gave positive RT-QuIC response. The ThT response for diluted sample was significantly lower, with only threshold positivity (Fig. 36A). The max ThT fluorescence for undiluted and diluted CSF was $19x10^4$ and $10x10^4$, respectively. The TTT was 5.5 hrs for undiluted CSF and 8 hrs for diluted CSF sample. The AUC for undiluted CSF was three times bigger with $6.3x10^6$ AU then for undiluted, which was $2.2x10^6$. The CSF sample from the 2nd case gave negative signal either undiluted or diluted (Fig. 36B).

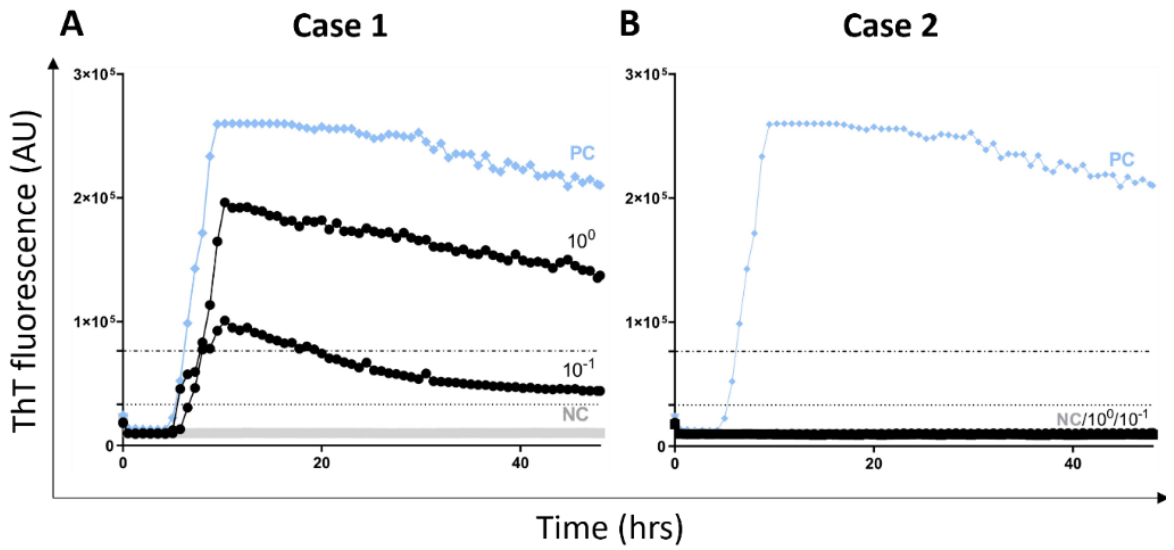

Figure 36. Detection of prion seeding activity in *post-mortem* ventricular cerebrospinal fluid from sibling gCJD patients with 5-OPRI in PRNP gene. Samples, showed in black, were analyzed both undiluted and 10x diluted in quadruplicates over 48 hrs. Samples were analyzed using rHAPrP90-231 as a substrate. The traces represent the mean of four wells at every time point. Blue trace shows representative CSF positive control with sCJD MM1 phenotype. Grey trace represents negative control seeded by dilution buffer (PBS, pH 7.4, 1x N-2 supplement, 0.1% SDS). The dotted line represents threshold for the positive RT-QuIC outcome of undiluted samples and dash-dotted for diluted CSF samples. (A) Kinetics of prion seeding activity in CSF from the 1st case. Both undiluted and diluted samples gave positive RT-QuIC outcome. (B) Analysis of CSF sample from the 2nd case with negative RT-QuIC response.

Finally, we analyzed skin samples obtained at autopsy from the area behind the ear at 10^{-2} dilution. The sample from the 1st case gave threshold positive signal with max ThT response of $10x10^4$ with corresponding TTT of 14.5 hrs. The AUC was $2.4x10^6$ (Fig. 37A). The sample from the 2nd case showed low seeding activity which did not reach the threshold. The max. ThT florescence corresponded to $4.9x10^4$ with AUC of $1.2x10^6$ (Fig. 37B).

To examine whether this low ThT signal was caused by the technical preparation of skin sample or by the presence of low prion seeding activity we reanalyzed newly prepared skin homogenate replicates (R2) by RT-QuIC. With new samples the seeding activity in the 1st case was very low with RT-QuIC response bellow the threshold. The max ThT signal was $3.1x10^4$ with just total AUC of $0.4x10^6$ (Fig. 37A). In the 2nd case, low seeding activity below the threshold was observed again with max ThT of $4x10^4$ and AUC of $0.7x10^6$ (Fig. 37B).

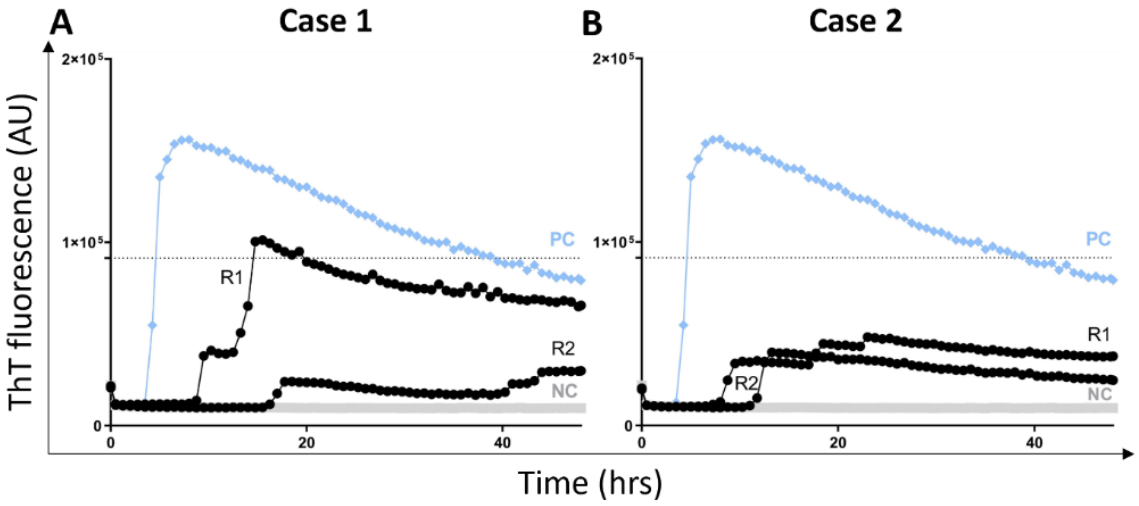

Figure 37. Detection of prion seeding activity in *post-mortem* skin from sibling gCJD patients with 5-OPRI in *PRNP* gene. Skin **s**amples, showed in black, were analyzed 100x diluted in quadruplicates using rHAPrP90-231 as a substrate. The traces represent the mean of four wells at every given time point. Blue traces show representative positive control from skin with sCJD MM1. Grey trace represents negative control seeded by dilution buffer (PBS, pH 7.4, 1x N-2 supplement, 0.1% SDS). The dotted line represents threshold for the positive RT-QuIC outcome. (A) Prion seeding activity in skin from the 1st case. The first replicate (R1) gave threshold positive signal, while the 2nd replicate (R2) gave negative response. (B) Prion seeding activity in skin from the 2nd case. Both replicates (R1 and R2) gave signals below the threshold.

4.11 Patients' cohort analyzed in retrospective analysis of brain and cerebrospinal fluid samples with definitive synucleinopathy

In total, 15 *post-mortem* brain and 14 *post-mortem* ventricular CSF samples were obtained from patients with definitive diagnosis of synucleinopathy during the autopsy (Table 8). Specifically, dementia with Lewy body (DLB, n=6), Alzheimer disease with amygdala Lewy body (AD/ALB, n=3) and patients with Creutzfeldt-Jakob disease and dementia with Lewy bodies (CJD/DLB, n=6) comorbidity. The CSF sample no. 11 from patient with CJD/DLB comorbidity was not provided for analysis. Definite diagnosis of synucleinopathies and other neurodegenerations were confirmed neuropathologically by immunohistochemistry during the autopsy.

The control group for BH consisted of patients with other neurodegenerative diseases (OND, n=17) as well as healthy corneal donors (CD, n=17). The control group for CSF samples consisted of distinct patients with other neurodegenerative diseases (n=18). Detailed characteristics of patients from both BHs and CSF neurological control groups is provided in Supplementary Table 2 and 3.

Table 8. Characteristic, demographic information and the RT-QuIC result of the analyzed patient's cohort. Patients positive for dementia with Lewy body depositions were classified according to Braak and McKeith staging system.

sample	age	sex	definite diagnosis	Braak staging	McKeith staging	RT-QuIC result for BH no SDS/ 0.0005% SDS	RT-QuIC results for CSF $10^0/10^{-1}$
01	83	M	DLB	4	II	+/+	+/+
02	71	M	DLB	6	III	+/+	+/+
03	78	M	DLB	6	III	+/+	+/+
04	74	F	DLB	6	III	+/+	+/+
05	88	F	DLB	5	II	+/+	+/+
06	87	M	DLB	5	III	+/+	+/+
07	97	F	AD (A3B3C3)/ ALB	-	-	+/+	+/+
08	84	F	AD (A3B3C3)/ ALB	-	-	+/+	+/+
09	80	M	AD (A3B3C3)/ ALB	-	-	+/+	+/-
10	60	F	CJD/DLB	3	I	+/+	+/+
11	71	F	CJD/DLB	3	I	+/+	N/A CSF
12	77	M	CJD/DLB	4	II	+/+	+/-
13	70	F	CJD/DLB	6	III	+/+	-/+
14	72	M	CJD/DLB	4	II	+/+	+/+
15	83	F	CJD/DLB	6	III	+/+	+/+

DLB – dementia with Lewy bodies, ALB – amygdala Lewy bodies, CJD – Creutzfeldt-Jakob disease

4.12 Detection of α-syn^D seeding activity in brain homogenate samples using RT-QuIC

To analyze α-syn^D seeding activity in brain, archive 10% BH (n=49) prepared from frontal cortices were tested using two different RT-QuIC conditions.

Firstly, samples were analyzed diluted in PBS, pH 7.4 in end-point dilution 10^{-2} – 10^{-8} using batch of rα-Syn (WT) dialyzed against water in the reaction mix. All *post-mortem* samples showed the positive seeding activity, although the overall signal was relatively low and overlapped with the signal of some controls (Fig. 38A).

In average, all cases gave clear ThT fluorescent signal when diluted up to 10^{-5}. DLB (n=6) cases gave the highest average ThT signal when diluted up to 10^{-4} whereas AD/ALB (n=3) and CJD/DLB (n=6) cases at 10^{-3} dilution (Fig. 39A-C). However, the dispersion of ThT values was the lowest at 10^{-3} dilution.

At 10^{-3} dilution, DLB cases gave the highest mean max ThT fluorescence of 13±1.9x10^4. Only one DLB sample with Braak stage 4 provided lower ThT signal comparing to others. The mean max ThT, for AD/ALB cases was 11±0.6x10^4. Cases with CJD/DLB comorbidity displayed the significantly ($P<0.0061$) lower mean max ThT fluorescence of 9.5±1.8x10^4 when compared to DLB cases (Fig. 38A). The corresponding time to threshold was 24.5±4.6 hrs for DLB, 26±4.2 hrs for AD/ALB and

25±4.2 hrs for CJD/DLB comorbidities. Similarly, area under the curve (AUC) at 10^{-3} dilution was biggest for DLB cases with $3.4x10^6$. AUC for AD/ALB and CJD/DLB samples was $2.9x10^6$ and $2.6x10^6$, respectively (Fig. 39A-C).

Interestingly, some control samples (n=8) also exhibited higher seeding activity when analyzed at 10^{-3} dilution (Fig. 40A). They included corneal donors (CD, n=2); Alzheimer disease (AD, n=4) and Huntington disease (HD, n=2) patients. The archive FFPE brain tissues of these AD and HD patients were reanalyzed by immunohistochemistry and in two AD patients α-syn pathology was found corresponding to ALB and DLB (Fig. 38A, green dots). The mean max ThT fluorescence for CD (n=17) samples was $3±4.6x10^4$ and for OND (n=17) it was $4±4.7x10^4$ (Fig. 38A). The mean time to threshold for false-positive CD samples (n=2) was 30±5 hrs and for OND samples including two unrecognized synucleinopathies (n=6) was 33±12.3 hrs. Mean AUC for CD samples was $1.1x10^6$ and for OND cases it was $1.3x10^6$ (Fig. 40A).

4.12.1 Enhanced detection of the α-syn^D seeding activity in the brain homogenate using RT-QuIC protocol with a low SDS concentration

Because the overall ThT fluorescence of BH samples was relatively low, two minor modifications were introduced to the original protocol to enhance the fluorescent signal. Again, BHs with synucleinopathy (n=15) were analyzed in end-point dilution 10^{-2} – 10^{-8}, however the samples were diluted in PBS (pH 7.4) containing 0.025% SDS, 1x N2-supplement and the rα-Syn (WT) used in the reaction was dialyzed against 40 mM PB (pH 8.0).

Similarly, all the samples with definite synucleinopathy (n=15) gave positive ThT signal suggesting the 100% sensitivity. However, at this setup the fluorescence was noticeably higher, hitting the detection limit of the fluorescent reader (~260 000 RFU) (Fig. 38B). Comparably, in average, DLB cases gave positive ThT signal even when diluted up to 10^{-6}, whereas AD/ALB and CJD/DLB comorbidities at 10^{-4} and 10^{-5} dilution, respectively (Fig. 39D-F). The lowest dispersion of mean ThT max values was noted at 10^{-4} dilution and the analysis was carried out for this sample dilution (data not shown). The calculated threshold (139,707AU) was little bit higher when comparing to RT-QuIC analysis without SDS.

The mean max ThT fluorescence at 10^{-4} dilution was $26±0.5x10^4$ for DLB, $25±1.4x10^4$ for AD/ALB and $26±0.1x10^4$ for CJD/DLB comorbidities (Fig. 38B). Mean time to threshold was also very similar, corresponding to 23±2 hrs for DLB cases, 25±2 hrs for AD/ALB and 25±3 hrs for CJD/DLB. The same pattern was preserved also for the AUC. The biggest AUC of $7x10^6$ corresponded to DLB cases, while the AUC for AD/ALB and CJD/DLB cases was $6.2x10^6$ and $6.3x10^6$ (Fig. 39D-F).

Again, few control samples gave higher fluorescence signal while the overall separation of the signals of positive and control samples improved (Fig. 40B). Five BHs control samples (n=34),

specifically CD samples (n=2) and patients with AD (N=3), analyzed in 10^{-4} dilution gave higher fluorescent ThT signal, therefore corresponding to 85.3% specificity. However, two positive AD samples were, after immunohistological reevaluation, reclassified as comorbidity synucleinopathies improving the assay specificity to 91.2%. One AD sample exhibited higher ThT signal, above the standard deviation, but did not reach the threshold and was classified as negative. The mean max ThT fluorescence for CD (n=17) was $4.5\pm6.8x10^4$ and for OND (n=17) was $6.8\pm5.6x10^4$ (Fig. 38B). The mean time to threshold for false positives was longer when comparing to the first setup of the assay. For CD (n=2) samples it was 36±7 hrs and for OND (n=3) it was 37±4 hrs. However, the mean AUC was comparable to the first setup, with $1x10^6$ for CD samples and $1.5x10^6$ for OND samples (Fig. 40B).

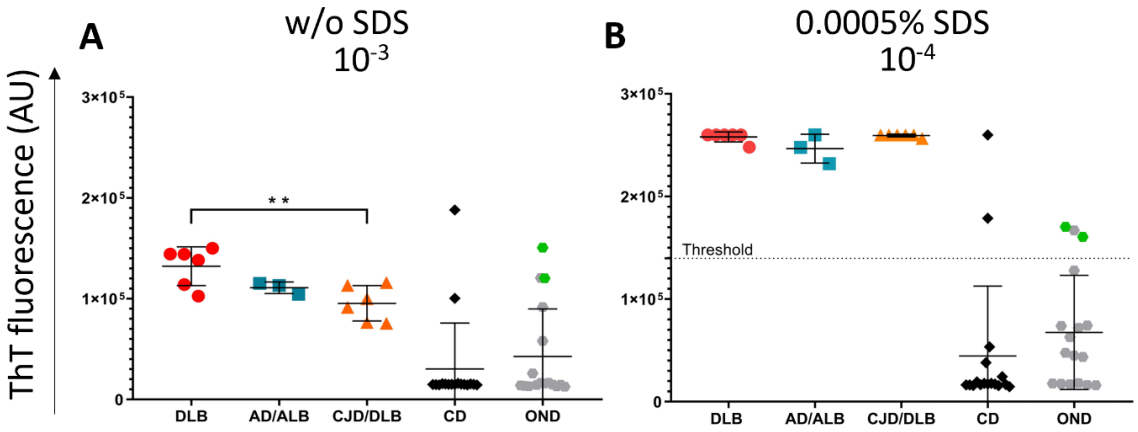

Figure 38. Dot plot of the max ThT fluorescence intensity detected in brain homogenates (BH) using two different RT-QuIC protocols. Synucleinopathies DLB (n=6), AD/ALB (n=3), CJD/DLB (n=6) and control CD (n=17) and OND (n=17) samples were analyzed in quadruplicates and were considered positive when the max ThT signal exceeded the threshold (dashed line). Every dot represents the mean max ThT signal from four wells of the tested sample. Green dots shows samples that were reanalyzed by immunohistochemistry and additionaly diagnosed with secondary synucleinoapthy. Bars show the mean ± standard deviation (SD). (A) The max ThT signal from the samples tested in the absence of SDS at 10^{-3} dilution. (B) The max ThT signal of the same samples tested in the presence of SDS (final concentration of 0.0005%) at 10^{-4} dilution.
AU – arbitrary fluorescence unit
DLB – Dementia with Lewy bodies, AD/ALB – Alzheimer disease/Amygdala Lewy body comorbidity, CJD/DLB – Creutzfeldt-Jakob disease/Dementia with Lewy bodies comorbidity, CD – corneal donors, OND – other neurodegenerative diseases

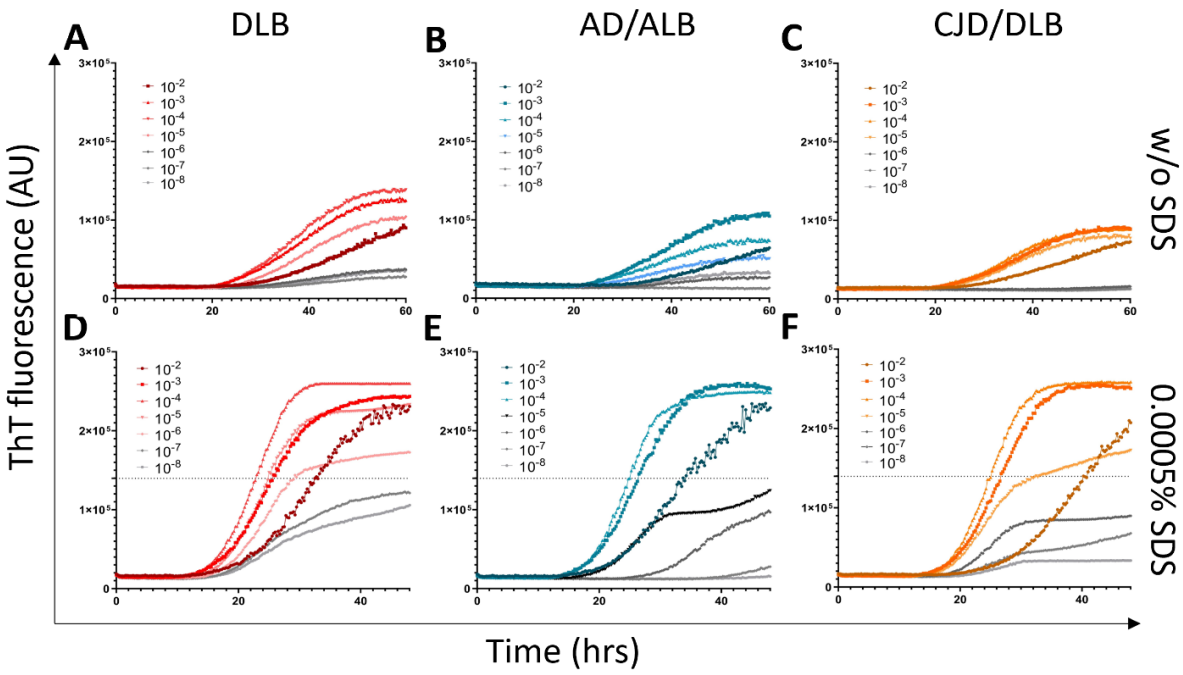

Figure 39: RT-QuIC analysis of α-syn^{D} seeding activity in brain homogenates (BH) by end-point dilution (10^{-2} – 10^{-8}) in the absence or presence of SDS. The samples were tested in quadruplicates and the reaction was seeded with 2 µl of the sample. Each dilution trace represents the mean ThT fluorescence of all tested samples in the experimental group. Dashed lines indicate the threshold of the assay for the positive RT-QuIC result. (A-C) The average kinetics of the α-syn^{D} seeding activity in the absence of SDS for DLB (n=6, red), AD/DLB (n=3, blue) and CJD/DLB (n=6, orange) cases over 60 hrs. (D-C) The enhancement of the mean kinetics of α-syn^{D} seeding activity in the presence of SDS (final concentration of 0.0005%) for synucleinopathy cases over 48 hrs.
AU – arbitrary fluorescence unit
DLB – Dementia with Lewy bodies, AD/ALB – Alzheimer disease/Amygdala Lewy body comorbidity, CJD/DLB – Creutzfeldt-Jakob disease/Dementia with Lewy bodies comorbidity, CD – corneal donors, OND – other neurodegenerative diseases

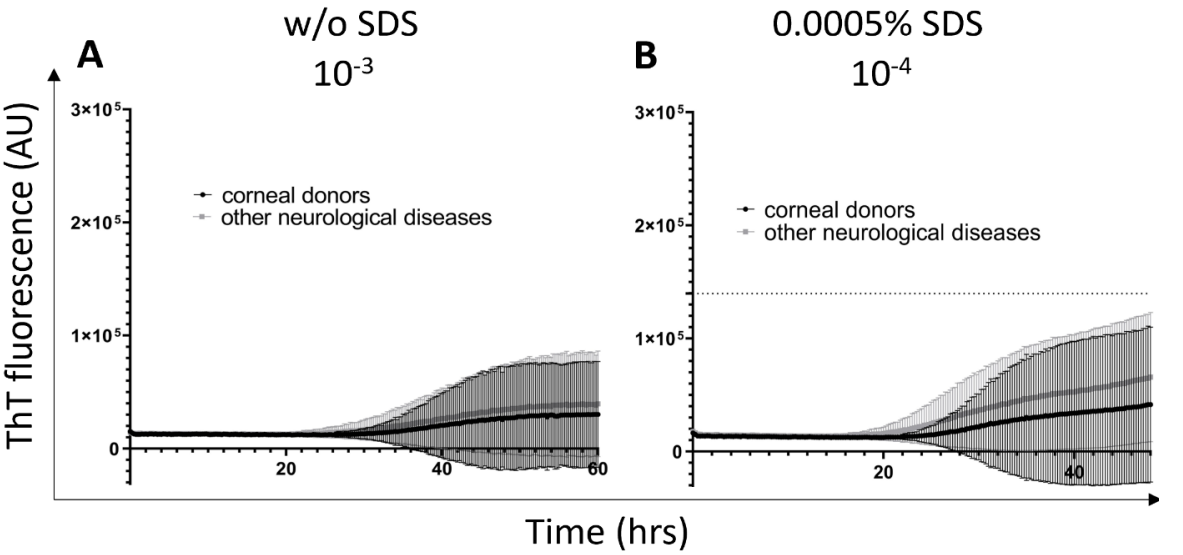

Figure 40: RT-QuIC analysis of α-syn^{D} seeding activity in control brain homogenates (BH) at the cut off dilution in the absence or presence of SDS. Controls samples CD (n=17) and OND (n=17) were analyzed in quadruplicates and the reaction was seeded with 2 µl of the sample. Each trace represents the mean ThT fluorescence ± standard deviation (SD) of all tested samples in the group. Dashed lines indicate the threshold for the positive RT-QuIC result. (A) The average RT-QuIC kinetics of CD (n=17, black) and OND (n=17, grey) in the absence of SDS. Samples were tested at cut off dilution of 10^{-3} over 60 hrs. (B) The average RT-QuIC kinetics of control samples in the presence of SDS (final concentration of 0.0005%). Samples were tested at cut off dilution of 10^{-4} over 48 hrs.

4.13 Detection of α-syn^{D} seeding activity in the ventricular cerebrospinal fluid using RT-QuIC

To validate the seeding activity in CSF, 14 *post-mortem* samples obtained at autopsy were analyzed according to previously published protocol (Groveman *et a*l., 2018). When tested undiluted, one CJD/DLB comorbidity sample did not reach the calculated threshold (56,900 AU) and was classified as negative, indicating 92.9% assay sensitivity. In parallel to BHs, the mean max ThT fluorescence of 20±1x10^{4}, obtained from DLB cases was significantly higher (P<0.0026) comparing to AD/ALB comorbidity samples. For the AD/ALB and CJD/DLB the mean max ThT signal was 11±5x10^{4} and 15.5±8x10^{4}, respectively (Fig. 41A). The mean time to threshold for DLB was 16,5±7 hrs, for AD/ALB was 31±22 hrs and for CJD/DLB 27.5±9 hrs. The AUC for DLB was 7.3x10^{6}, for AD/ALB 3.5x10^{6} and for CJD/DLB it was 4.3x10^{6} (Fig. 42A). Control group consisted only of OND samples (n=18). The specificity corresponds to 83.3% with three samples, specifically two AD cases and one sample not defined, gave ThT signal above the threshold (Fig. 41A). The mean max ThT for undiluted CSF controls was 3.3±2.3x10^{4}. The mean time to threshold for the false positives (n=3) was 17±29 hrs. The mean AUC was 1.4x10^{6} (Fig. 42A).

To decrease the inhibitors of the assay, that are often present in *post-mortem* CSF, the samples were analyzed also diluted 10x in PBS (pH 7.4). However, after the dilution the sensitivity of the assay lowered. One AD/ALB and one CJD/DLB comorbidity did not reach the calculated threshold (85,110 AU), corresponding to 85.7% assay sensitivity. The mean ThT max, for DLB was 23.5±4 .8x10^{4} which was significantly higher (P = 0.048) only when comparing to CJD/DLB comorbidity which mean max ThT was 15.6±6.6x10^{4}. For AD/DLB, it was 16±12.3x10^{4} (Fig. 41B). The mean time to threshold 16.4±3 hrs for diluted DLB samples was almost the same as for the undiluted samples. However, it was noticeably shorter for AD/ALB within 22±10 hrs and for CJD/DLB comorbidities within 24±4 hrs. The mean AUC for diluted samples was 9.5x10^{6} for DLB, 5.8x10^{6} for AD/ALB and 5.4x10^{6} for CJD/DLB samples (Fig. 42B).

The specificity of the assay was higher for diluted CSF samples corresponding to 94.4%. Only one control AD sample gave fluorescence signal above the threshold. The mean max ThT signal for the CSF control group was 3.9±3x10^{4} (Fig. 41B). The time to threshold for the false-positive AD sample was 34 hrs. Finally, the mean AUC was 1.4x10^{6} (Fig. 42B).

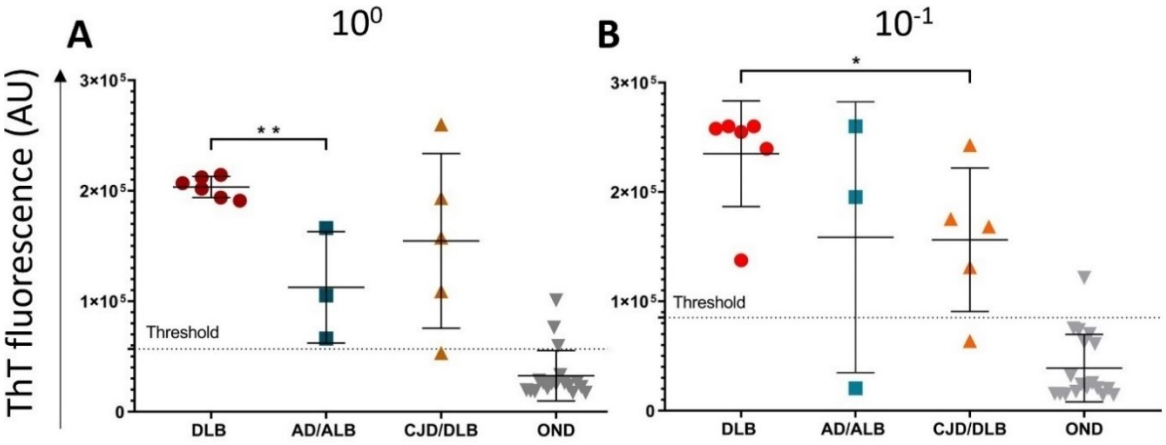

Figure 41: Dot plot of the max ThT fluorescence intensity detected in *post-mortem* CSF samples by α-syn RT-QuIC. Samples were analyzed in quadruplicates and were considered positive when the max ThT signal exceeded the calculated threshold (dashed line). Every dot represents the mean max ThT signal from four wells of the tested sample. Bars show the mean ± standard deviation (SD). (A) The max ThT signal of CSF samples from DLB (n=6), AD/ALB (n=3), CJD/DLB (n=5) and OND (n=18) tested undiluted. (B) The max ThT signal of the same diluted CSF samples with synucleinopathy and controls.

AU – arbitrary fluorescence unit

DLB – Dementia with Lewy bodies, AD/ALB – Alzheimer disease/Amygdala Lewy body comorbidity, CJD/DLB – Creutzfeldt-Jakob disease/Dementia with Lewy bodies comorbidity, OND – other neurodegenerative diseases

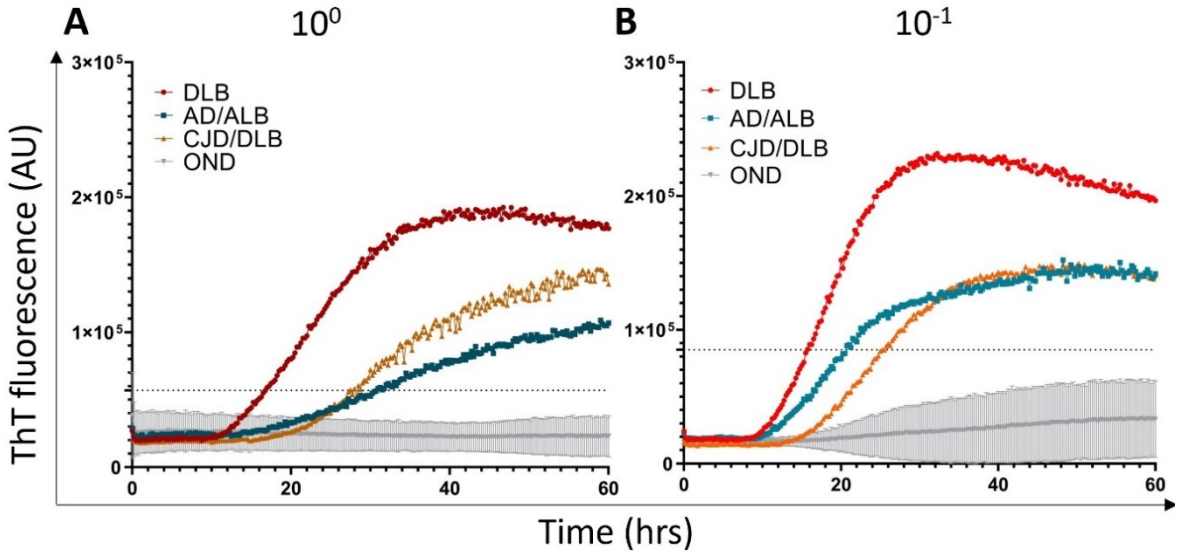

Figure 42: RT-QuIC analysis of α-syn^D seeding activity in *post-mortem* ventricular CSF samples. CSF samples were analyzed in quadruplicates over 60 hrs and the reaction was seeded with 15 µl of the sample. Each trace for the synucleinopathies represents the mean ThT fluorescence and for the control samples the mean ThT fluorescence ± standard deviation. Dashed lines represent the threshold for the positive results. (A) The mean kinetics of α-syn^D seeding activity from DLB (n=6, red), AD/ALB (n=3, blue), CJD/DLB (n=5, orange) and OND (n=18, grey) cases in undiluted CSF. (B) The mean kinetics of α-syn^D seeding activity from the synucleinopathies and control samples in 10x diluted CSF.

AU – arbitrary fluorescence unit

DLB – Dementia with Lewy bodies, AD/ALB – Alzheimer disease/Amygdala Lewy body comorbidity, CJD/DLB – Creutzfeldt-Jakob disease/Dementia with Lewy bodies comorbidity, OND – other neurodegenerative diseases

4.14 Detection of the prion seeding activity in CJD/DLB comorbidity samples

Cases with CJD/DLB comorbidity were also tested for the presence of the prion seeding activity. Both BHs (n=6) and CSF (n=5) samples were analyzed according to previously published

protocol (Moško *et al*., 2021). The threshold for BH (65,413 AU) and CSF undiluted (33,166 AU) and diluted (76,436 AU) samples was calculated for the previous retrospective study done in our laboratory.

BHs were analyzed in end-point dilution $5x10^{-6}$ – $5x10^{-10}$ (Fig. 44A). All BH samples were classified as positive, up to $5x10^{-7}$ dilution, resulting in 100% assay sensitivity. At $5x10^{-8}$ only two samples gave positive ThT signal and at $5x10^{-10}$ dilution none were positive (Fig. 44A). The mean max ThT fluorescent signal at $5x10^{-6}$ dilution was $14.9\pm2.3x10^{4}$ (Fig. 43A) and the mean time to threshold was 4.25±0.7 hrs. The mean AUC for BHs was $4.6x10^{6}$ (Fig. 44A).

Similarly, the sensitivity was 100% for both undiluted and diluted CSF samples. The mean max ThT fluorescence was $15.6\pm5x10^{4}$ for undiluted samples and $11.7\pm3x10^{4}$ for diluted samples (Fig. 43B). The mean time to threshold for undiluted and diluted CSF was very similar, about 6.9±0.8 hrs and 6±1.5 hrs, respectively. The mean AUC for undiluted CSF samples was $5.3x10^{6}$ and for diluted samples it was $3.9x10^{6}$ (Fig. 44B).

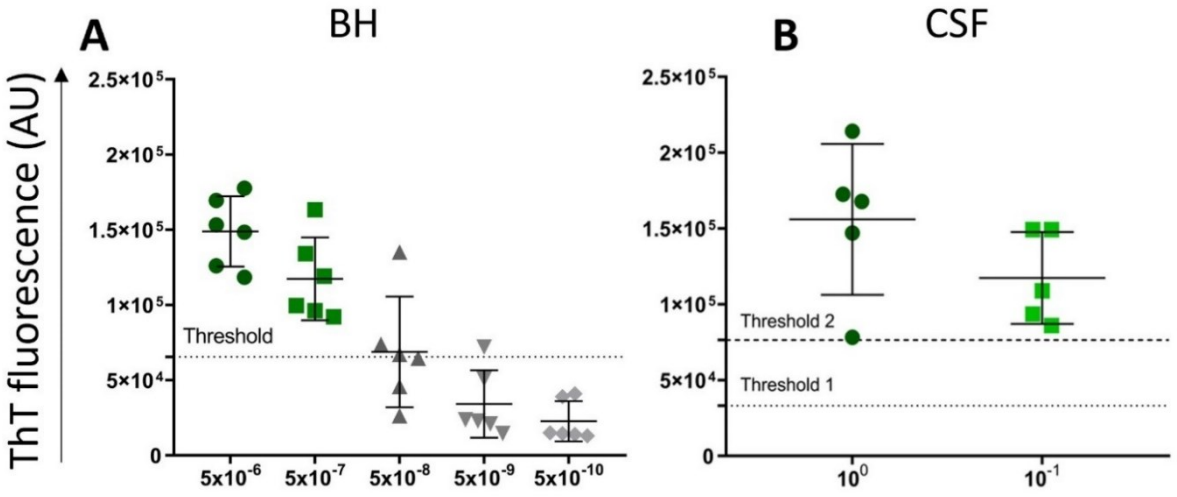

Figure 43: Dot plot of the max ThT fluorescence intensity detected in *post-mortem* BH and CSF samples with CJD/DLB comorbidity using prion RT-QuIC. Samples were analyzed in quadruplicates and were considered positive when the max ThT signal exceeded the threshold (dashed line). Every dot represents the mean max ThT from four wells of the tested sample. Bars show the mean ± standard deviation (SD). (A) The max ThT signal of BH samples (n=6) analyzed in end-point dilution $5x10^{-6}$ – $5x10^{-10}$. (B) The max ThT signal of ventricular CSF samples (n=5) analyzed undiluted or 10x diluted.
AU – arbitrary units

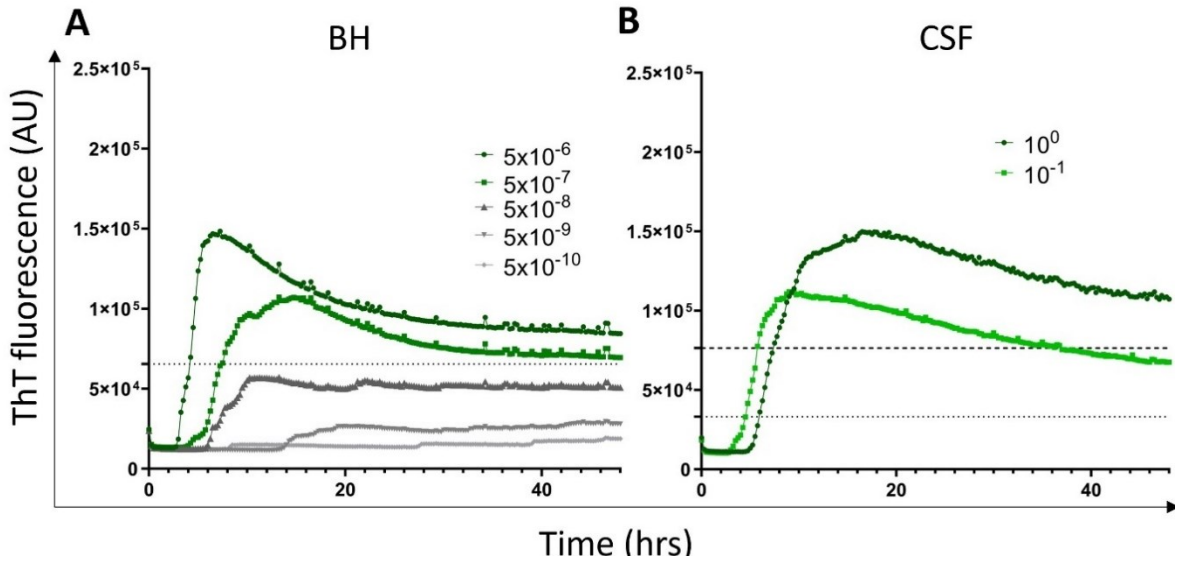

Figure 44: RT-QuIC analysis of prion seeding activity in *post-mortem* BH and CSF samples with CJD/DLB comorbidity. Samples were analyzed in quadruplicates and the reaction was seeded either with 2 µl of BH or 15 µl of CSF into the final volume of 100 µl. Each trace shows the mean ThT fluorescence of all tested samples during the 48 hrs. Dashed lines represents threshold for the positive result. (A) The mean kinetics of prion seeding activity from BHs samples (n=6) analyzed in end-point dilution, $5x10^{-6}$ – $5x10^{-10}$. (B) The mean kinetics of prion seeding activity from CSF samples (n=5) analyzed undiluted or 10x diluted.
AU- arbitrary fluorescence unit
CJD/DLB – Creutzfeldt-Jakob disease/ Dementia with Lewy bodies

5 Discussion

Although many advancements were made in diagnosis of neurodegenerative diseases in the last decade, there is still no reliable definite *ante-mortem* diagnosis of prionopathies and α-synucleinopathies used in clinical practice. To date, many studies demonstrated highly specific and sensitive detection of prion seeding activity and 'prion-like' seeding activity of α-syn utilizing either Protein Misfolding Cyclic Amplification (PMCA) or Real-Time Quaking-Induced Conversion (RT-QuIC) assay. However, great exists variability among the different protocols and the value of these techniques for the diagnosis is intensively debated. To shed a light on the complexity of the diagnosis of neurodegenerations, we analyzed different types of samples using different approaches to exploit the potential of RT-QuIC assay as a diagnostic tool for prionopathies and synucleinopathies.

In our retrospective study (Baranová *et al*., 2024), we have analyzed *post-mortem* CSF and skin samples from patients with definite diagnosis of prionopathy, specifically sporadic and genetic forms of Creutzfeldt-Jakob disease (CJD). Utilization of *ante-mortem* CSF was previously reported in many studies and to date it is the most common type of sample used in RT-QuIC assay (Bongianni *et al*., 2017; Foutz *et al*., 2017; Atarashi 2022). However, the number of studies conducted on *post-mortem* CSF samples is still very limited. The analysis is complicated by the fact, that the composition of *post-mortem* CSF differs from the *intra-vitam* CSF. It is known that the concentration of total protein in CSF can be 20 times higher after the death (Mangin *et al*., 1983). Also, the inhibition of RT-QuIC reaction caused by the contaminants such as cell debris or the high concentration of proteins (more than 2.5 mg/ml) in CSF was reported previously by Mok *et al*. (2021). During our analysis, *post-mortem* CSF samples that gave negative RT-QuIC result undiluted have 1.7 higher concentration of proteins that the positive samples. However, two patients that gave highly positive RT-QuIC result had the highest protein content around 10 mg/ml. Conversely, the samples that gave lower ThT fluorescent signal had lower protein content around 2.5 mg/ml. These results suggests that the inhibition of RT-QuIC reaction is specific in every patient and depends also on the composition of CSF and not solely on its protein concentration. Although, it is not clear what components caused this phenomenon. Some components were shown to inhibit the *in vitro* seeding assays, such as blood or plasma (Orrú *et al*., 2012). However, Hoover *et al*. (2017) also reported the inhibition of prion amyloid formation caused by brain polar lipids and Davenport *et al*. (2018) reported inhibitors in saliva from mucin family.

Based on our previous experiences, we have decided to analyze *post-mortem* CSF samples both undiluted and 10x diluted to avoid false-negative RT-QuIC results. Interestingly, control samples that were 10x diluted gave higher ThT background and three control samples showed

notably elevated ThT fluorescence in one or two wells. However, after repeating RT-QuIC analysis, the max ThT signal of these samples lowered. The threshold for the positive outcome of the RT-QuIC was established from the mean max ThT fluorescence of all control samples plus five standard deviations (SD) calculated separately for undiluted and diluted CSF samples. Utilization of second-generation RT-QuIC assay with rHAPrP90-231 as a substrate led to positive result in less than 20 hours in all tested samples with definite diagnosis of prionopathy. Noticeably, in undiluted samples, the mean time to threshold was longer possibly caused by the presence of inhibitors which could interact with the seeding activity. Only one sample with rare VPSPr gave threshold positive signal even after dilution, with longer time to threshold and the lag phase when comparing to other CJD phenotypes. Similar result for VPSPr cases were demonstrated confirmed also by different studies, where the RT-QuIC response was lower in these cases (Baiardi *et al*., 2022; Uchino *et al*., 2023).

Due to the heterogenous nature of the samples, the analysis of skin was more complex than for the corresponding CSF samples. In previous studies, various body regions like abdomen, thigh, neck, arm, or area behind the ear were examined and the most consistent results were provided from neck and ear areas aligning with our approach in the retrospective study (Orrú *et al*., 2017; Mammana *et al.,* 2020; Xiao *et al*., 2021). The skin was obtained at autopsy from the area behind the ear, before opening the skull to avoid cross-contamination. The skin was prepared for the RT-QuIC by simple tissue lysis using collagenase A as described previously by Orrú *et al*. (2017). The homogenate was 10x diluted before seeding the RT-QuIC reaction.

At the beginning, we assumed that the seeding activity in skin is naturally lower, therefore we utilized the same protocol as for the *post-mortem* CSF samples using higher volume (15 µl) to seed the reaction. However, control samples showed higher fluorescent signal, partially overlapping with the positive samples. To decrease the rate of spontaneous aggregates in the control group and to increase the ThT signal in positive samples, we added N-2 supplement into the samples. N-2 supplement is a commercial product consisting of human recombinant insulin, holo-transferrin, progesterone, putrescine, and selenite and is added to the RT-QuIC reaction to prevent loses of the PrP^{TSE} in higher dilutions. Interestingly, in our experience, it also may provide better outcome of the RT-QuIC reactions, but the mechanistic reason behind this phenomenon is unknown. With this approach, we were able to decrease rate of spontaneous aggregations in the control group, but still the heterogeneity of control group results has prevented calculation of useful threshold for positive reactions. Finally, utilization of just 2 µl of sample to seed the reaction with N-2 supplement led to the marked inhibition of spontaneous aggregation of control group samples while preserving good aggregation response in positive samples. CSF and skin samples were analyzed using the same reader with the exact same settings so we could directly compare the obtained data. The overall ThT fluorescence was noticeably lower after seeding with skin samples when comparing to the

corresponding CSF samples which were often hitting the detection limit of the reader (~260,000 AU). On the contrary, the mean lag phase of skin samples was a little bit shorter than of the undiluted CSF samples. The reason behind these variations is not clear, however, it underlines the complexity of *in-vitro* seeding activity analysis, the possible effect of the analytical matrix and the effect of the template used in the reaction. When analyzing skin samples with definite prionopathy, seven were classified as negative, as their mean ThT fluorescence was lower than the established threshold. After these samples were reanalyzed, three displayed higher prion seeding activity, exceeding the threshold, and improving the sensitivity of the skin RT-QuIC assay to 89.5%. At the same time, six control skin samples gave elevated ThT fluorescent signal, most of them just in one well and with the mean ThT signal safely under the established threshold, suggesting the assay specificity 100%. Only one control skin sample gave elevated ThT signal in all four wells and it was the sample which provided the elevated signal also in all our previous analysis implying that some of the skin samples may on occasion be prone to provide false positive results. After repeating the RT-QuIC analysis within these six samples, their fluorescence signal lowered, confirming 100% assay specificity. Recently, similar sensitivity and specificity utilizing skin samples were reported also in the large-scale study by Zhang *et al*. (2024) utilizing rHAPrP90-231 and rBVPrP (full-length) as substrates.

Surprising findings of our study was that representative *post-mortem* skin mixed samples showed higher SD_{50} in end-point dilution analysis when comparing to the corresponding representative *post-mortem* CSF mixed samples irrespective of the tested CJD type. Our data suggest that the skin homogenate samples contain one order of magnitude higher amount of prion seeding activity that the ventricular CSF. Recently, Xiao *et al*. (2021) reported higher prion seeding activity and RT-QuIC sensitivity (91%) in skin samples comparing to the sensitivity (45%) of CSF samples in living Chinese patients with probable diagnosis of prionopathy.

To further clarify the potential of skin samples in *ante-mortem* diagnosis of prionopathies, we have utilized mouse animal model of prion infection to establish the ability of RT-QuIC to detect prions before the onset of clinical symptoms. RT-QuIC assay was performed utilizing brain and skin tissue (head apex and ear lobe) at different time points after the mice were inoculated either intracerebrally or subcutaneously with RML prion strain or PBS as controls. The assay threshold was calculated from mice control group inoculated intracerebrally with PBS. Similarly, to *post-mortem* human skin, skin samples from the control mice gave slightly elevated fluorescent signal, which resulted in calculation of the higher threshold. Therefore, some samples were classified as negative, even though the presence of prion seeding activity was detected in all four wells, but the mean fluorescence did not reach the threshold. Moreover, infected mice were co-housed in a cage together with control mice to observe the possibility of the cross-contamination between animals.

One control mouse showed positive RT-QuIC signal in brain tissue 112 dpi. The reason behind this finding needs further investigation but our data suggests that cohabitating of RML prions infected and noninfected mice did not lead to presence of detectable prion converting activity in the brains of noninfected mice.

PK-resistant PrP^{TSE} in brain became detectable by WB 84 dpi, 56 days before the first mouse became terminally ill, although the signal was noticeably weaker. The signal became stronger 140 dpi in all three inoculated mice. The prion seeding activity in brain was detectable even earlier (56 dpi) by RT-QuIC assay in two mice which is 84 days before the onset of the symptoms in the first mouse. Interestingly, when analyzing skin samples, some low prion seeding activity was detected as soon as 28 dpi in the skin of three mice. Possible explanation is that it was caused by the contamination of the skin on the head by intracerebrally administered RML inoculum. Alternative explanation that there was rapid replication of PrP^{TSE} in skin is less likely as the signal decreased 56 dpi. Unequivocal positive prion seeding activity in all three i.c. RML inoculated mice was observed 140 dpi, when the mice started to show clinical symptoms. Similarly, Wang *et al*., (2019) also reported detectable prion seeding activity in humanized Tg mice inoculated intracranially with sCJD MM1 prions after 140 dpi (20 wpi), before the terminal stage of the symptoms occurred. Curiously, they were able to detect prion seeding activity in skin samples from the back of 263K-inoculated hamster as soon as 3 wpi. Even though the overall RT-QuIC signal was lower in the ear samples, no difference in the sample's positivity was observed in comparison to the skin samples from the apex of the head.

In subcutaneously inoculated mice, the infection progressed was slower as it was anticipated, and the onset of symptoms was more heterogenous than in i.c. inoculated mice. The PK-resistant PrP^{TSE} was detected in the brain by WB 140 dpi, 40 days before the first mouse started displaying symptoms. However, the RT-QuIC positive prion seeding activity in the brain of all three RML inoculated mice became detectable earlier at 112 dpi. Surprisingly, one control mouse brain sample also showed positive, even though lower, RT-QuIC signal. The positive seeding activity in the skin was first detected in two out of three mice 168 dpi, 12 days before the onset of clinical symptoms, but 56 days after the brain became RT-QuIC positive. All three mice were classified positive only in one cage (204, 211 dpi) suggesting the lower concentration of PrP^{TSE} in the skin from subcutaneously inoculated mice. During the analysis of skin from ear lobe, the first samples positive for RT-QuIC was detected in one mouse out of three 140 dpi, 40 days before the onset of clinical symptoms.

Our results indicate, differences in the spread of PrP^{TSE} and prion converting activity in intracerebrally and subcutaneously inoculated mice. The course of the disease in intracerebrally inoculated mice was faster and the RT-QuIC positive prion seeding activity of the skin (apex and ear

lobe) samples was detected only after the onset of clinical symptoms. On the contrary, in mice inoculated subcutaneously, the spread of prions was slower, but the positive RT-QuIC signal was detectable shortly before the occurrence of the symptoms.

To further explore the application of RT-QuIC assay in the prion research, we aimed to establish a method utilizing archive formalin-fixed paraffin-embedded brain samples. This approach would allow us to investigate the prion seeding activity in different parts of the brain, that are not usually available as frozen brain homogenates. Moreover, it should enable deeper analysis of archival samples from different, rare phenotypes of prionopathies over longer period. In our retrospective study, we examined corresponding FFPE brain samples from patient's cohort of the CSF/skin study. Overall, 30 TSE and 30 non-TSE FFPE microtone sections were processed and analyzed in end-point dilution by RT-QuIC assay. The seeding activity was confirmed in all TSE samples, although not every sample gave positive RT-QuIC outcome. The RT-QuIC analysis of two TSE (VV2 and GSS) samples that gave negative results due to not reaching the positivity threshold and four non-TSE samples with elevated fluorescent signal was repeated. The results improved in non-TSE control samples, indicating that higher non-specific ThT signal in control samples could be caused by technical origin while processing wax curls. Similarly, previously negative TSE VV2 sample improved and gave threshold positive signal when RT-QuIC was repeated. However, the GSS sample remained negative in both runs. Interestingly, also the skin sample of this GSS patient was negative in RT-QuIC, suggesting the lower converting activity or concentration of PrP^{TSE} in these samples. Noteworthy observation was the shift in the range of the dilutions in which the seeding activity was detectable. In FFPE samples the prion seeding activity was observed from the lowest dilution of 10^{-2}. On the contrary, when analyzing frozen brain homogenates, the seeding activity at dilution of 10^{-2} is presumably inhibited by the high concentration of inhibitors that are present in the brain tissue (Henderson *et al*., 2015). In comparison, the lowest dilution of $5x10^{-6}$ is standardly used in our laboratory when analyzing frozen brain tissues. Therefore, we assume that some inhibitors are being removed during the washes of xylene and ethanol during the sample preparation. However, discussion of what exactly cause this inhibition is still ongoing. To our best knowledge, only Hoover *et al*. (2016) previously reported detection of prion seeding activity in FFPE obex samples from deer infected with chronic wasting disease by RT-QuIC. Similarly, to our results, they also observed seeding activity in lower dilutions comparing to frozen brains. However, more studies were conducted on FFPE samples to confirm the seeding activity of $\alpha\text{-syn}^{D}$ in brain, skin, submandibular glands, and even in gastrointestinal tract (Manne *et al*., 2020; Shin *et al*., 2022).

Genetic prion diseases are historically divided into three main groups (gCJD, GSS, and FFI) based on the clinical and neuropathological findings, although this does not cover the whole spectrum of diverse phenotypes caused by different mutations in *PRNP* gene (Kim *et al*., 2018; Mok

et al., 2021). Specifically, rare octapeptide repeats insertion and novel Y163X mutation (Capellari *et al*., 2018) cause a great phenotype heterogeneity which make their diagnosis much more difficult. Moreover, the RT-QuIC sensitivity examined in rare genetic prionopathies varies between laboratories (Orrú *et al*., 2015; Shi *et al*., 2021). Therefore, we analyzed the prion seeding activity in frontal lobe, cerebellum, ventricular CSF, and skin samples from two siblings (case 1 and 2) diagnosed with a novel 5-OPRI mutation (Schmitz *et al*., 2017). The course of the disease presented as a slow cognitive decline for over more than 10 years in both siblings. The tissue samples from the case 1 gave clear positive RT-QuIC results in every tested sample with exception of the skin. Strikingly, all samples from the case 2 gave negative RT-QuIC results. We confirmed this negative result utilizing also rBVPrP (full-length) substrate in the RT-QuIC reaction, which was considered as a universal substrate for gCJD (Orrú *et al*., 2015). Moreover, we also decided to examine prion seeding activity in FFPE cerebellum which was according to the immunohistochemistry evaluation the most affected area in the brain. Still, in the case 2 no seeding activity was detected. The only sample that showed ambivalent prion seeding activity was skin sample. Skin was analyzed as two separate biological replicates. When comparing to classical sCJD MM1 skin, the sample from case 1 with 5-OPRI gave lower ThT signal with longer lag phase and the second replicate displayed just low ThT fluorescence below the threshold. The findings suggest that skin samples from individuals with OPRI exhibit reduced prion seeding activity, indicating a diminished suitability of skin as diagnostic specimens in OPRI cases. Similar low seeding activity below threshold was observed also in the skin sample from the case 2. It is not clear, if it was caused by spontaneous aggregation or by the low level of PrP^{TSE} present in the skin. Similarly, Mok *et al*. (2021) reported negative RT-QuIC assay in two patients with 4-OPRI and in one patient out of three with 6-OPRI mutations utilizing rBVPrP substrate. Later, the same group reported different patients with 5-OPRI and 6-OPRI with negative presymptomatic RT-QuIC prion seeding activity in CSF using both rBVPrP and recombinant human prion protein with P102L mutation (rHuPrP P102L) as a substrate (Mok *et al*., 2023). Moreover Hamada *et al*. (2023) described two siblings with 5-OPRI mutation with long disease duration (more than 10 years) that both displayed negative RT-QuIC seeding activity. On the other hand, the positive seeding activity was detected in tears from patient with 5-OPRI mutation utilizing rHuPrP with E200K mutation as a substrate (Schmitz *et al*., 2023). These ambivalent results indicate great heterogeneity not only between the clinical onset and symptoms but perhaps also in prion characteristics present in individual gCJD OPRI patient.

Our next aim was to establish RT-QuIC assay for synucleinopathies in our laboratory. Previously was RT-QuIC for prions successfully adapted to synucleinopathies utilizing brain, CSF, olfactory mucosa, skin, or colon tissue (Bargar *et al*., 2021; Bongianni *et al.,* 2022; Donadio *et al*., 2021; Han *et al.*, 2021). Moreover, to our best knowledge, just limited numbers of studies analyzed

seeding activity of α-syn^{D} in related brains and CSF samples. To examine complexities of co-pathologies we have analyzed archived *post-mortem* BH and CSF samples of patients with primary or secondary, concomitant, synucleinopathy.

Exploiting the approach of Dr. Caughey's lab, at the beginning, we were able to confirm the positive seeding activity for all BH samples. Although we observed quenching of the seeding activity at the lowest BH dilution of 10^{-2}, possibly due to the presence of inhibitors in the brain. The seeding ability of BH was increased at 10^{-3} dilution. This phenomenon, like in prionopathies, occurring in synucleinopathy brains was also observed by others (Chen *et al.* 2022). Still, the overall ThT fluorescence was relatively low, while partially overlapping with the control group samples which was in contrast with other reported studies (Groveman *et al*., 2018; Han *et al*., 2020). Moreover, the lag phases were relatively long when the aggregation of rα-Syn (WT) started only after 20 hrs of the assay. To improve the outcome of the assay for BH samples, we have decided to utilize low conc. of SDS, to accelerate the aggregation and N-2 supplement to prevent loses of α-syn^{D} at higher sample dilutions. Similar approach for BH samples was exploited by Jin *et al*. (2022) who used 0.0006% SDS in the reaction mix. After adding 0.0005% SDS and N-2 supplement, we were able to significantly increase the fluorescence signal and at the same time shorten the lag phase of the RT-QuIC below 20 hours. It is important to note, that because we wanted to compare two conditions of the RT-QuIC reaction, we used the same settings for the fluorescence measurement. Therefore, almost all BH samples with SDS reached the detection limit of the reader and we could not analyze differences between the synucleinopathy groups.

Importantly, we confirmed the presence of 'prion-like' seeding activity in frontal lobe in of patients with Alzheimer disease with amygdala Lewy bodies where no α-syn^{D} deposits were detected by immunohistochemistry. In comparison to classical DLB cases, the seeding activity of α-syn in AD/ALB patients was lower which was also reported by Bentivenga *et al*. (2024) in patients with amygdala predominant LB pathology. Similarly to our results, Jin *et al*. (2022) reported α-syn seeding activity in temporal cortex with AD and LBD pathology. However, it is not clear whether this phenomenon is caused by a new different strain of α-syn present in frontal lobe or by the propagation of the strain that is present in amygdala. Moreover, to our best knowledge, we are the first to analyze both α-synuclein and prion seeding activity in BH with CJD/DLB co-pathology utilizing specific RT-QuIC assays.

Analysis of control group samples utilizing the same assay conditions, did not provide 100% specificity. In OND control group we have observed positive seeding activity not only in some AD samples which is consistent with previous studies (Manne *et al*., 2019; Jin *et al*., 2022; Bongianni *et al*., 2019; Bentivenga *et al*., 2024) but also in both patients with Huntington disease. However, after optimization of the assay, we got positive results only for the same AD patients (Supplementary

Table 2). To rule out the possibility that the seeding activity observed in those AD patients was caused by the presence of α-syn^{D} seeds in brain (Visanji *et al*., 2019), the brain FFPE samples were reanalyzed by immunohistochemistry and different brain areas other than frontal lobe were examined. Indeed, in two AD patients the secondary synucleinopathy was confirmed. The first patient was additionally diagnosed with an early stage of DLB (Braak 3, McKeith 1) with α-synuclein pathology mostly found in the brain stem and the second patient with isolated ALB synucleinopathy. These findings illustrate the power of RT-QuIC assay in possible improvement of standard diagnostic procedures of neurodegenerative diseases that are conducted after the autopsy. Interestingly, in CD control group, we observed two samples that were repeatedly highly RT-QuIC positive. Unfortunately, because organ donors are anonymized and no additional tissues were available, we could not conclude the reason behind the same RT-QuIC positivity.

The RT-QuIC analysis of the corresponding *post-mortem* ventricular CSF samples was more straightforward and the differences between synucleinopathy groups were more significant comparing to BH samples. Based on the previous experiences, we have decided to analyze CSF samples both undiluted and diluted to prevent possible false-negative results caused by the presence of inhibitors (Moško *et al.,* 2021). We have been able to confirm RT-QuIC positive seeding activity in all CSF samples.

Undiluted CSF of DLB cases gave the highest ThT signal with the lowest dispersion of max ThT values, similarly to BH samples. Also, the initiation of aggregation was noticeably faster comparing to AD/ALB and CJD/DLB samples suggesting the presence of higher α-syn^{D} seeding activity. Comparable RT-QuIC results for DLB cases, with very high sensitivity and specificity, were reported by many others in the last years (Fairfoul *et al*., 2016; Rossi *et al*., 2020; Mammana *et al*., 2021). Moreover, we also confirmed positive seeding activity in all *post-mortem* CSF samples with secondary α-synucleinopathies. At first, one CJD/DLB sample did not reach the threshold and was classified as negative, however, after the dilution the sample became positive. Therefore, it is probable that the negative result was caused by the inhibitors of seed amplification. When comparing to DLB samples, the seeding activity was lower and the dispersion of max ThT values was higher specifically in AD/ALB cases. Comparably to our results, Bongianni *et al*. (2019) confirmed seeding activity in 14 out of 15 patients CSF with LBD/AD and in 2 out of 3 patients with CJD/LBD diagnosis. Also, Hall *et a*l. (2022) reported less robust RT-QuIC read outs when testing samples from patients with amygdala or brainstem restricted LB. Analyzing control group samples which consisted of patients with OND, we again observed positive ThT signal in two AD samples and one sample with hypoxic/anoxic brain injury. RT-QuIC positivity in CSF from AD patients was already observed by different groups (Fairfoul et al., 2016; Hall *et al*., 2022; Bentivenga *et al*., 2024) and it is not clear

if this phenomenon is caused by the presence of unrecognized synucleinopathy comorbidity or perhaps by cross seeding of synuclein aggregation by amyloid beta or tau fibrils.

When analyzing diluted *post-mortem* CSF, the average ThT fluorescence for DLB samples increased, however for AD/ALB and CJD/DLB samples we did not observe any significant improvement. After the dilution, the aggregation of α-synuclein was initiated earlier but there was bigger dispersion of max ThT fluorescence values especially for samples with comorbidities. Moreover, one AD/ALB and one CJD/DLB case that were positive when tested undiluted, did not reached the threshold, and were classified as negative, possibly because of dilution of $\alpha\text{-syn}^{D}$ in the sample. From OND control group, only one sample with AD gave the positive signal which could be again caused by the presence of $\alpha\text{-syn}^{D}$.

In conclusion, we confirmed the prion and α-synuclein seeding activity in all *post-mortem* samples with prionopathy or primary/secondary synucleinopathy. More essentially, we observed seeding activity in frontal lobe within brains with amygdala restricted LB. We report high sensitivity and specificity of RT-QuIC adapted for synucleinopathies, although special attention should be paid to cases with Alzheimer disease where $\alpha\text{-syn}^{D}$ can be present due to comorbidity or the aggregation of synuclein substrate may be occasionally initiated by cross seeding on the present amyloid fibrils.

6 Conclusion

As of today, there is still lack of early and reliable diagnosis of neurodegenerative diseases during the patient's lifetime and the definite diagnosis is made only *post-mortem* during the autopsy. Therefore, our main aim of presented dissertation thesis was to examine the prion seeding activity in different types of patient's tissues (brain, CSF, and skin) utilizing ultra-sensitive Real-Time Quacking-Induced Conversion assay, to assess its diagnostic potential. Moreover, we established RT-QuIC assay adapted to α-syn^{D} in our laboratory to further investigate the utilization of its 'prion-like' seeding activity for laboratory diagnostics of synucleinopathies. We believe that our efforts contribute to better understanding of diagnostic potential of seed amplification assays which will help to introduce these methods into clinical practice as diagnostic tools for early diagnosis of neurodegenerative diseases.

- We have successfully purified rHAPrP90-231 and rBVPrP (full-length) for prion RT-QuIC assay along with rα-Syn (WT) for the assay adapted to synucleinopathies. Subsequently, we tested the suitability of the purified recombinant protein substrates through quality control assay utilizing RT-QuIC.
- We have confirmed the presence of prion seeding activity in *post-mortem* CSF and corresponding skin samples in the retrospective study. Moreover, we have determined the median seeding dose of CSF and skin samples across various CJD phenotypes.
- We have assessed the diagnostic potential of skin samples in the presymptomatic stage of the disease by analyzing samples (brain, skin from apex and ear lobe) from mice sacrificed at different time points after inoculation. We also compared the differences caused by different inoculation routes.
- We have established RT-QuIC assay employing formalin-fixed paraffin-embedded (FFPE) archive brain tissue.
- We have evaluated prion seeding activity in two siblings with genetic CJD with a novel five octapeptide repeat insertions (5-OPRI) in the *PRNP* gene. We have examined different tissue types (frontal lobe, ventricular CSF, ski and FFPE cerebellum tissue) utilizing different RT-QuIC substrates. We were able to detect positive seeding activity only in one sibling suggesting possible presence of two different prion strains.

- We have established and optimized RT-QuIC assay adapted to detect α-syn^{D} seeding activity in patient's samples.
- We have analyzed α-syn^{D} seeding activity in *post-mortem* BH and CSF from patients with definite primary or secondary synucleinopathy. Moreover, we have detected α-syn^{D} co-pathology in two control patients with definite diagnosis of Alzheimer disease.
- We have confirmed high-diagnostic potential of various tissue types and possible usefulness of RT-QuIC assay in *ante-mortem* diagnosis of prionopathies and synucleinopathies.

7 Literature

ALPER, Tikvah, et al. Does the agent of scrapie replicate without nucleic acid?. *Nature*, 1967, 214.5090: 764-766.

ASKANAS, Valerie, et al. Novel immunolocalization of α-synuclein in human muscle of inclusion-body myositis, regenerating and necrotic muscle fibers, and at neuromuscular junctions. *Journal of Neuropathology & Experimental Neurology*, 2000, 59.7: 592-598.

ATARASHI, Ryuichiro. RT-QuIC as ultrasensitive method for prion detection. *Cell and Tissue Research*,2023, 392.1: 295-300.

ATARASHI, Ryuichiro, et al. Ultrasensitive detection of scrapie prion protein using seeded conversion of recombinant prion protein. *Nature methods*, 2007, 4.8: 645-650.

BAIARDI, Simone, et al. Phenotypic heterogeneity of variably protease-sensitive prionopathy: a report of three cases carrying different genotypes at PRNP codon 129. *Viruses*, 2022, 14.2: 367.

BALESTRINO, Roberta; SCHAPIRA, A. H. V. Parkinson disease. *European journal of neurology*, 2020, 27.1: 27-42.

BALTIC, Svetlana, et al. α-Synuclein is expressed in different tissues during human fetal development. *Journal of Molecular Neuroscience*, 2004, 22: 199-203.

BARAL, Pravas K., et al. Transition of the prion protein from a structured cellular form (PrPC) to the infectious scrapie agent (PrPSc). *Protein Science*, 2019, 28.12: 2055-2063.

BARANOVÁ, Soňa, et al. Detection of prions in matching post-mortem skin and cerebrospinal fluid samples using second-generation real-time quaking-induced conversion assay. *Scientific Reports*, 2024, 14.1: 6294.

BARGAR, Connor, et al. Streamlined alpha-synuclein RT-QuIC assay for various biospecimens in Parkinson's disease and dementia with Lewy bodies. *Acta neuropathologica communications*, 2021, 9: 1-13.

BENTIVENGA, Giuseppe Mario, et al. Performance of a seed amplification assay for misfolded alpha-synuclein in cerebrospinal fluid and brain tissue in relation to Lewy body disease stage and pathology burden. *Acta Neuropathologica*, 2024, 147.1: 18.

BERNARDI, Livia; BRUNI, Amalia C. Mutations in prion protein gene: pathogenic mechanisms in C-terminal vs. N-terminal domain, a review. *International Journal of Molecular Sciences*, 2019, 20.14: 3606.

BEYER, Katrin, et al. Identification and characterization of a new alpha-synuclein isoform and its role in Lewy body diseases. *Neurogenetics*, 2008, 9: 15-23.

BINOLFI, Andrés, et al. Interaction of α-synuclein with divalent metal ions reveals key differences: A link between structure, binding specificity and fibrillation enhancement. *Journal of the American Chemical Society*, 2006, 128.30: 9893-9901.

BONGIANNI, Matilde, et al. Diagnosis of human prion disease using real-time quaking-induced conversion testing of olfactory mucosa and cerebrospinal fluid samples. *JAMA neurology*, 2017, 74.2: 155-162.

BONGIANNI, Matilde, et al. α-Synuclein RT-QuIC assay in cerebrospinal fluid of patients with dementia with Lewy bodies. *Annals of clinical and translational neurology*, 2019, 6.10: 2120-2126.

BONGIANNI, Matilde, et al. Olfactory swab sampling optimization for α-synuclein aggregate detection in patients with Parkinson's disease. *Translational neurodegeneration*, 2022, 11.1: 37.

BOUGARD, Daisy, et al. Detection of prions in the plasma of presymptomatic and symptomatic patients with variant Creutzfeldt-Jakob disease. *Science translational medicine*, 2016, 8.370: 370ra182-370ra182.

BRAAK, Heiko, et al. Staging of brain pathology related to sporadic Parkinson's disease. *Neurobiology of aging*, 2003, 24.2: 197-211.

BROWN, H. R., et al. The mRNA encoding the scrapie agent protein is present in a variety of non-neuronal cells. *Acta neuropathologica*, 1990, 80: 1-6.

BROWN, Paul, et al. Iatrogenic Creutzfeldt-Jakob disease, final assessment. *Emerging infectious diseases*, 2012, 18.6: 901.

CAPELLARI, Sabina, et al. Two novel PRNP truncating mutations broaden the spectrum of prion amyloidosis. *Annals of clinical and translational neurology*, 2018, 5.6: 777-783.

CASTILLA, Joaquín, et al. Crossing the species barrier by PrPSc replication in vitro generates unique infectious prions. *Cell*, 2008, 134.5: 757-768.

CAUGHEY, Byron, et al. Pathogenic prion structures at high resolution. *PLoS Pathogens*, 2022, 18.6: e1010594.

CHOHAN, Gurjit, et al. The role of cerebrospinal fluid 14-3-3 and other proteins in the diagnosis of sporadic Creutzfeldt–Jakob disease in the UK: a 10-year review. *Journal of Neurology, Neurosurgery & Psychiatry*, 2010, 81.11: 1243-1248.

COLBY, David W.; PRUSINER, Stanley B. Prions. *Cold Spring Harbor perspectives in biology*, 2011, 3.1: a006833.

COLLINGE, John. Mammalian prions and their wider relevance in neurodegenerative diseases. *Nature*, 2016, 539.7628: 217-226.

COON, Elizabeth A.; SINGER, Wolfgang. Synucleinopathies. *CONTINUUM: Lifelong Learning in Neurology*, 2020, 26.1: 72-92.

CRONIER, Sabrina, et al. Detection and characterization of proteinase K-sensitive disease-related prion protein with thermolysin. *Biochemical Journal*, 2008, 416.2: 297-305.

DAVENPORT, Kristen A., et al. Modified protein misfolding cyclic amplification overcomes real-time quaking-induced conversion assay inhibitors in deer saliva to detect chronic wasting disease prions. *Journal of clinical microbiology*, 2018, 56.9: 10.1128/jcm. 00947-18.

DONADIO, Vincenzo, et al. In vivo diagnosis of synucleinopathies: a comparative study of skin biopsy and RT-QuIC. *Neurology*, 2021, 96.20: e2513-e2524.

DUFFY, Philip, et al. Possible person-to-person transmission of Creutzfeldt-Jakob disease. *The New England journal of medicine*, 1974, 290.12: 692-693.

ELFARRASH, Sara, et al. Organotypic slice culture model demonstrates inter-neuronal spreading of alpha-synuclein aggregates. *Acta Neuropathologica Communications*, 2019, 7: 1-16.

EMAMZADEH, Fatemeh Nouri. Alpha-synuclein structure, functions, and interactions. *Journal of Research in Medical Sciences*, 2016, 21.1: 29.

FAIRFOUL, Graham, et al. Alpha-synuclein RT-Qu IC in the CSF of patients with alpha-synucleinopathies. *Annals of clinical and translational neurology*, 2016, 3.10: 812-818.

FERREIRA, Sara A.; ROMERO-RAMOS, Marina. Microglia response during Parkinson's disease: alpha-synuclein intervention. *Frontiers in cellular neuroscience*, 2018, 12: 247.

FIORINI, Michele, et al. High diagnostic accuracy of RT-QuIC assay in a prospective study of patients with suspected sCJD. *International Journal of Molecular Sciences*, 2020, 21.3: 880.

FOUTZ, Aaron, et al. Diagnostic and prognostic value of human prion detection in cerebrospinal fluid. *Annals of neurology*, 2017, 81.1: 79-92.

FRANCESCHINI, A., et al. Regional pattern of microgliosis in sporadic Creutzfeldt-Jakob disease in relation to phenotypic variants and disease progression. *Neuropathology and Applied Neurobiology*, 2018, 44.6: 574-589.

FUJIWARA, Hideo, et al. α-Synuclein is phosphorylated in synucleinopathy lesions. *Nature cell biology*, 2002, 4.2: 160-164.

FULCHER, James M., et al. Enhancing top-down proteomics of brain tissue with FAIMS. *Journal of proteome research*, 2021, 20.5: 2780-2795.

GAJDUSEK, Daniel Carleton; GIBBS, CJ, Jr; ALPERS, Michael. Experimental Transmission of a Kuril-Like Syndrome to Chimpanzees. 1966.

GAMBETTI, Pierluigi, et al. A novel human disease with abnormal prion protein sensitive to protease. *Annals of Neurology: Official Journal of the American Neurological Association and the Child Neurology Society*, 2008, 63.6: 697-708.

GESCHWIND, Michael D. Prion diseases. *CONTINUUM: Lifelong Learning in Neurology*, 2015, 21.6: 1612-1638.

GONZÁLEZ, Nazareno, et al. Effects of alpha-synuclein post-translational modifications on metal binding. *Journal of Neurochemistry*, 2019, 150.5: 507-521.

GRAU-RIVERA, Oriol, et al. Clinicopathological correlations and concomitant pathologies in rapidly progressive dementia: a brain bank series. *Neurodegenerative Diseases*, 2015, 15.6: 350-360.

GREEN, Alison JE. RT-QuIC: a new test for sporadic CJD. *Practical neurology*, 2019, 19.1: 49-55.

GRIFFITH, John S. Self-replication and scrapie. 1967.

GRINBERG, Lea Tenenholz, et al. Brainstem pathology and non-motor symptoms in PD. *Journal of the neurological sciences*, 2010, 289.1-2: 81-88.

GROVEMAN, Bradley R., et al. Rapid and ultra-sensitive quantitation of disease-associated α-synuclein seeds in brain and cerebrospinal fluid by αSyn RT-QuIC. *Acta neuropathologica communications*, 2018, 6.1: 1-10.

GROZDANOV, Veselin; DANZER, Karin M. Intracellular alpha-synuclein and immune cell function. *Frontiers in Cell and Developmental Biology*, 2020, 8: 562692.

HALL, Sara, et al. Performance of αSynuclein RT-QuIC in relation to neuropathological staging of Lewy body disease. *Acta neuropathologica communications*, 2022, 10.1: 90.

HAMADA, Shinsuke, et al. Genetic Creutzfeldt–Jakob disease with 5-octapeptide repeats presented as frontotemporal dementia. *Human Genome Variation*, 2023, 10.1: 10.

HAN, Jung-Youn, et al. RT-QuIC-based detection of alpha-synuclein seeding activity in brains of dementia with Lewy Body patients and of a transgenic mouse model of synucleinopathy. *Prion*, 2020, 14.1: 88-94.

HAN, Jung-Youn; SHIN, Chaewon; CHOI, Young Pyo. Preclinical detection of alpha-synuclein seeding activity in the colon of a transgenic mouse model of synucleinopathy by RT-QuIC. *Viruses*, 2021, 13.5: 759.

HASHIMOTO, Makoto, et al. NACP, a synaptic protein involved in Alzheimer's disease, is differentially regulated during megakaryocyte differentiation. *Biochemical and biophysical research communications*, 1997, 237.3: 611-616.

HASS, Ethan W., et al. Disease-, region-and cell type specific diversity of α-synuclein carboxy terminal truncations in synucleinopathies. *Acta neuropathologica communications*, 2021, 9.1: 146.

HEAD, Mark W., et al. Variably protease-sensitive prionopathy in the UK: a retrospective review 1991–2008. *Brain*, 2013, 136.4: 1102-1115.

HENDERSON, Davin M., et al. Quantitative assessment of prion infectivity in tissues and body fluids by real-time quaking-induced conversion. *Journal of General Virology*, 2015, 96.1: 210-219.

HOLEC, Sara AM, et al. The E46K mutation modulates α-synuclein prion replication in transgenic mice. *PLoS Pathogens*, 2022, 18.12: e1010956.

HOOVER, Clare E., et al. Detection and quantification of CWD prions in fixed paraffin embedded tissues by real-time quaking-induced conversion. *Scientific reports*, 2016, 6.1: 25098.

HOOVER, Clare E., et al. Endogenous brain lipids inhibit prion amyloid formation in vitro. *Journal of Virology*, 2017, 91.9: 10.1128/jvi. 02162-16.

CHATZIKONSTANTINOU, Simela, et al. A meta-analysis on RT-QuIC for the diagnosis of sporadic CJD. *Acta Neurologica Belgica*, 2021, 121: 341-349.

CHEN, Dong-Dong, et al. Application of α-syn real-time quaking-induced conversion for brain and skin specimens of the chinese patients with Parkinson's disease. *Frontiers in Aging Neuroscience*, 2022, 14: 898516.

IRANZO, Alex, et al. Detection of α-synuclein in CSF by RT-QuIC in patients with isolated rapid-eye-movement sleep behaviour disorder: a longitudinal observational study. *The Lancet Neurology*, 2021, 20.3: 203-212.

IRONSIDE, James W.; RITCHIE, Diane L.; HEAD, Mark W. Prion diseases. *Handbook of clinical neurology*, 2018, 145: 393-403.

ISAACS, J. D.; JACKSON, G. S.; ALTMANN, D. M. The role of the cellular prion protein in the immune system. *Clinical & Experimental Immunology*, 2006, 146.1: 1-8.

JHA, Narendra Nath, et al. Complexation of NAC-derived peptide ligands with the C-terminus of α-synuclein accelerates its aggregation. *Biochemistry*, 2018, 57.5: 791-804.

JIN, Yunjung, et al. APOE4 exacerbates α-synuclein seeding activity and contributes to neurotoxicity in Alzheimer's disease with Lewy body pathology. *Acta neuropathologica*, 2022, 143.6: 641-662.

KIM, Mee-Ohk, et al. Genetic PrP prion diseases. *Cold Spring Harbor perspectives in biology*, 2018, 10.5: a033134.

KOO, Hyun-Jung; LEE, Hak-Joo; IM, Hana. Sequence determinants regulating fibrillation of human α-synuclein. *Biochemical and biophysical research communications*, 2008, 368.3: 772-778.

KOVÁCS, Gábor G., et al. Genetic prion disease: the EUROCJD experience. *Human genetics*, 2005, 118: 166-174.

KOVACS, Gabor G., et al. Genetic Creutzfeldt-Jakob disease associated with the E200K mutation: characterization of a complex proteinopathy. *Acta neuropathologica*, 2011, 121: 39-57.

KRAUS, Allison, et al. High-resolution structure and strain comparison of infectious mammalian prions. *Molecular cell*, 2021, 81.21: 4540-4551. e6.

KUPFER, L.; HINRICHS, W.; GROSCHUP, M. H. Prion protein misfolding. *Current molecular medicine*, 2009, 9.7: 826-835.

KUZKINA, Anastasia, et al. Combining skin and olfactory α-synuclein RT-QuIC-towards biomarker-driven phenotyping in synucleinopathies. 2022.

LADOGANA, Anna; KOVACS, Gabor G. Genetic Creutzfeldt–Jakob disease. In: *Handbook of Clinical Neurology*. Elsevier, 2018. p. 219-242.

LATTANZIO, Francesca, et al. Prion-specific and surrogate CSF biomarkers in Creutzfeldt-Jakob disease: diagnostic accuracy in relation to molecular subtypes and analysis of neuropathological correlates of p-tau and Aβ42 levels. *Acta neuropathologica*, 2017, 133: 559-578.

LEGNAME, Giuseppe. Elucidating the function of the prion protein. *PLoS pathogens*, 2017, 13.8: e1006458.

LI, Jia-Yi, et al. Lewy bodies in grafted neurons in subjects with Parkinson's disease suggest host-to-graft disease propagation. *Nature medicine*, 2008, 14.5: 501-503.

LINDGREN, P., et al. Cost of Parkinson's disease in Europe. *European Journal of Neurology*, 2005, 12: 68-73.

LUK, Kelvin C., et al. Exogenous α-synuclein fibrils seed the formation of Lewy body-like intracellular inclusions in cultured cells. *Proceedings of the National Academy of Sciences*, 2009, 106.47: 20051-20056.

LUK, Kelvin C., et al. Pathological α-synuclein transmission initiates Parkinson-like neurodegeneration in nontransgenic mice. *Science*, 2012, 338.6109: 949-953.

MAMMANA, Angela, et al. Detection of prions in skin punch biopsies of Creutzfeldt–Jakob disease patients. *Annals of Clinical and Translational Neurology*, 2020, 7.4: 559-564.

MAMMANA, Angela, et al. RT-QuIC detection of pathological α-Synuclein in skin punches of patients with Lewy body disease. *Movement Disorders*, 2021, 36.9: 2173-2177.

MANGIN, P., et al. Forensic significance of postmortem estimation of the blood cerebrospinal fluid barrier permeability. *Forensic Science International*, 1983, 22.2-3: 143-149.

MANNE, Sireesha, et al. Ultrasensitive detection of aggregated α-synuclein in glial cells, human cerebrospinal fluid, and brain tissue using the RT-QuIC assay: new high-throughput neuroimmune biomarker assay for parkinsonian disorders. *Journal of Neuroimmune Pharmacology*, 2019, 14: 423-435.

MANNE, Sireesha, et al. Blinded RT-QuIC analysis of α-Synuclein biomarker in skin tissue from Parkinson's disease patients. *Movement Disorders*, 2020, 35.12: 2230-2239.

MANNE, Sireesha, et al. α-Synuclein real-time quaking-induced conversion in the submandibular glands of Parkinson's disease patients. *Movement Disorders*, 2020, 35.2: 268-278.

MEAD, Simon, et al. Balancing selection at the prion protein gene consistent with prehistoric kurulike epidemics. *Science*, 2003, 300.5619: 640-643.

MEAD, S., et al. Inherited prion disease with 5-OPRI: phenotype modification by repeat length and codon 129. *Neurology*, 2007, 69.8: 730-738.

MINIKEL, Eric Vallabh, et al. Quantifying prion disease penetrance using large population control cohorts. *Science translational medicine*, 2016, 8.322: 322ra9-322ra9.

MITROVÁ, Eva, et al. Experience with preventive genetic testing of corneal donors in slovakia. *Cornea*, 2011, 30.9: 987-990.

MODA, Fabio, et al. Prions in the urine of patients with variant Creutzfeldt–Jakob disease. *New England Journal of Medicine*, 2014, 371.6: 530-539.

MOK, Tze How, et al. Bank vole prion protein extends the use of RT-QuIC assays to detect prions in a range of inherited prion diseases. *Scientific reports*, 2021, 11.1: 5231.

MOK, Tze How, et al. Seed amplification and neurodegeneration marker trajectories in individuals at risk of prion disease. *Brain*, 2023, 146.6: 2570-2583.

MORALES, Rodrigo; ABID, Karim; SOTO, Claudio. The prion strain phenomenon: molecular basis and unprecedented features. *Biochimica et Biophysica Acta (BBA)-Molecular Basis of Disease*, 2007, 1772.6: 681-691.

MOREL, Etienne, et al. The cellular prion protein PrPc is expressed in human enterocytes in cell-cell junctional domains. *Journal of Biological Chemistry*, 2004, 279.2: 1499-1505.

MOŠKO, Tibor, et al. Detection of prions in brain homogenates and CSF samples using a second-generation RT-QuIC assay: a useful tool for retrospective analysis of archived samples. *Pathogens*, 2021, 10.6: 750

National CJD. Surveillance Unit. Creutzfeldt-Jakob disease in the UK. *NCJDRSU* www.cjd.ed.ac.uk/sites/default/files/figs.pdf

ORRÚ, Christina D.; CAUGHEY, Byron. Prion seeded conversion and amplification assays. *Prion proteins*, 2011, 121-133.

ORRU, Christina D., et al. New generation QuIC assays for prion seeding activity. *Prion*, 2012, 6.2: 147-152.

ORRÚ, Christina D., et al. Rapid and sensitive RT-QuIC detection of human Creutzfeldt-Jakob disease using cerebrospinal fluid. *MBio*, 2015, 6.1: 10.1128/mbio. 02451-14.

ORRÚ, Christina D., et al. Bank vole prion protein as an apparently universal substrate for RT-QuIC-based detection and discrimination of prion strains. *PLoS pathogens*, 2015, 11.6: e1004983.

ORRÚ, Christina D., et al. Prion seeding activity and infectivity in skin samples from patients with sporadic Creutzfeldt-Jakob disease. *Science translational medicine*, 2017, 9.417: eaam7785.

ORRÚ, Christina D., et al. Ring trial of 2nd generation RT-QuIC diagnostic tests for sporadic CJD. *Annals of Clinical and Translational Neurology*, 2020, 7.11: 2262-2271.

OUESLATI, Abid. Implication of alpha-synuclein phosphorylation at S129 in synucleinopathies: what have we learned in the last decade?. *Journal of Parkinson's disease*, 2016, 6.1: 39-51.

PANIGAJ, Martin, et al. Expression of prion protein in mouse erythroid progenitors and differentiating murine erythroleukemia cells. *PloS one*, 2011, 6.9: e24599.

PARCHI, Piero, et al. Incidence and spectrum of sporadic Creutzfeldt–Jakob disease variants with mixed phenotype and co-occurrence of PrP Sc types: an updated classification. *Acta neuropathologica*, 2009, 118: 659-671.

PARCHI, Piero; SAVERIONI, Daniela. Molecular pathology, classification, and diagnosis of sporadic human prion disease variants. *Folia neuropathologica*, 2012, 50.1: 20-45.

PEDEN, Alexander H., et al. Sensitive and specific detection of sporadic Creutzfeldt–Jakob disease brain prion protein using real-time quaking-induced conversion. *Journal of general virology*, 2012, 93.2: 438-449.

RAHIMI, Jasmin; KOVACS, Gabor G. Prevalence of mixed pathologies in the aging brain. *Alzheimer's research & therapy*, 2014, 6: 1-11.

RAMESH, Sairam; ARACHCHIGE, Arosh S. Perera Molligoda. Depletion of dopamine in Parkinson's disease and relevant therapeutic options: A review of the literature. *AIMS neuroscience*, 2023, 10.3: 200.

ROSSI, Marcello, et al. Ultrasensitive RT-QuIC assay with high sensitivity and specificity for Lewy body-associated synucleinopathies. *Acta neuropathologica*, 2020, 140: 49-62.

RÖNTGEN, Alexander, et al. Modulation of α-synuclein in vitro aggregation kinetics by its alternative splice isoforms. *Proceedings of the National Academy of Sciences*, 2024, 121.7: e2313465121.

RUBENSTEIN, Richard; CHANG, Binggong. Re-assessment of PrPSc distribution in sporadic and variant CJD. *PloS one*, 2013, 8.7: e66352.

SARNATARO, Daniela; PEPE, Anna; ZURZOLO, Chiara. Cell biology of prion protein. *Progress in molecular biology and translational science*, 2017, 150: 57-82.

SCHMITZ, Matthias, et al. Hereditary human prion diseases: an update. *Molecular neurobiology*, 2017, 54: 4138-4149.

SCHMITZ, Matthias, et al. Detection of prion protein seeding activity in tear fluids. *New England Journal of Medicine*, 2023, 388.19: 1816-1817.

SCHWEIGHAUSER, Manuel, et al. Structures of α-synuclein filaments from multiple system atrophy. *Nature*, 2020, 585.7825: 464-469.

SHI, Qi, et al. Genetic prion disease: insight from the features and experience of China National Surveillance for Creutzfeldt-Jakob Disease. *Neuroscience Bulletin*, 2021, 37: 1570-1582.

SHIN, Eui Cheol, et al. Expression patterns of α-synuclein in human hematopoietic cells and in Drosophila at different developmental stages. *Molecules and cells*, 2000, 10: 65-70.

SHIN, Chaewon, et al. In vivo and autopsy validation of alpha-synuclein seeding activity using RT-QuIC assay in the gastrointestinal tract of patients with Parkinson's disease. *Parkinsonism & Related Disorders*, 2022, 103: 23-28.

SHTILERMAN, Mark D.; DING, Tomas T.; LANSBURY, Peter T. Molecular crowding accelerates fibrillization of α-synuclein: could an increase in the cytoplasmic protein concentration induce Parkinson's disease?. *Biochemistry*, 2002, 41.12: 3855-3860.

SMITH, Jeffrey D., et al. Prion protein expression and functional importance in skeletal muscle. *Antioxidants & redox signaling*, 2011, 15.9: 2465-2475.

SORRENTINO, Zachary A., et al. Unique α-synuclein pathology within the amygdala in Lewy body dementia: implications for disease initiation and progression. *Acta neuropathologica communications*, 2019, 7: 1-22.

SOTO, Claudio; SABORIO, Gabriela P.; ANDERES, Laurence. Cyclic amplification of protein misfolding: application to prion-related disorders and beyond. *Trends in neurosciences*, 2002, 25.8: 390-394.

STEPHENS, Amberley D.; ZACHAROPOULOU, Maria; SCHIERLE, Gabriele S. Kaminski. The cellular environment affects monomeric α-synuclein structure. *Trends in biochemical sciences*, 2019, 44.5: 453-466.

TAKADA, Leonel T., et al. Genetic prion disease: experience of a rapidly progressive dementia center in the United States and a review of the literature. *American Journal of Medical Genetics Part B: Neuropsychiatric Genetics*, 2017, 174.1: 36-69.

TANJI, Kunikazu, et al. Analysis of PrPc mRNA by in situ hybridization in brain, placenta, uterus and testis of rats. *Intervirology*, 1995, 38.6: 309-315.

TELLING, Glenn C., et al. Prion propagation in mice expressing human and chimeric PrP transgenes implicates the interaction of cellular PrP with another protein. *Cell*, 1995, 83.1: 79-90.

TESAR, Adam, et al. Clinical Variability in P102L Gerstmann–Sträussler–Scheinker Syndrome. *Annals of neurology*, 2019, 86.5: 643-652.

TOBY, Timothy K., et al. Proteoforms in peripheral blood mononuclear cells as novel rejection biomarkers in liver transplant recipients. *American Journal of Transplantation*, 2017, 17.9: 2458-2467.

UCHIKADO, Hirotake, et al. Alzheimer disease with amygdala Lewy bodies: a distinct form of α-synucleinopathy. *Journal of Neuropathology & Experimental Neurology*, 2006, 65.7: 685-697.

UCHINO, Akiko, et al. An autopsy case of variably protease-sensitive prionopathy with Met/Met homogeneity at codon 129. *Neuropathology*, 2023.

UVERSKY, Vladimir N.; LI, Jie; FINK, Anthony L. Evidence for a partially folded intermediate in α-synuclein fibril formation. *Journal of Biological Chemistry*, 2001, 276.14: 10737-10744.

UVERSKY, Vladimir N.; LI, Jie; FINK, Anthony L. Pesticides directly accelerate the rate of α-synuclein fibril formation: a possible factor in Parkinson's disease. *FEBS letters*, 2001, 500.3: 105-108.

VILLAR-PIQUÉ, Anna; LOPES DA FONSECA, Tomás; OUTEIRO, Tiago Fleming. Structure, function and toxicity of alpha-synuclein: the Bermuda triangle in synucleinopathies. *Journal of neurochemistry*, 2016, 139: 240-255.

VISANJI, Naomi P.; LANG, Anthony E.; KOVACS, Gabor G. Beyond the synucleinopathies: alpha synuclein as a driving force in neurodegenerative comorbidities. *Translational neurodegeneration*, 2019, 8: 1-13.

VITAL, Anne, et al. The nigrostriatal pathway in Creutzfeldt-Jakob disease. *Journal of Neuropathology & Experimental Neurology*, 2009, 68.7: 809-815.

WANG, Zerui, et al. Early preclinical detection of prions in the skin of prion-infected animals. *Nature communications*, 2019, 10.1: 247.

WATSON, Neil, et al. The importance of ongoing international surveillance for Creutzfeldt–Jakob disease. *Nature Reviews Neurology*, 2021, 17.6: 362-379.

WEBER, Petra, et al. Generation of genuine prion infectivity by serial PMCA. *Veterinary microbiology*, 2007, 123.4: 346-357.

WESTERGARD, Laura; CHRISTENSEN, Heather M.; HARRIS, David A. The cellular prion protein (PrPC): its physiological function and role in disease. *Biochimica et Biophysica Acta (BBA)-Molecular Basis of Disease*, 2007, 1772.6: 629-644.

WILHAM, Jason M., et al. Rapid end-point quantitation of prion seeding activity with sensitivity comparable to bioassays. *PLoS pathogens*, 2010, 6.12: e1001217.

WHITTAKER, Heather T., et al. Multiple system atrophy: genetic risks and alpha-synuclein mutations. *F1000Research*, 2017, 6.

XIAO, Kang, et al. Validation and application of skin RT-QuIC to patients in China with probable CJD. *Pathogens*, 2021, 10.12: 1642.

XU, Wei; TAN, Lan; YU, Jin-Tai. The link between the SNCA gene and parkinsonism. *Neurobiology of aging*, 2015, 36.3: 1505-1518.

YANG, Yang, et al. Structures of α-synuclein filaments from human brains with Lewy pathology. *Nature*, 2022, 610.7933: 791-795.

YOKOYAMA, Takashi, et al. Heparin enhances the cell-protein misfolding cyclic amplification efficiency of variant Creutzfeldt–Jakob disease. *Neuroscience letters*, 2011, 498.2: 119-123.

ZERR, Inga. RT-QuIC for detection of prodromal α-synucleinopathies. *The Lancet Neurology*, 2021, 20.3: 165-166.

ZERR, Inga, et al. Creutzfeldt–Jakob disease and other prion diseases. *Nature Reviews Disease Primers*, 2024, 10.1: 14.

ZHANG, Weiguanliu, et al. Large-scale validation of skin prion seeding activity as a biomarker for diagnosis of prion diseases. *Acta Neuropathologica*, 2024, 147.1: 1-16.

ZHU, Caihong; AGUZZI, Adriano. Prion protein and prion disease at a glance. *Journal of Cell Science*, 2021, 134.17: jcs245605.

8 Supplement

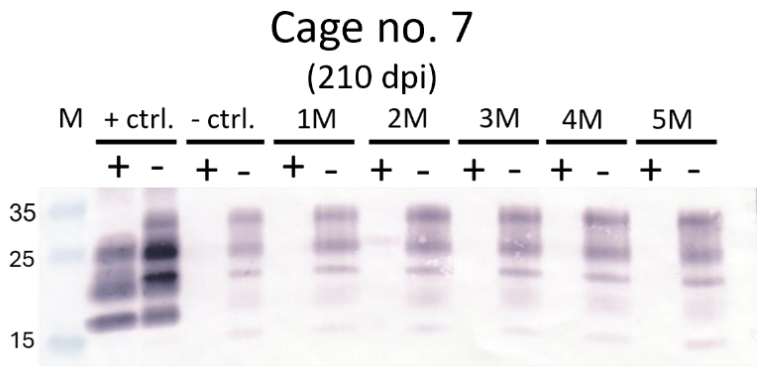

Supplementary Figure 6. Western blot detection of pathogenic prion protein (PrP^{Sc}) in brain from control mice intracerebrally inoculated with PBS. Samples were both untreated (-) and treated (+) with proteinase K (PK) and subsequently stained with a mix of AH6 and 6D11 primary mice antibodies. As a positive control (+ctrl), 10% brain homogenate from mice inoculated with RML prion strain in terminal stage was used. As a negative control (-ctrl.), 10% brain homogenate from healthy mouse was used. All control mice were negative for PrP^{Sc}.

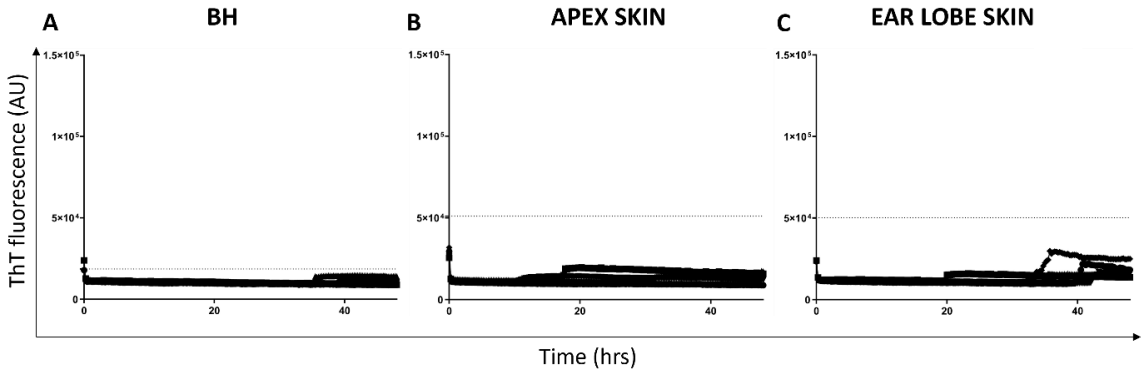

Supplementary Figure 7. RT-QuIC detection of prion seeding activity in brain and skin (apex, ear lobe) from control mice inoculated intracerebrally with PBS. Samples were analyzed in quadruplicates over 48 hrs utilizing rHAPrP90-231 as a substrate. Traces represents the mean from four wells for every tested mouse (n=5). Control mice were sacrificed 210 dpi. The dotted line represents calculated threshold for every type of the sample. All control mice gave negative ThT fluorescence signal, safely below the threshold.
AU – arbitrary units

Supplementary Table 1. Characteristics and RT-QuIC results analyzed archive FFPE samples from control patients with other neurodegenerative diseases. The definite diagnosis of non-TSE was confirmed at neuropathological examination of brain by immunohistochemistry and western blot during the autopsy.

	n	mean age ± SD	male (n)/ female (n)	mean max. ThT±SD (AU) x10^4	mean AUC (AU) x10^6
AD	12	79 ± 8	8/4	2.3±1	0.7
DLB	2	89, 78	2/0	1.7; 1.4	0.7; 0.6
FTLD*	8	74 ± 6	5/3	2.5±1.2	0.7
VaD	1	94	0/1	2.7	0.8
Syn	1	56	1/0	1.4	0.5
ND-A	1	56	1/0	3.7	1.1
lymphoma infiltration	1	54	0/1	1.7	0.7
H/ABI	3	43 ± 8	1/2	2±0.8	0.7
encephalitis, DLBCL	1	66	0/1	1.7	0.7

AD – Alzheimer disease, DLB – dementia with Lewy body, FTLD – frontotemporal dementia, VaD – vascular dementia, Syn – synucleinopathy, ND – A – non-dementia alcoholism, H/ABI – hypoxic/anoxic brain injury, DLBCL – diffuse large B-cell lymphoma

Supplementary Table 2. Characteristics of control patients and RT-QuIC results of tested BHs in the absence or presence of low concentration of SDS. Definite diagnosis was confirmed at autopsy by immunohistochemistry. Secondary synucleinopathy was confirmed in two patients (marked in green) that were reanalyzed after the positive RT-QuIC outcome.

sample	age	sex	definite diagnosis	RT-QuIC result for BH no SDS/ 0.0005% SDS
92/16	72	F	AD/DLB (Braak 3, McKeith 1)	+/+
116/17	80	F	AD	-/-
127/13	62	M	AD	+/+
155/13	60	M	AD/ALB	+/+
129/18	89	M	AD + others	+/-
119/18	75	F	AD + others	-/-
102/18	72	M	AD + others	-/-
25/18	69	M	FTLD-tau	-/-
80/18	84	M	FTLD-tau	-/-
38/18	64	F	FTLD-tau	-/-
135/17	73	F	FTLD-tau	-/-
93/15	67	F	FTLD-TDP	-/-
110/16	72	F	FTLD-TDP	-/-
60/19	66	M	FTLD-TDP	-/-
76/15	51	M	FTLD-TDP	-/-
121/12	80	M	HD	+/-
37/13	61	F	HD	+/-

AD – Alzheimer disease, DLB – dementia with Lewy bodies, ALB – amygdala Lewy body, FTLD – frontotemporal dementia, HD – Huntington disease

Supplementary Table 3. Characteristics of control patients and RT-QuIC results of tested undiluted and diluted CSF samples. Definite diagnosis was confirmed at autopsy by western blot and immunohistochemistry.

sample	age	sex	definite diagnosis	RT-QuIC result for CSF 10^0/ 10^{-1}
78/18	73	F	AD	+/-
61/18	74	M	AD	-/-
85/18	88	M	AD	+/+
83/19	94	F	FTLD-tau + VaD	-/-
38/18	64	F	FTLD-tau	-/-
40/19	71	M	FTLD-UPS	-/-
30/19	75	M	CJD (MM1)	-/-
88/19	70	F	CJD (MM1+2)	-/-
75/19	63	F	CJD (MM1+2)	-/-
130/19	73	M	CJD (MV1)	-/-
13/19	65	F	CJD (MV1)	-/-
35/20	75	F	CJD (MV1)	-/-
27/19	87	M	CJD (MM1)	-/-
111/18	73	M	CJD (VPSPr)	-/-
60/20	73	M	CJD (VV2)	-/-
62/18	34	M	H/A BI	+/-
10/19	49	F	H/A BI	-/-
74/19	56	M	ND-A	-/-

AD – Alzheimer diseas, FTLD – frontotemporal dementia, VaD – vascular dementia, CJD – Creutzfeldt-Jakob disease, H/A BI – hypoxic/anoxic brain injury, ND-A – non-dementia alcoholism

List of publications

1. Publications *in extenso* which are the basis for dissertation thesis

Detection of prions in matching *post-mortem* skin and cerebrospinal fluid samples using second-generation real-time quaking-induced conversion assay.

Baranová S., Moško T., Průžová M., Haldiman T., Kim Ch., Safar J.G., Matěj R., Holada K.

Scientific reports. 2024, doi.org/10.1038/s41598-024-56789-6

Impact factor: 4.6

Detection of Prions in Brain Homogenates and CSF Samples Using a Second Generation RT-QuIC Assay: A Useful Tool for Retrospective Analysis of Archived Samples.

Moško T., Galušková S., Matěj R., Průžová M., Holada K.

Pathogens, 2021, **doi.org/10.3390/pathogens10060750**

Impact factor: 3.7

New possibilities of laboratory diagnostics of diseases associated with amyloid formation.

Galušková S., Moško T., Dušek P., Matěj R., Holada K.

Česká a Slovenská Neurologie a Neurochirurgie, 2021, doi.org/10.48095/cccsnn2021334

Impact factor: 0.5

Univerzita Karlova v Praze, 1. lékařská fakulta
Kateřinská 32, Praha 2

Prohlášení zájemce o nahlédnutí

do závěrečné práce absolventa studijního programu uskutečňovaného na 1. lékařské fakultě Univerzity Karlovy v Praze

Jsem si vědom/a, že závěrečná práce je autorským dílem a že informace získané nahlédnutím do zpřístupněné závěrečné práce nemohou být použity k výdělečným účelům, ani nemohou být vydávány za studijní, vědeckou nebo jinou tvůrčí činnost jiné osoby než autora.

Byl/a jsem seznámen/a se skutečností, že si mohu pořizovat výpisy, opisy nebo kopie závěrečné práce, jsem však povinen/a s nimi nakládat jako s autorským dílem a zachovávat pravidla uvedená v předchozím odstavci.

Příjmení, jméno (hůlkovým písmem)	Číslo dokladu totožnosti vypůjčitele (např. OP, cestovní pas)	Signatura závěrečné práce	Datum	Podpis